JPL Publication 05-8

Technology Plan for the Terrestrial Planet Finder Coronagraph

Edited by:

Jennifer A. Dooley and Peter R. Lawson

Jet Propulsion Laboratory
California Institute of Technology
Pasadena, California

National Aeronautics and
Space Administration

Jet Propulsion Laboratory
California Institute of Technology
Pasadena, California

March 2005

This research was carried out at the Jet Propulsion Laboratory, California Institute of Technology, under a contract with the National Aeronautics and Space Administration.

TECHNOLOGY PLAN

TERRESTRIAL PLANET FINDER CORONAGRAPH

Approvals

Prepared By:

Jennifer A. Dooley, March 2, 2005
TPF Project Technologist — Date

Approved By:

Daniel R. Coulter, March 2, 2005
TPF Project Manager — Date

Michael Devirian, March 2, 2005
Navigator Program Manager — Date

Larry Simmons, 3/4/05
Director, JPL Astronomy & Physics Directorate — Date

Zlatan Tsvetanov, 3/07/2005
TPF Program Scientist — Date

Lia LaPiana, 3/7/05
TPF Program Executive — Date

Abstract

The Terrestrial Planet Finder (TPF) is envisaged as a series of two space observatories: an 8-m class optical coronagraph, to be launched around 2016; and a mid-infrared formation-flying interferometer, to be launched sometime prior to 2020. The goal of these missions, broadly stated, is to understand the formation and evolution of planets and, ultimately, of life beyond our Solar System. In support of this goal, the TPF missions will be capable of (1) searching for and detecting terrestrial planets should they exist in the habitable zones of nearby stars, (2) characterizing the atmosphere of planets they detect and searching for indicators of the presence of life, (3) undertaking a program of comparative study of the constituents of planetary systems, and (4) enabling a broad program of general astrophysics. These two missions provide a unifying context for all missions within NASA's Navigator Program. They are being managed by the Jet Propulsion Laboratory and supported by the Goddard Space Flight Center, on behalf of the Universe Division of NASA's Science Mission Directorate.

This document details the technology plan for the first of the TPF missions, the Terrestrial Planet Finder Coronagraph (TPF-C). TPF-C is currently in the first (or pre-Phase A) stage of the NASA project life cycle, and is undertaking a suite of technology development projects to demonstrate technological readiness leading to its Mission Concept Review, currently planned for late FY2006. Contained in these pages is an overview of planned pre-Phase A technology development activities, as well as activities planned through Phase C/D.

A central theme in the TPF-C technology plan is that of verification. It will likely be impossible to test the entire observatory under flight-like conditions prior to launch. Predictability of success and minimization of risk are therefore paramount. Verification of TPF-C flight hardware will be accomplished by subsystem and component testing at the most detailed level. The results of these tests will be used to confirm analytic models, and these models will then be linked together to estimate the overall performance of TPF-C. By comparing the interaction of individually tested elements (represented by verified independent models), confidence in the overall systems model will be obtained. The fidelity of the models and their analytic interfaces will be verified. Proof that these tolerances can be achieved in a repeatable and robust manner will be completed prior to the start of Phase C/D. Such proof will be obtained by taking measurements of appropriately scaled testbeds and components and correlating these results with models whose scalability and linearity can be verified.

The approach to verification will be an integral part of the architecture and design process to ensure that what is ultimately designed will be testable. Where adequate design margins or nagging uncertainties may persist, despite the best modeling techniques, the systems will have the ability to adjust out the system anomalies that might only be discovered in flight. During pre-Phase-A and phases A and B, the design approaches for these components and subsystems will be developed and verified by breadboard or testbed experiments.

The TPF-C Project is committed to maintaining strong industry and university involvement and will solicit, award, and manage a set of industry and university contracts to develop and demonstrate the needed technologies for TPF-C. The development of TPF-C will take advantage of the rich technology inheritance from many outside sources of key technologies and the many NASA missions currently under development.

Recent Highlights

Technical progress against the previous development plan (*Technology Plan for the Terrestrial Planet Finder*, March 2003) has been dramatic, particularly in the past year.

The critical technologies for TPF-C have been identified as those required for starlight suppression in both narrow and broad bands. The primary testbed for demonstration in this area, the High Contrast Imaging Testbed (HCIT), had achieved a contrast of 10^{-5} by March of 2003. As of December 2004, a contrast of 0.9×10^{-9}, an improvement of better than 4 orders of magnitude, had been achieved with laser light as shown in Figure i-1. Broadband experiments have also begun during this interval, achieving a contrast of 5×10^{-9} over a 40-nm bandpass. These contrast values refer to an average contrast within the half-dark hole extending from 4 to 10 λ/D. These achievements represent significant progress against the milestones agreed upon for entry into Phase A.

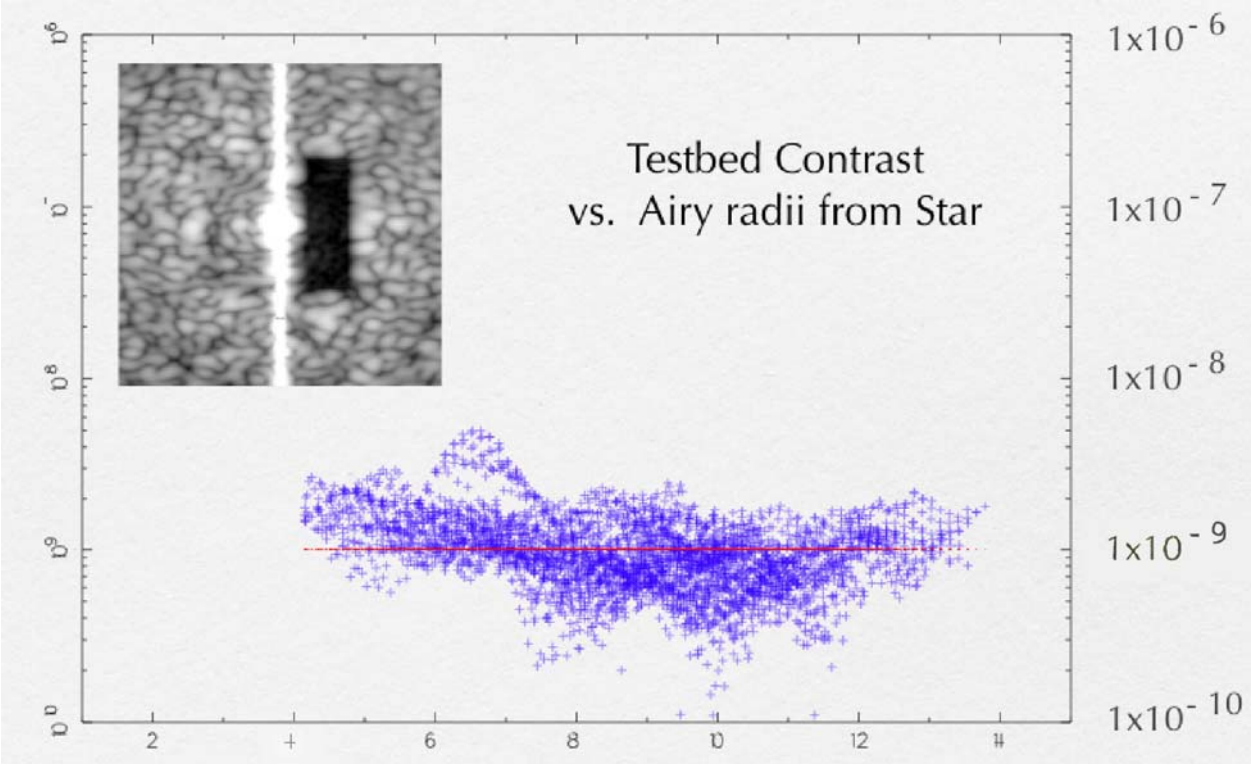

Figure i-1. Laboratory results from the HCIT showing an average contrast of 0.9×10^{-9} for laser light, as measured in the half dark hole (shown on a logarithmic scale in the upper-left corner) over angles from 4 to 10 λ/D.

Progress in two component technologies was essential to achieving the performance the HCIT demonstrated. The first was the fabrication of gray scale masks consistent with the 10^{-9} contrast achieved, and the second was continued development of the deformable mirrors (DMs).

Linear 1-sinc^2 masks patterned with controlled optical density profiles have been written in high-energy electron beam sensitive (HEBS) glass. The HEBS glass darkens to greater opacity with increased electron beam exposure. Significant progress has been made both in the processes for fabrication of the glass and electron beam writing as well as in the characterization of the finished masks. Figure i-2 shows the linear mask and the corresponding image recorded in the HCIT. Measurement of phase retardation, optical density, optical constants, and polarization properties are underway or in work. An alternative binary mask design employs electron beam lithography of aluminum on glass. Development has produced test articles, shown in Figure i-3, which are currently under test in the HCIT for comparison with the gray scale mask performance.

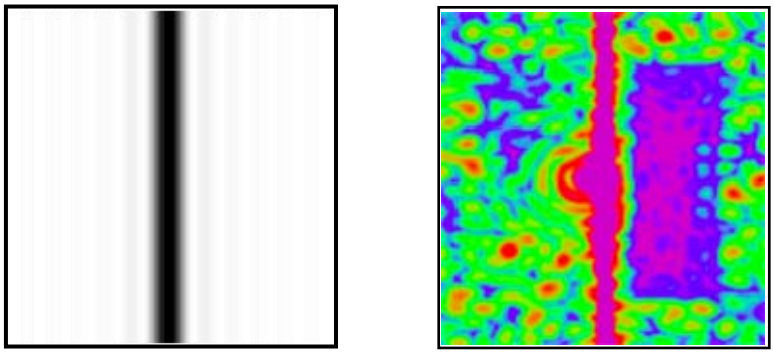

Figure i-2. Mask (left) and image (right). The mask is included in the optical train of the HCIT where the corresponding image is recorded.

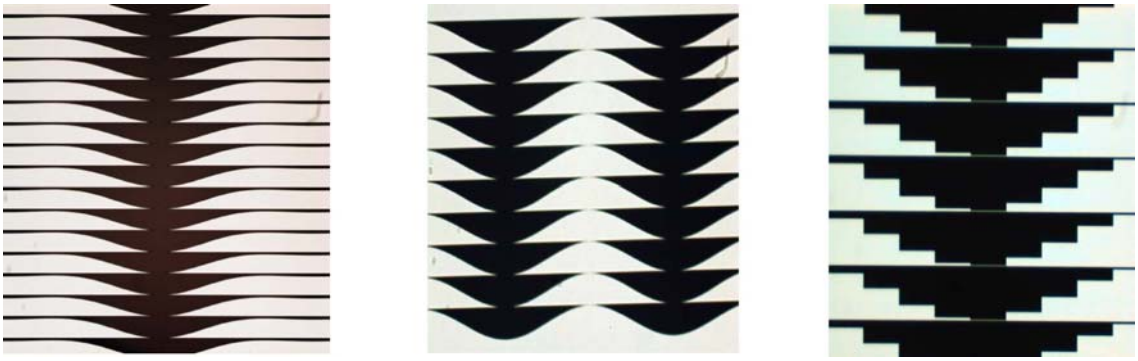

Figure i-3. Binary 1-sinc^2 mask (left) produced by electron-beam lithography of aluminium on glass for f/28.55 and wavelength 785 nm, binary continuous sin^2 mask pattern (middle), and binary discontinuous sin^2 mask pattern (right).

In 2003 Xinetics produced 32 × 32 mm, 1024-actuator DM modules that demonstrated 0.1-nm rms surface deformation control on the HCIT. Advances in the connector technology have made it possible to combine multiple modules behind a single facesheet. Currently, 4096-actuator DMs built up of four individual modules driving a single 64 × 64-mm facesheet have been delivered, and 96 × 96-mm DMs are in production. Examples are shown in Figure i-4. Thermal control, improved calibration, and electronics development have yielded command resolution of <0.10 Å surface/step and position stability of <0.20 Å surface/hour.

Figure i-4. Deformable mirror delivered by Xinetics to the HCIT.

The very recent development and adoption of an eighth-order mask design to replace the fourth-order masks previously baselined have had a major impact on the design and the 2005 technology plan detailed here. At the expense of some system throughput, the system sensitivity to aberrations is greatly reduced, by more than two orders of magnitude in some cases, as summarized in Table i-1. This translates into relaxation of a number of the more challenging mechanical and thermal requirements on the system. This development originated with an outside collaborator funded through a university contract and was eagerly adopted by the project.

Table i-1. Selected Error Budget Terms at Contrast = 1×10^{-12} at 4λ/D

Aberration	New (8^{th} Order)	Old (4^{th} Order)	Relaxation Ratio
Tilt	4.3×10^{-2}	2.7×10^{-3}	16
Focus	3.8 × 10-3	2.9×10^{-5}	132
Astigmatism	5.3 × 10-3	4.0 × 10-5	132
Coma	1.0×10^{-3}	5.6×10^{-6}	185
Trefoil	2.3×10^{-3}	1.7×10^{-5}	132
Spherical	3.5×10^{-5}	4.9×10^{-6}	7.2

*Aberration units are waves rms at 550 nm.

Acknowledgements

The *Technology Plan for the Terrestrial Planet Finder Coronagraph* has been put together with the efforts of many individuals. The editors are pleased to acknowledge contributions at the Jet Propulsion Laboratory by Virginia Ford, Andrew Lowman, Stuart Shaklan, Marie Levine, Rhonda Morgan, Bala Balasubramanian, Douglas Lisman, Joseph Green, Eri Cohen, John Trauger, B. Martin Levine, Mary White, James Alexander, Zakos Mouroulis, Greg Moore, Allan Eisenman, and Karl Stapelfeldt; and at the Goddard Space Flight Center by Dave Content, Andy Smith, Clifton Jackson, Alice Liu, Carl Blaurock, Claef Hakun, Chuck Bowers, Lou Fantano, and Jordan Camp. Contributions by Industry Contractors Larry Dewell (Lockheed Martin) and Terry Cafferty (TC Technologies) are also gratefully acknowledged.

The TPF Project is also pleased to acknowledge the constructive criticism and support of the TPF Technology Advisory Committee, listed in Appendix D, and the Navigator Program's External Independent Readiness Board, chaired by Vernon Weyers.

Table of Contents

1 Introduction

1.1 Purpose and Scope

The Terrestrial Planet Finder (TPF) is a suite of two complementary space observatories: a visible-light coronagraph and a mid-infrared formation-flying interferometer (depicted in Figure 1-1). The combination of these two missions, observing over a wide wavelength range, will provide definitive characterization of extra-solar planets and planetary systems and yield a reliable and robust assessment of habitability and the presence of signatures of life.

The primary purpose of this document is to detail the technology development activities for the Terrestrial Planet Finder Coronagraph (TPF-C) that will take place in pre-Phase A, leading up to the Mission Concept Review planned toward the end of FY2006. The focus of the technology plan is therefore to lay out the scope, depth, and inter-relatedness of activities that will enable TPF-C to achieve its technology milestones, supporting its entry to Phase A.

The TPF-C technology plan nonetheless takes a longer perspective and outlines the approach to technology verification that will lead the project through Phase A and onward to Phase C/D. TPF-C will be a technologically demanding mission. The size of the observatory, its complexity, system tolerances, and sensitivity to environmental conditions are such that it may never be possible to undertake a full end-to-end test of the observatory prior to launch. Much of this technology plan is therefore devoted to describing the approach to verification and validation of the expected performance of TPF-C.

This document is intended to be very specific concerning plans for the immediate future up until the end of pre-Phase A and somewhat detailed for plans in Phase A, but to provide only a broad outline of the approach that will be undertaken towards the latter phases of development leading up to launch. Whereas detailed budget information is considered in planning of pre-Phase A activities, no attempt is made to incorporate comprehensive budget information for subsequent Phases.

Within these pages are documented the critical component, subsystem, and system technologies and a schedule of development that includes the progression of NASA Technology Readiness Levels (TRLs). Error budgets are also presented that justify the current technology goals, with the understanding that these error budgets are subject to revision as the technology matures.

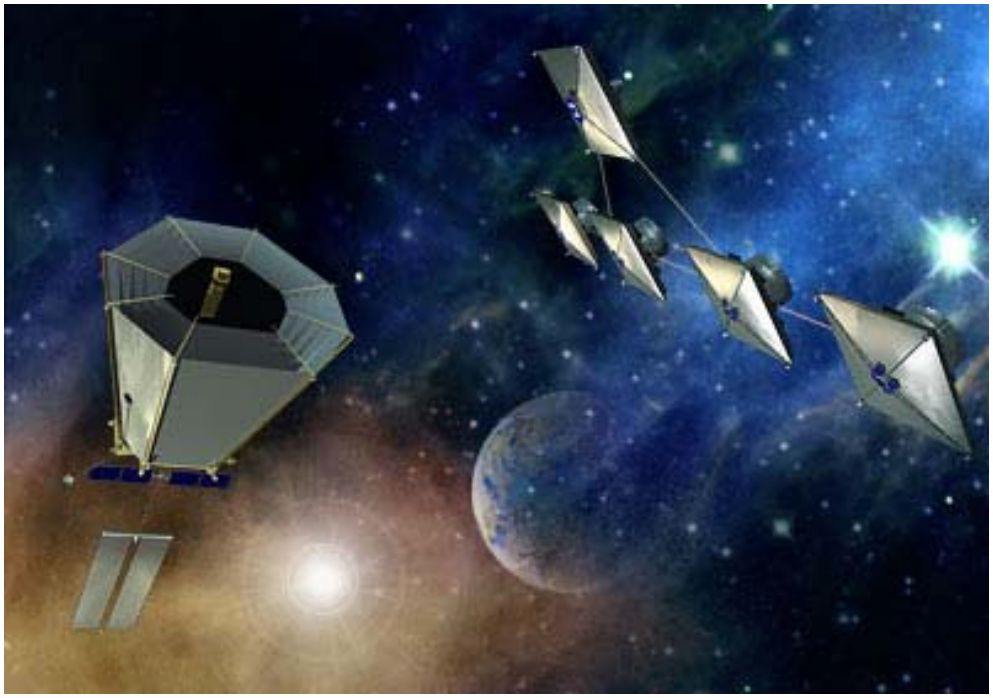

Figure 1-1. Artist's impression of the Terrestrial Planet Finder Coronagraph (TPF-C, left) and the Terrestrial Planet Finder Interferometer (TPF- I, right).

A previous version of the TPF Technology Plan was prepared in 2003 and charted the path for the current technology development for both TPF-C and the Terrestrial Planet Finder Interferometer (TPF-I). This updated plan, focusing solely on TPF-C, documents the progress that has been made since the earlier plan was put in place.

1.2 Relationship to Technology Development for Other Missions

TPF-C is largely pioneering the field of space-based high-contrast imaging. The technology demands are so stringent that there are relatively few missions that TPF-C can rely on for technology heritage in coronagraphy. Nonetheless, four missions stand out as technology precursors.

a) Hubble Space Telescope (HST): Advanced Camera for Surveys (ACS), High Resolution Channel (HRC), in use since 2002.

b) Space Interferometry Mission (SIM): planned for launch in 2010.

c) James Webb Space Telecope (JWST): planned for launch in 2011.

d) Laser Interferometer Space Antenna (LISA): planned for launch in 2011.

The Hubble Space Telescope has provided the first stellar coronagraph in space, and HST's coronagraph on the Advanced Camera for Surveys provides practical experience with space-based optical coronagraphy. However, the extent of technology inheritance is limited because

the dynamic range of the ACS/HRC is only a factor of 10. This is due primarily to the absence of a deformable mirror (DM) to correct residual wavefront errors.

Work for the development of the Space Interferometry Mission has included the design of space qualified laser metrology systems for nanometer control and picometer sensing of its optical surfaces. TPF-C will require active sensing and compensation of relative motions of its primary and secondary mirrors, as well as other mirrors in its optical train. The development of metrology lasers that are stable for periods corresponding the integration times of the coronagraph, which may be as long as 24 hours, are of interest to TPF-C. In this regard, there is direct technology heritage from LISA, whose lasers have very similar requirements. Precision laser metrology, stabilized lasers, corner-cubes, active control, vibration isolation and suppression, and precision optics are all candidate areas for technology inheritance. TPF-C will also benefit from parallel technology development for TPF-I.

JWST funded and developed the infrastructure for the measurement of materials properties that TPF-C will use. SIM funded microdynamics technology experiments on two flight experiments (Interferometry Program Experiment (IPEX) I and II) in 1996 and 1997. Although scaling of microdynamics behavior is not yet well understood, TPF-C benefits from both of these activities and their related database of measurements.

For additional technology, such as development of wavefront sensing techniques, controlling of wavefront through algorithms and mechanisms, adoption of an integrated modeling approach, thermal shielding deployments, and materials and temperature stabilization, the basis of the TPF-C approach derives from the Spitzer Space Telescope and JWST.

1.3 Applicable Documents

a) Science Requirements for the Terrestrial Planet Finder (Executive Summary), April 2004.
b) *Precursor Science for the Terrestrial Planet Finder*, October 2004, JPL Pub. 04-014.
c) *Biosignatures and Planetary Properties to be Investigated by the TPF Mission*, October 2001, JPL Pub. 01-008.
d) Terrestrial Planet Finder Coronagraph Mission Concept Report, Jan. 2005, JPL D-30415 (internal to JPL).
e) TPF-C Technology Overview, SPIE Proceedings, vol. 5487, Glasgow, June 2004.
f) *Technology Plan for the Terrestrial Planet Finder*, March 2003, JPL Pub. 03-007.
g) *TPF: Terrestrial Planet Finder*, May 1999, JPL Pub. 99-3.
h) TPF-C WBS Work Agreements (WAs), December 2004 (internal to JPL).

Document 1.3 (a) briefly describes the TPF science requirements as developed by the TPF Science Working Group (SWG) in 2003–2004. The technology requirements for TPF-C are derived from the science requirements tabled in this document. Documents 1.3 (b) and (c) provide further background information concerning the science objectives of TPF and relevant biomarkers. Document 1.3 (d) provides a detailed description of the mission concept for TPF-C as developed by the TPF-C Design Team, with input from the TPF SWG. Numerous technology papers describing technology testbeds for TPF-C are included in the three-volume SPIE proceedings of Document 1.3 (e). Document 1.3 (f) is the previous technology plan for TPF, written at a time when the focus of efforts was the architecture down-select between TPF-C and TPF-I. Document 1.3 (g) is the *TPF Book*, which, despite its emphasis on mid-infrared

interferometry, continues to be an excellent source of information related to TPF and the search for life on other planets. Document 1.3 (h) is the group of standard JPL documents that capture, at a high level of detail, the plans for implementing each Work Breakdown Structure (WBS) task. The WAs are signed by the doing organizations and, hence, represent commitments to the Project that the work will get done for the agreed upon budget and schedule. Most of these documents can be downloaded from the TPF Library at: http://planetquest.jpl.nasa.gov/TPF/tpf_index.html.

1.4 Science Objectives of TPF-C

The major scientific objectives of TPF-C are to:

a) Search for and detect any Earth-like planets in the habitable zone around nearby stars
b) Characterize Earth-like planets and their atmospheres, assess habitability and search for signatures of life
c) Carry out a program of comparative planetology
d) Enable a program of "revolutionary" general astrophysics

The main scientific goal of TPF-C is to detect directly and characterize Earth-like planets around nearby stars. The requirements that flow down from this goal define the characteristics of the observatory design and the mission. In particular, the ability to directly detect planets implies that TPF-C must be capable of separating the planet light from the starlight. Moreover, the facility must provide a sensitivity that will enable spectroscopic measurements of the light from the planet to determine the type of planet, its gross physical properties, and its main atmospheric constituents; the ultimate goal, of course, is to assess whether life or habitable conditions exist there.

The science requirements for the mission, as derived by the TPF Science Working Group, are shown in Table 1-1. One would expect Earth-like planets to be found around stars that are roughly similar to the sun, and so TPF-C target stars should include main sequence F, G, and K stars. The habitable zones to be studied span at least the orbital distances of Mars to Venus (scaled by the square-root of the stellar luminosity), and planets with a half-Earth area should be detectable. For the search to be statistically meaningful, at least 35 and preferably an additional 130 stars should be included in the search.

TPF-C must use the spectrum of a planet to characterize its surface and atmosphere. The spectrum of Earth, scaled for semi-major axis and star luminosity, would be used as a reference. The required spectral resolution is 70 in the visible. TPF must be capable of measuring O_2, H_2O, and O_3 in the visible. In this context, a measurement of a species is defined as the determination of the equivalent width of a spectral feature of that species to 20% accuracy. We desire that TPF measure Rayleigh scattering, photosynthetic pigments, CO_2, and CH_4 at visible wavelengths. The desired spectral resolutions are 2 times the required values.

TPF-C will also directly detect and characterize the spectrum of planets outside the habitable zone and determine the spatial and mineralogical distribution of material in the exozodiacal dust clouds of target systems. This will permit an understanding of the nature of terrestrial planets within a broader framework that includes the properties of other planetary system constituents.

The need to study outer planets generally implies a large outer working angle requiring a field of view extending out to at least 5 AU for the nearest target stars.

Other requirements and goals are listed in Table 1-1. It is worth noting that neither the comparative planetology nor the general astrophysics programs will be design drivers for the mission. These programs are intended to be carried out at little or no additional expense to the project.

1.5 TPF-C Mission Description

The current reference mission concept calls for TPF-C to be an 8 m class visible wavelength coronagraph operating in L2 orbit. The key mission parameters are summarized as follows.

a) L2 Orbit
b) Launch Vehicle – evolved expendable launch vehicle with 5 m × 19 m fairing
c) Mass 6200 kg (margin 32 %)
d) Power 3 kW
e) Lifetime 5 years (goal 10 years)

The TPF-C Mission Concept Report describes an advanced telescope system with a Cassegrain design having an off-axis elliptical primary mirror measuring 8.0 by 3.5 m along its major and minor axes, respectively (see Figure 1-2). A Cassegrain system was chosen, as opposed to a Gregorian, because it allows the primary mirror to be optically slower, thus reducing the

Table 1-1. Science Objectives of the TPF-C

Key Parameter	Requirement	Goal
Star types	F through K	F through K
Habitable zone	0.7 to 1.5 AU scaled $L^{0.5}$	0.7 to 1.5 AU scaled $L^{0.5}$
Orbit phase space	Semi-major axis: uniform inclination: uniform eccentricity: 0–0.35	Semi-major axis: uniform inclination: uniform eccentricity: 0–0.35
Number of stars to be searched	35 core stars	165 (130 additional stars)
Completeness per core star	90%	90%
Completeness per set of additional stars	N/A	90% integrated over the ensemble
Minimum planet area	1/2 Earth area	1/2 Earth area
Geometric albedo	Earth	Earth
Flux ratio	At least 3 broad wavelength bands	At least 3 broad wavelength bands
Spectral range	0.5–0.8 μm	0.5–1.05 μm
Characterization completeness	50%	50%
Giant planets	Jupiter brightness at 5 AU, 50% of stars	Jupiter brightness at 5 AU, 50% of stars
Average (Maximum) tolerable exozodi	3 (10) zodi	3 (10) zodi

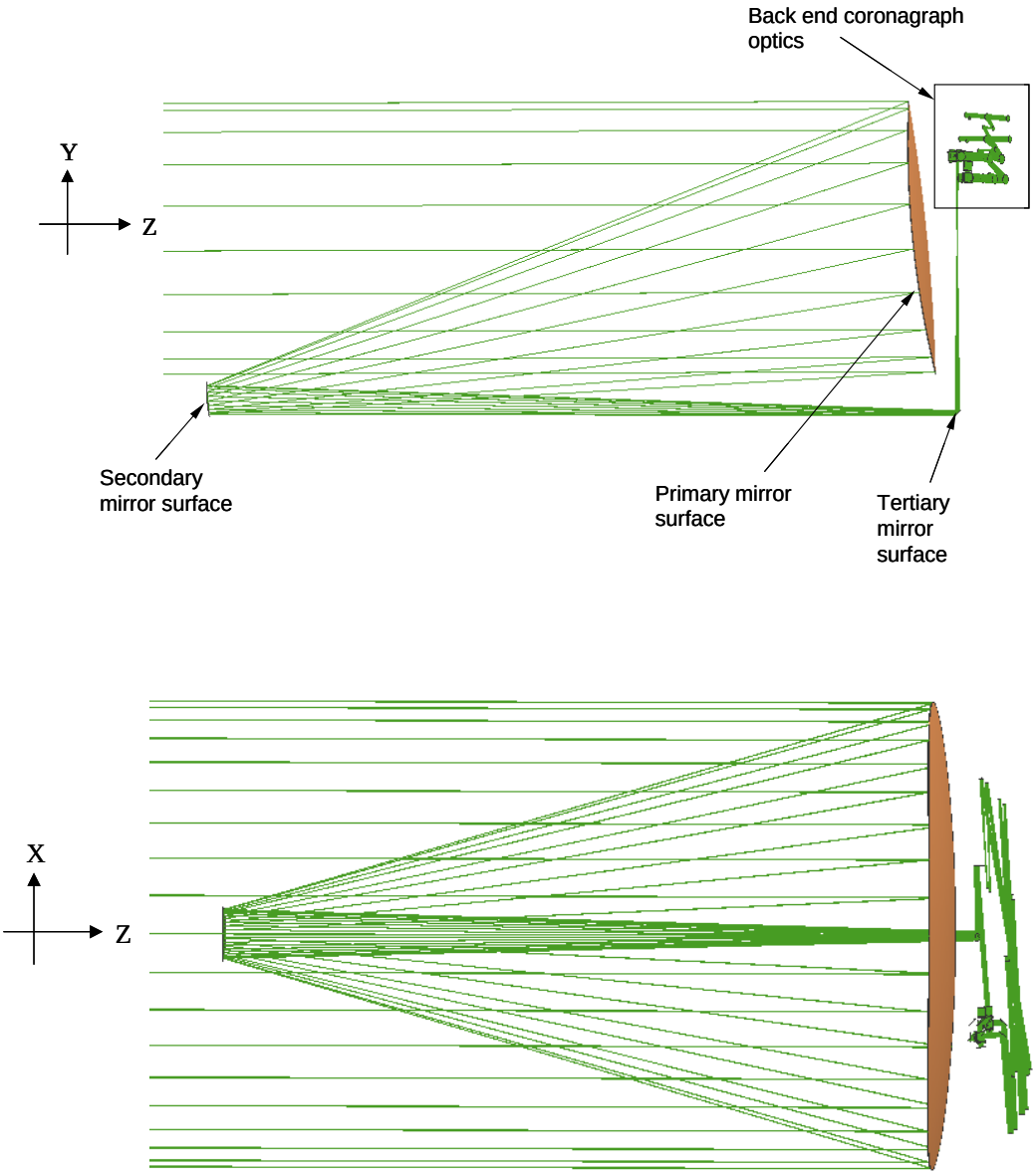

Figure 1-2. Raytrace diagram showing the overall optical layout of TPF-C, with side view (top) and front view (bottom).

sensitivities to misalignments and polarization effects that would result from higher angles of incidence. The primary-secondary separation is 12 m, and the secondary mirror is also an off-axis mirror, elliptical in profile, but with major and minor axes of 83.0 cm and 36.5 cm, respectively. The effective focal length of the system is 146 m, providing a field-of-view of 3.6 arcsec. As shown in Figure 1-3, the light from the secondary is directed by a flat tertiary mirror to an optical bench that lies underneath the primary. The optical bench houses a wavefront-correction system, followed by a coronagraph. Further details of the coronagraph optics are described in the subsequent sections of this document.

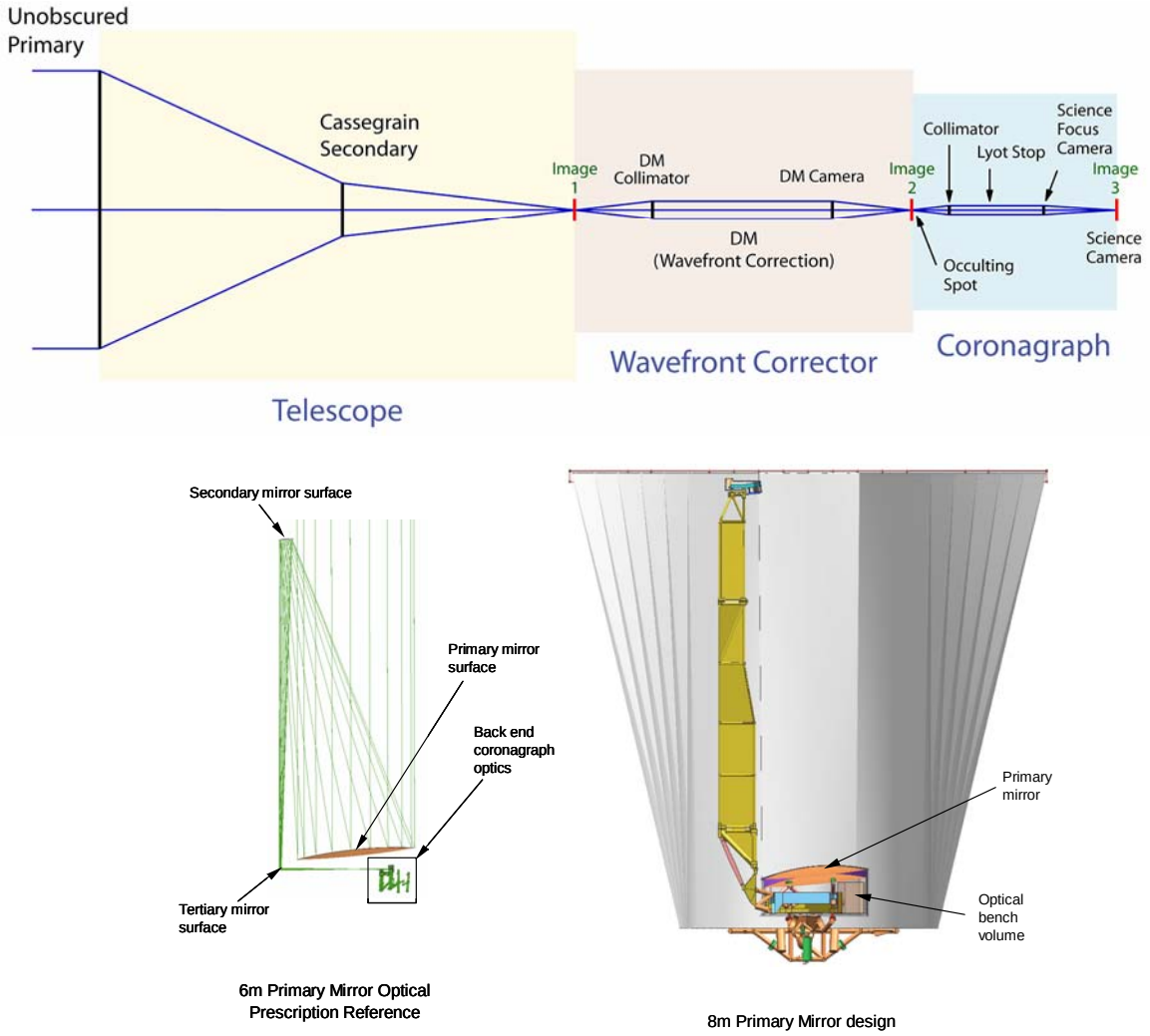

Figure 1-3. Optical system schematic and opto-mechanical layout.

After an initial on-orbit calibration and checkout period, the instrument will begin a 5-year science mission to obtain detailed and highly accurate coronagraphic measurements in search of planets orbiting nearby stars. Scheduled for launch in 2016, this mission will make measurements with far greater accuracy than is possible from the ground and will complement subsequent measurements to be made by TPF-I.

1.6 Preliminary TPF-C Instrument Description

The optics of TPF-C are currently structured around an off-axis Cassegrain telescope, followed by a wavefront compensation system, and finally an advanced coronagraph. The flow of the subcomponents of this system is shown schematically in Figure 1-4 and described in detail in the subsections that follow. Table 1-2 gives the mirror design parameters. The structure that supports the telescope and optics includes thermal isolation and actuators to reposition the secondary mirror, as well as separate thermal enclosures for the primary and secondary mirror.

Surrounding the whole telescope is a large multi-vane sunshield, whose design provides thermal stability for the facility as a whole and whose packaging allows for deployment in space.

The design of TPF-C provides the necessary wavefront correction to allow high contrast imaging, as well as the control necessary to maintain wavefront control over long exposure times. The approach to starlight suppression and planet detection is described following the instrument description.

1.6.1 Telescope Design

The focal length for the telescope is 146 m, and the paraxial focal ratio is f/18.2. The real focal ratios along each axis are 20.7 and 44.3 along the fast and slow axes, respectively. The axial separation between the primary and secondary mirrors is 12 m, and the distance from the secondary to the telescope focus is 15 m. The fold mirror is located 0.5 m behind the primary mirror vertex. After the fold mirror, the light passes to a second fold mirror, shown in Figure 1-5, then a collimating mirror, and then to a polarizing beamsplitter. The polarizing beamsplitter

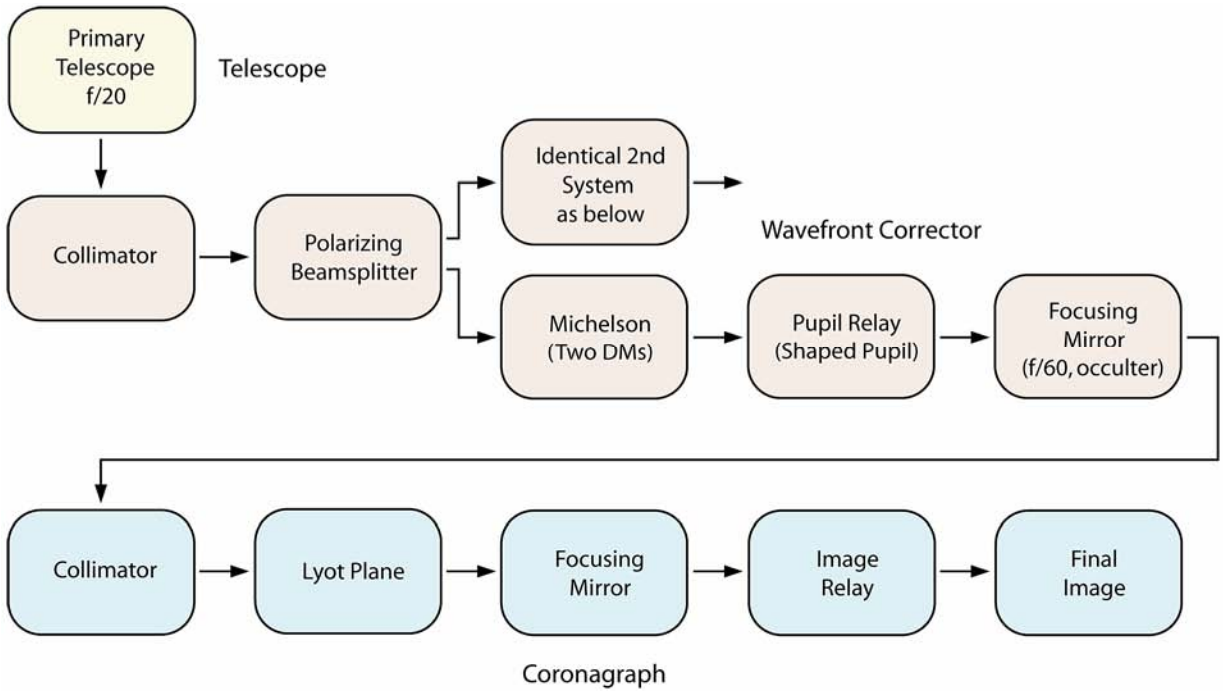

Figure 1-4. Schematic overview of the TPF-C optical layout.

Table 1-2. Design parameters for the primary, secondary, and tertiary mirrors of TPF-C

Mirror	Radius (mm)	Conic	Aperture (mm)	Off-axis decenter (mm)
Primary	26756.027	-1.001939	8000 × 3500	2300
Secondary	3034.830	-1.470716	830 × 365	237
Fold	Infinity	0.0	140 × 90	N/A

separates the × and *y* polarizations, and hereafter the optics are duplicated for each polarization and the light in each polarization is treated separately. The following description considers one polarization only.

1.6.2 Wavefront Compensator

The light now passes to a Michelson interferometer, shown in Figure 1-6. The arms of the interferometer are relatively short, and each terminates in a deformable mirror. The light is retro-reflected off the DMs, is recombined, and then sent onward to the coronagraph. This step is necessary so that the incoming wavefront can be corrected in both amplitude and phase. The two DMs provide the two degrees of freedom (DOF) necessary to correct both amplitude and phase. When the beam is recombined, it has been corrected not only for errors that exist on the telescope mirrors but also for errors due to the non-uniformity in the mirror coatings. Using a single DM, as the High Contrast Imaging Testbed (HCIT) does currently, it is possible to correct both phase and amplitude errors over a half-dark hole, or the phase errors over a full-dark hole yielding a reduced contrast.

1.6.3 Coronagraph Design

This near-perfect wavefront is then relayed to a pupil plane where a mask is inserted to block starlight. The pupil-plane mask diffracts the starlight away from the field of the habitable zone. The light is then imaged at a focal plane where an occulting mask is inserted to block the central star-light that passes through. The next step is to re-collimate the beam, which will send any diffracted light out to the edges of the field. This ring of light is blocked by a Lyot stop. Finally, the beam is relayed into a focus mirror which images it onto the science camera.

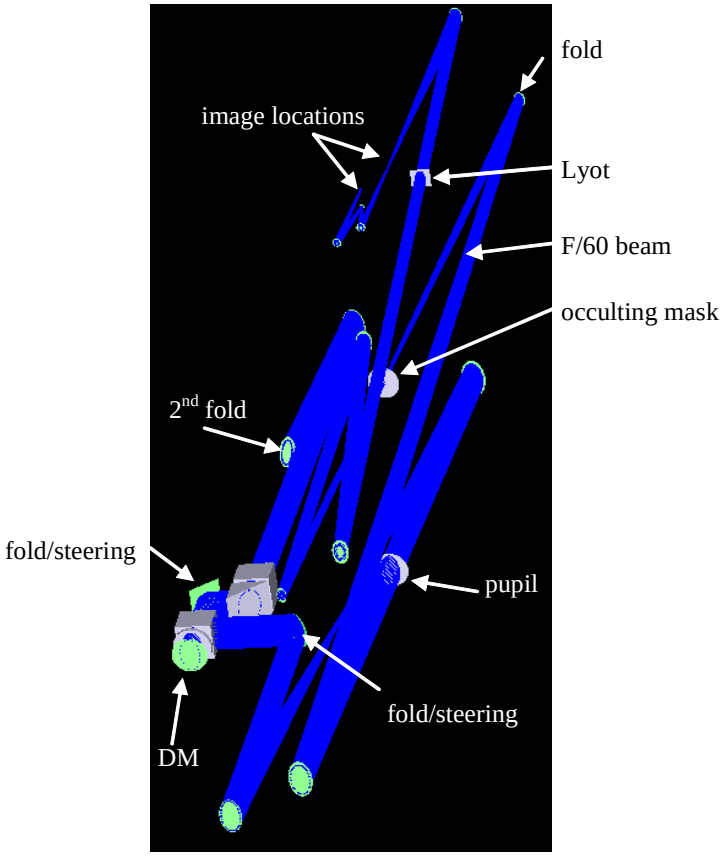

Figure 1-5. Coronagraph optical layout.

After the telescope is rolled, the residual background light can be subtracted and the camera will see an image similar to what is shown in Figure 1-7. The half of a square-shaped dark hole is created because of the square arrangement of the deformable mirror actuators. If the actuators were arranged in a hexagonal pattern, the dark hole would also be hexagonal. If the speckles were caused only by phase errors, the full dark hole with a bright line running through would

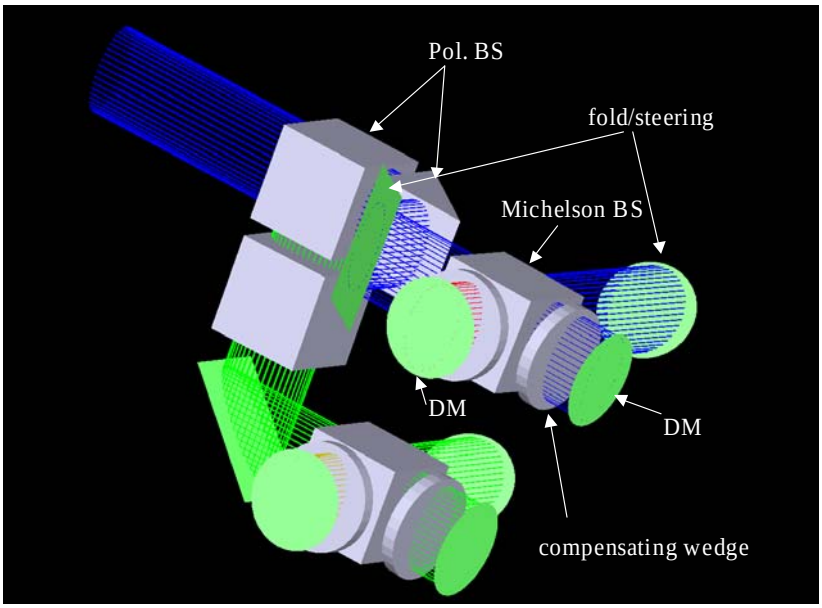

Figure 1-6. Polarizing beamsplitter with Michelson interferometers used for wavefront correction of amplitude and phase. The arms of the interferometers terminate in deformable mirrors, shown above.

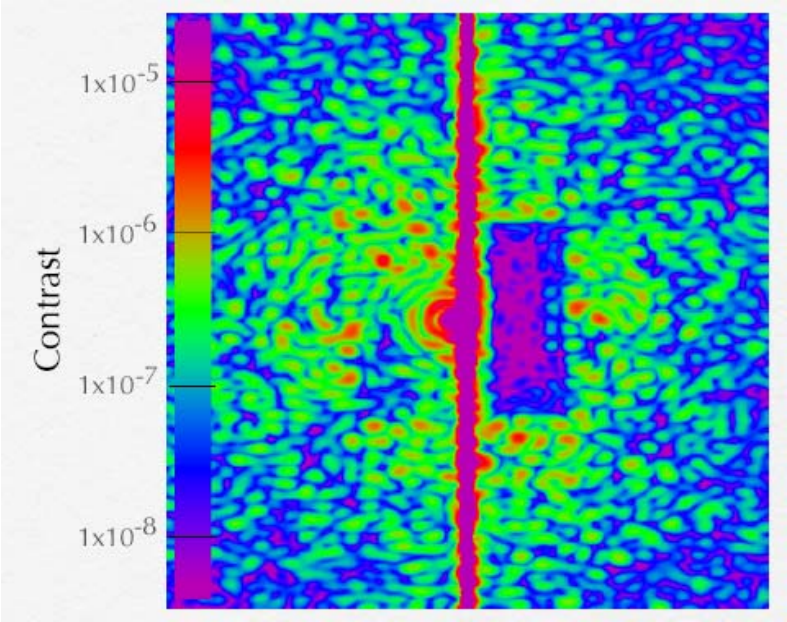

Figure 1-7. Results of laboratory tests showing starlight suppression to a level better than 1 part in 10^8.

be seen. Only half of the hole is dark because of the need to correct both phase and amplitude errors. In the dark hole, planets can be seen outside of the star light that has not been totally eliminated.

1.6.4 Thermal and Structural Design

As shown in Figure 1-8, the back of the primary mirror is surrounded by a heated thermal enclosure that maintains a steady controlled temperature gradient through the primary mirror, the coronagraph, and the science instruments. The temperature will be close to room temperature to allow the primary mirror to operate at the same temperature that it was fabricated. There is a similar smaller enclosure around the secondary mirror that also keeps its temperature steady at room temperature.

Behind the secondary mirror is an actuated hexapod with dual stage actuators that provide both coarse and fine position adjustment. The support of the actuated hexapod is thermally isolated from the secondary tower. The secondary mirror and primary mirror will have a 6-beam laser metrology system that will permit positional monitoring of the secondary mirror relative to the primary mirror at all times. The secondary tower itself will not be thermally controlled.

The tower is attached to an aft metering structure through three thermally-isolated bipods. The aft metering structure supports the telescope components: the primary mirror and the secondary tower. The aft metering structure is also attached to a payload support structure that integrates the telescope to the instruments.

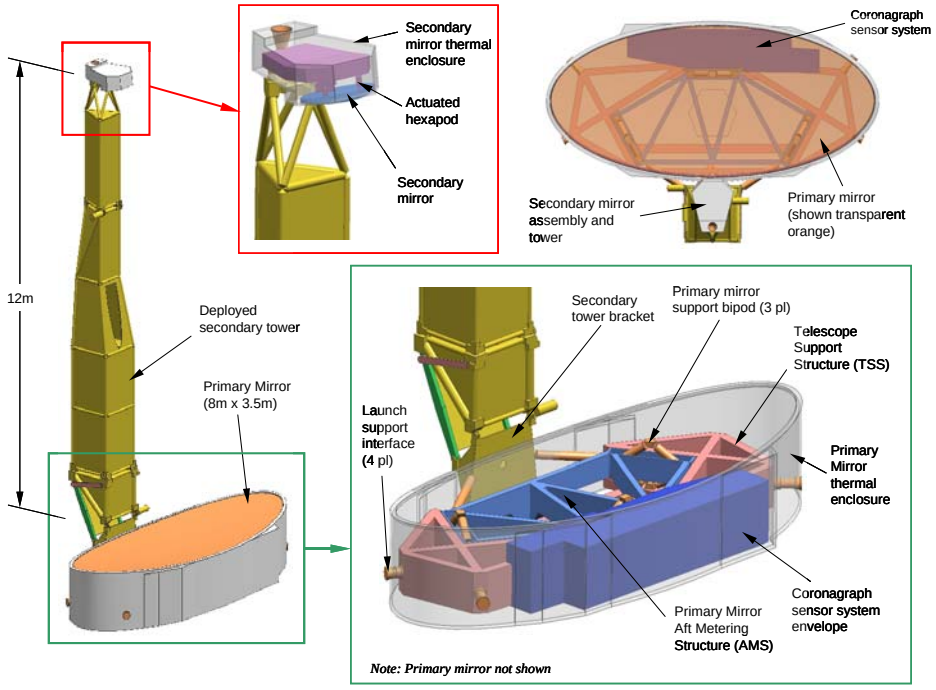

Figure 1-8. Exploded view showing the thermal and structural design of supports for the TPF-C primary and secondary mirrors.

1.6.5 Sunshield

The telescope is protected from the Sun by a six-vane v-groove radiator. This radiator rejects the heat from the Sun so that the telescope can rotate about its observing axis without significant deformation of the wavefront in the telescope. Extreme thermal stability is required so the optical wavefront will remain stable enough to allow for subtraction of the diffracted speckle pattern created by the telescope. The v-groove radiator is based on technology developed for the James Webb Space Telescope. The radiator must be deployed in space because it will not fit into a launch vehicle. Deployment from the stowed configuration behind the primary mirror is very challenging, requiring both radial and axial motion and tensioning of the thin vanes. The current concept for the sun shade deployment is shown in Figure 1-9.

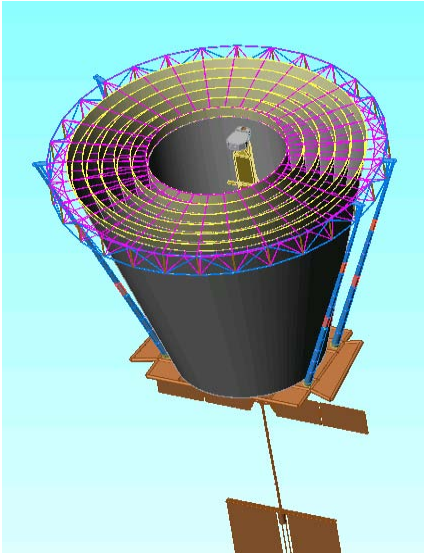

Figure 1-9. Concept for the TPF-C Deployable Sunshield

1.7 How TPF-C Detects Planets

TPF-C is designed as a high-performance coronagraph. The ability of TPF-C to detect a planet as separate from its host star is determined by the diffraction pattern of the primary mirror, as viewed through the optics of the coronagraph. There are two issues to contend with: (1) the primary mirror must be sufficiently large to provide the angular resolution necessary to resolve the planet as separate from the star, and (2) the sidelobes, stray light, and speckles in the diffraction pattern must be controlled and suppressed so that the faint planet light is detectable above the otherwise bright glare of the background.

Diffraction effects are minimized by having an unobstructed primary mirror (using an off-axis telescope design) and requiring the mirror surface to be sufficiently flat at spatial scales corresponding to the angular separation of star and planet, thus reducing the halo of speckles arising from imperfections in the mirror itself.

Scattered light is further controlled using two deformable mirrors that operate in concert to correct for both amplitude and phase irregularities in the wavefront. The remaining scattered light (after wavefront compensation) is blocked by a Lyot stop located in a pupil plane, and the diffraction pattern is further tapered using an image-plane stop.

The key conflict arises that a larger telescope at least in principle improves the ability to separate the planet light from the star, because the planet will appear further away from the image of the star, but this makes the observatory larger, more technologically challenging, and more expensive. The principal design trade is therefore to arrive at a primary mirror diameter that does not impose unrealistic constraints on the coronagraph performance.

1.8 Key Technical Challenges of TPF-C

The TPF-C telescope represents a large step between current or near-future heritage and what is required for a successful mission. To a large extent, this step deals with alignment, shape, and dynamic positional stabilities that are hard to achieve even in a small-scale laboratory instrument, let alone a huge space telescope.

When deployed, the TPF-C telescope fills a volume with its sunshield that is 16 m in diameter and 14 m long enclosing the 8-m primary mirror. Underneath this, the spacecraft, solar arrays, and solar wind compensating panel add another 23 m, for a total length of about 37 m. This entire 16 × 37 m system must be stowed for launch within a 4.5 × 16 m fairing. Furthermore the weight of the telescope and its sunshade cannot exceed 6200 kg to still allow for a 32% mass margin.

1.8.1 Correction of Static Wavefront Errors

Once deployed and commissioned, the telescope needs to deliver a ~10-nm rms wavefront to the coronagraph, where a deformable mirror will further reduce the wavefront error to an unprecedented sub-nm level. The wavefront correction must be maintained over the entire observation period.

1.8.2 Suppression of Dynamic Wavefront Errors

If the star image blooms because of a change in focus (a despace between the primary and secondary mirror of 50 nm or a sagitta change of the primary mirror of a mere 80 pm) or other decrease in wavefront quality, more light will spill past the apodizing mask and reduce the contrast necessary to distinguish the planet from the background noise. Additionally, decenter between the star image and the occulting disk needs to be limited to 400 nm.

TPF-C will be a very large, lightweight, 8-m telescope whose precision loadpath has potential elastic and inelastic discontinuities associated with the hinges and latches and mechanisms necessary to deploy it, residual strains resulting from 1-g assembly and 0-g operation that may not be fully stable, and a thermal environment which also may have milli- or micro-Kelvin temperature instabilities, all of which can conspire against these unprecedented stability levels. Recognizing this and the need to improve our design and analysis methods to reduce these uncertainties to levels that are acceptable, a series of component- and testbed-level development activities have been planned and are described in this report.

1.9 Technology Development Philosophy

The planet detection and characterization objectives described above drive the core of the TPF-C technology efforts, particularly in the early phase (pre-Phase A). The comparative planetology objective primarily impacts the design and engineering efforts and does not drive the technology efforts. The general astrophysics objective is not a driver for the design or technology efforts. The previous TPF Technology Development Plan was developed in 2002–2003 to support the

expected architecture downselect from either a TPF-C or TPF-I in 2006, before the decision was made to proceed with both observatories.

With the recent decision to move forward first with TPF-C on a schedule consistent with launch readiness in 2016, the nature of the technology efforts must be reconsidered. The ultimate goal of the technology development program is an operational TPF-C flight observatory. The project must accelerate and complete pre-Phase A technology development activity in approximately two years to a level sufficient for NASA to approve entry into the formulation phase (Phase A/B) in 2007 and into the implementation phase (Phase C/D) in the 2011 timeframe, with the eventual goal of NASA approval for a 2016 launch.

Briefly, to complete pre-Phase A successfully, three major activities must be implemented in an integrated manner: testbed demonstrations, mission models, and error budget allocations. A development flow is established to retire each identified technical risk by end of formulation through laboratory demonstrations, validated models, and iteration of the error budget allocations based on technology achievements. The critical technologies and the feasibility of the mission based on the current design combined with mission models and error budgets must be demonstrated. As laid out in the NASA Code S Management Handbook, in order to complete Phase A, all technologies must be demonstrated to TRL 5, defined as "component and/or breadboard validation in a relevant environment (ground or space)," and the engineering must be within reach. The TRL levels attempt to standardize the description of technology maturity and are discussed in more detail in Appendix E. To complete Phase B and enter implementation, all technologies must be at TRL 6, defined as "system/subsystem model or prototype demonstration in a relevant environment," and a preliminary design must be shown analytically with validated models to achieve the flight performance necessary to realize the mission science objectives. The testbeds and models, with the error budget assumptions, developed during the formulation phase of the Project must achieve the stated maturity, but must also be conceived with an eye for their eventual programmatic purpose in the flight system test and verification activities and investigation of potential anomalies during operation.

Ideally, one tests a flight system end-to-end at flight levels in a flight environment. In the case of TPF-C, it will not be feasible to test the full system in this way due to the physical scale of the observatory and the difficulty of creating an environment that sufficiently approximates flight for the complete system. Confidence that the system will perform as expected on orbit will be developed through validated models of the system. Verification of TPF-C flight hardware will be accomplished via subsystem and component testing at the highest level to which these entities can be confidently tested. The TPF-C technology development program will validate the physics and scalability of these models at flight levels in flight environments. These models will then be linked together to estimate the performance of TPF-C. The fidelity of the models in the high-precision (picometer and milli-Kelvin) regimes and the model interfaces must have bounded and verified performance as well. Recognizing that our models will never be fully complete, the project will continuously review the mission models for omissions or errors based on testbed performance results. In some cases, the most stringent requirements on testbed performance will be levied by their role in model validation as opposed to technology demonstration. While it will not be necessary to improve on flight performance levels in order to validate the models, it will be necessary to design the testbed in such a way that it can be modeled accurately and the components can be characterized and exercised to determine sensitivities. The remaining

uncertainties in the system will be addressed with the capacity for on-orbit diagnostics and adjustments.

To support this progression, the TPF-C team has identified the technical risks, based primarily on the system error budget, to successfully implementing TPF-C. It is recognized that the observing mode that imposes the most stringent performance requirements must form the basis of the technology development program; for example, stability of the system is likely to be driven by the planet detection objective, while the planet characterization objective is likely to drive the bandwidth requirements. However, these relationships are not clear-cut; realizing this, the Project will continuously evaluate the relationship between the requirements and the observing mode. These risks are summarized in Table 1-3 and detailed later in chapters 3, 4, and 5. Risks are categorized as technology risks, representing requirements that are beyond the state-of-the-art, and engineering risks, which represent challenging engineering or design requirements. Additional risks are expected to be identified or given increased priority as the design and the corresponding error budget continues to evolve. The mission error budget is continuously updated to reflect the actual hardware performance. This allows the system architect to relax performance requirements in one area if performance can be improved more easily in another, or if the benefit of the performance increase is not significant for the overall system performance. Milestone definition is also updated to reflect this evolving understanding to ensure that the project resources are applied in the most effective way.

Clear paths to mitigate each risk area are being developed. A roadmap showing the testbed or technology activity mitigating each identified risk is given in Section 7.1. The error budget and predicted and laboratory performance must be consistent in order to consider a risk retired. The technical risk mitigation approach will be reviewed by the TPF-Technology Advisory Committee (TPF-TAC), the TPF-Science and Technology Definition Team (TPF-STDT), and HQ. A work plan that outlines this risk mitigation approach and includes measurable quantitative technical targets for functionality and performance will be developed and documented in this Technology Plan. The strategy will be informed by technology heritage from JWST, SIM, HST, Large Binocular Telescope Interferometer, Starlight and Keck-I for individual technologies as well as for integration and test (I&T) approaches which include validation through analytical modeling. It is recognized that the transfer of technology to the system implementers is a critical component of a successful development program. The project plan for technology transfer will be addressed in the implementation plan as part of the acquisition strategy and in future updates to this plan.

As the project moves into formulation, the technology development must be balanced within the funding and programmatic constraints. As the technical risks are better understood, and the details of the formulation phase technology plan evolve, some risks may have to be accepted without complete mitigation. Technology risks will need to be retired on the schedule described above, while certain engineering (or design) risks may be accepted. The project will engage the JPL Quality Assurance organization, the TPF-TAC, the TPF-STDT, HQ, and other stakeholders to gain agreement on the risk assessment and the details of the mitigation approach. In parallel, the TPF-C integration and test plan will be evolving along with the baseline system technical design. By the end of pre-Phase A, a preliminary description of essential tasks and tests will be developed based on the project technical risk mitigation strategy, consistent with the project acquisition strategy. By the end of formulation, the integration and test plan will be fully defined describing a risk-mitigation-driven technical approach supported by doing organization resource

Table 1-3. TPF-C Technology and Engineering Risks

Optics and Starlight Suppression Technology	TPF-C Preliminary Error Budget Allocations	Development Task Where Addressed	Page Refs
Technology Risks			
Broadband mask physics	Masks consistent with 10^{-10} contrast requirement	Apodizing Masks and Stops High Contrast Imaging Testbed	28 112 49 105
Amplitude and phase wavefront control	Demonstrate sensing and control to 10^{-5} wave in mid-spatial frequencies in a flight-like system	High Contrast Imaging Testbed Wavefront Sensing and Control Deformable Mirror Planet Detection Simulator	49 105 37 114 38 115 52 110
Optical coating performance and characterization	10^{-3} reflectivity uniformity	Coatings Technology Demonstration Mirror	42 117 33 113
Straylight	10^{-11} background	Scatterometer	45 118
Transmissive Optics	Sub-Angstrom wavelength transmission uniformity	Transmissive Optics Characterization	41 116
Engineering Risks			
Large primary mirror fabrication	<25 kg/m^2, <7 nm rms surface error at 4–100 cycles\aperture, 8 m class	Technology Demonstration Mirror	33 113
Contamination	Small optics better than class 100	Scatterometer High Contrast Imaging Testbed	45 118 49 105
Structural, Thermal and Spacecraft Technology			
Technology Risks			
Primary mirror surface figure stability	Sub-nm for up to 24 hours	Technology Demonstration Mirror Sub-scale EM Primary Assembly Testbed	33 113 78 129
Stability of structures	10–30 nm stability*	Precision Structural Stability Testbed Secondary Mirror Tower Partial Structure Testbed Vibration Isolation Testbed	58 122 70 126 64 123
Secondary mirror position control system	25 nm multi-axis control	Metrology Components Precision Hexapod Closed-loop Secondary Mirror Position Control	55 120 56 121 68 125
Material property characterization		Precision Structural Stability Testbed	58 122
Engineering Risks			
Thermal control system	mK-class thermal control of primary mirror and instrument	Sub-scale EM Primary Assembly Testbed Sub-scale EM Sunshield and Isothermal Enclosure	78 129 75 128
Sunshade deployment		Sunshade deployment testing	
Pointing control	5 mas rigid body pointing	Pointing Control Testbed	71 127
Integrated Modeling and Model Validation			
Technology Risks			
Thermo-mechanical analytical modeling fidelity	Validation of the tools at a contrast level of 10^{-10}	Sub-scale EM Primary Assembly Testbed Sub-scale Em Sunshield and Isothermal Enclosure Integrated Modeling Tools	78 129 75 128 91 130
End-to-end system testbed modeling and simulation	Contrast better than 10^{-10} at <4 λ/D; 0.5–0.8 microns	High Contrast Imaging Testbed Planet Detection Simulator Sub-scale EM Primary Assembly Testbed Sub-scale EM Sunshield and Isothermal Enclosure Closed-loop Secondary Mirror Position Control	49 105 52 110 78 129 75 128 68 125

*Time constants vary: secondary tower monitored by laser gauges, thus 1 Hz requirement; other optics are unmonitored, and so a 1×10^{-4} Hz requirement.

estimates. At this time a full test at flight levels of the instrument assembly, consisting of the starlight suppression system, is planned. A full test of the optical telescope assembly (OTA) is planned and the nature of this test is being evaluated. A programmatic end-to-end performance gate will be defined as part of the I&T plan.

In order to respond to changing priorities, this Technology Plan will be updated yearly with the first update to occur in March of 2006. Modifications to this document may result from a combination of factors: shifting instrument error allocations, changing risk prioritization, shifting budget priorities, and the challenge of performing state-of-the-art technical work on a tight schedule. Approvals for revised versions of the Plan will be obtained prior to issuance.

1.10 TPF-C High-level Technology Milestones

Three significant technology milestones have been set to gauge the developmental progress of the project and have been imposed as a requirement for the project to proceed from pre-Phase A to Phase A. Completion of the milestones is documented by the project, reviewed by the TPF-TAC and HQ, and approved by HQ. Listed below, these pre-Phase A milestones focus on demonstrating the critical technologies and the feasibility of the mission. The critical technologies for TPF-C have been identified as starlight suppression in both narrow and broad bands.

Milestone #1: Starlight Suppression

Demonstrate that the High Contrast Imaging Testbed (HCIT) is capable of achieving a baseline contrast of 1×10^{-9} (goal 1×10^{-10}) at a 4 λ/D inner working angle, at λ=785 nm, and stable for at least one hour.

Planned Completion Date: Q3 FY05

Milestone #2: Broadband Starlight Suppression

Demonstrate that the HCIT is capable of achieving a baseline contrast of 1×10^{-9} (goal 1×10^{-10}) at a 4 λ/D inner working angle over a 60-nm bandpass (goal 100 nm) with the center wavelength in the range of 0.5 µm to 0.8 µm.

Planned Completion Date: Q3 FY06

Milestone #3: Model Validation and Performance Feasibility

3A: Demonstrate that starlight suppression performance predictions from high-fidelity optical models of the HCIT**,** utilizing measured data on specific testbed components, are consistent with actual measured results on the testbed. Correlation of model predictions with experimental testbed results validates models at a baseline contrast ratio of better than 1×10^{-9} (goal 1×10^{-10}) over a 60-nm bandwidth.

Planned Completion Date: Q4 FY06

3B: Demonstrate, using the modeling approach validated against the HCIT performance combined with appropriate telescope models and the current mission error budget, that TPF-C could achieve a baseline contrast of 1×10^{-10} over the required optical bandwidth necessary for detecting Earth-like planets, characterizing their properties and assessing habitability.

Planned Completion Date: Q1 FY07

Milestone Development

Quantitative milestones for entry into Phase B and C will be developed by the project based on the error budget and technical risk mitigation strategy; reviewed by the TPF-TAC, TPF-STDT, and HQ; and approved by HQ. Approval of the milestones from HQ is required before the project enters Phase A. Descriptions of the testbed on which the gates are accomplished are provided in Section 3.2.1.

1.11 TPF-C Project Schedule

The TPF Project is in the first (pre-Phase A) stage of the NASA Project Life Cycle. In pre-Phase A, a wide range of missions and technology concepts are explored, and the emphasis is on establishing top-level goals, science requirements, and the technological feasibility of the mission. For planning purposes, the TPF-C project is focused on achieving its pre-Phase A technology goals no later than FY2006 to support a Phase A start in FY2007 and a launch by ~2016. Figure 1-10 shows the TPF-C life cycle schedule.

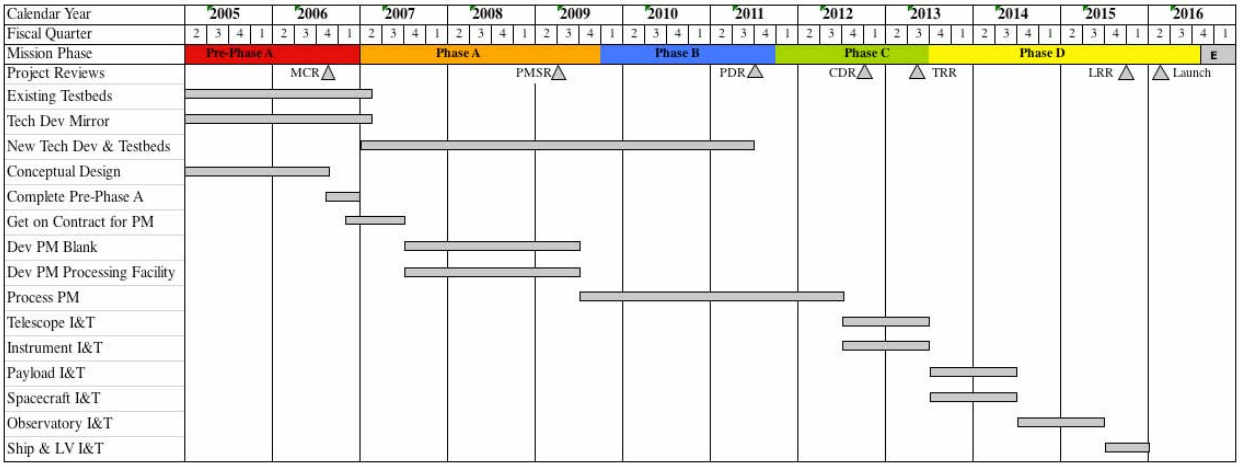

Figure 1-10. TPF-C Life Cycle Schedule

1.12 Technology Development Approach

It is convenient to divide TPF-C technology development into three, somewhat overlapping, segments:

- component technology development
- technology demonstration
- technology infusion

Component development deals with the design, build and test of breadboards for each novel hardware unit. These breadboards are taken through TRL 5, defined as "component and/or breadboard validation in a relevant environment (ground or space)." For TPF-C the relevant test environment for a component is typically a ground testbed where the component is shown to interface properly with other components and provide performance in a system setting. Technology demonstration is the province of TPF-C's subsystem and system level testbeds. In addition to serving as proving grounds for technology components (and software), the testbeds provide technology validation at a higher level of integration, consistent with TRL 6 (defined as "system/subsystem model or prototype demonstration in a relevant environment"). Technology infusion, for TPF-C, is the process of transferring the knowledge, techniques and "lessons learned" garnered during technology development and demonstration to the Flight System development team.

2 Error Budgets

2.1 Contrast Error Budget

Error Budget Description

An efficient stellar coronagraph blocks virtually all of the light from a target star by presenting a highly corrected wavefront to an efficient diffraction control system. At any point in the image plane, the ratio of the residual light level to the light that would appear if the stellar image was centered at that point is termed the "contrast." For TPF-C, the residual diffracted and scattered starlight in the image plane must be many orders of magnitude below the direct light from the target star to detect terrestrial planets via reflected starlight. The contrast describes the fundamental performance required of the observatory system, and so has been chosen as the top-level metric. The requirement is a contrast of 10^{-10} over an angle representing the habitable zone (where liquid water could exist), stable to a level of 2.5×10^{-11} for up to 24 hours.

The contrast error budget (CEB) rolls up the allocations for individual error contributions into an observatory system contrast. The CEB is an on-going process, with the document held by the system architect and iterated regularly to reflect changing design baselines and system understanding. It is used to manage the allocation of challenging requirements between system components and to manage the reserve margins on each of those allocations. The CEB guides directly the technology effort, serving to highlight requirements beyond the state-of-the-art, thereby triggering development activities.

The error budget allocation process begins with a first-order sensitivity analysis. Engineering judgment is used to partition allowable errors throughout the subsystems. In some cases, the allocations point directly to the difficult requirements, such as primary mirror stability, while in others requirements are derived indirectly through engineering analysis, as is the case for temperature stability requirements on the primary mirror. Reserve factors are allocated for each source and account for the performance reserve, the modeling uncertainty factor, and the error in the modeling. The modeling uncertainty relates to aspects of the model that do not accurately reflect physical behavior, while the modeling error refers to inaccuracies in the as-built model or physical properties. These reserve allocations are initially chosen based on engineering judgment and over time modified to reflect bounding of model calculations via testbed results. The TPF-C high-level error budget is shown in Figure 2-1.

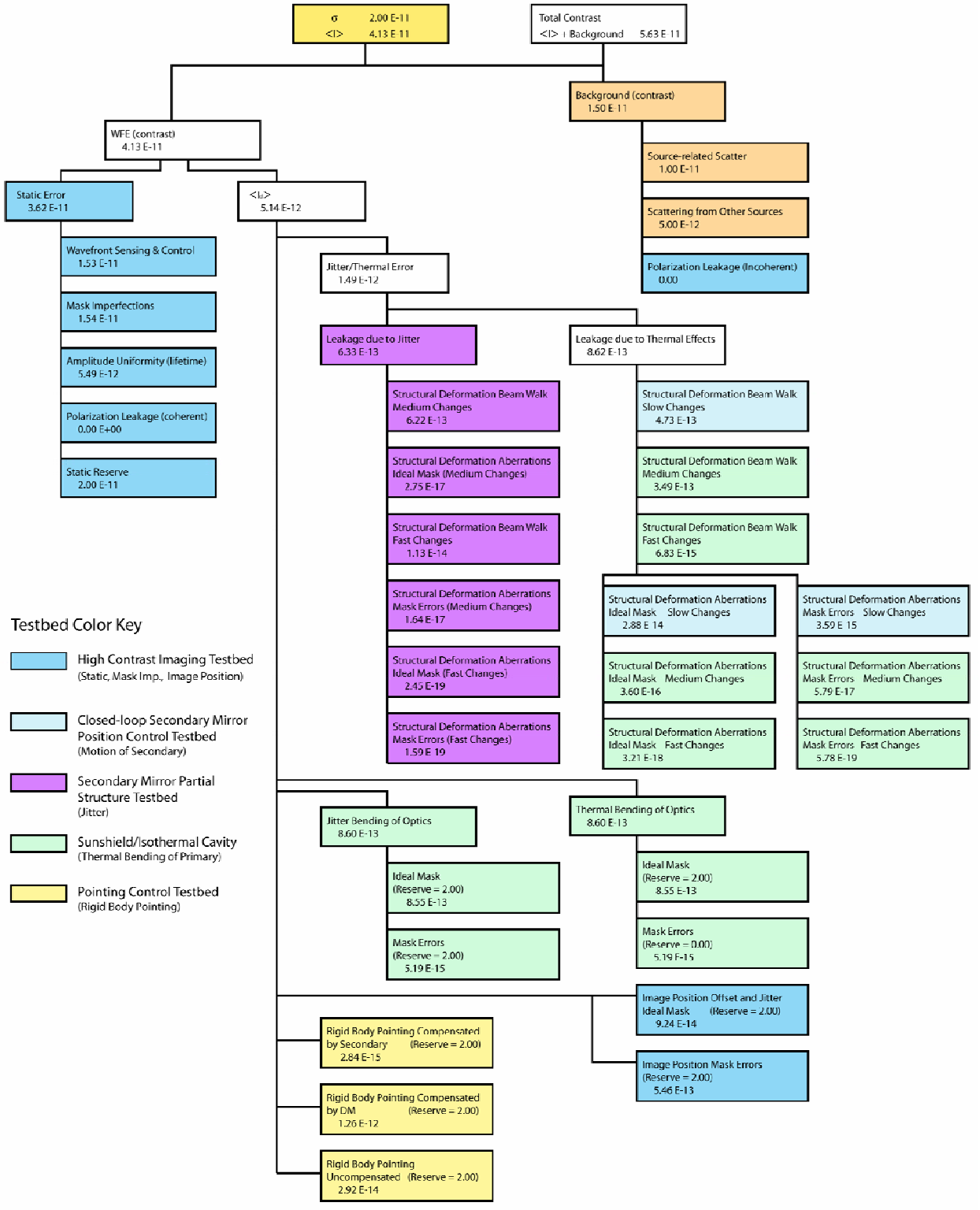

Figure 2-1. TPF-C high-level error budget. Values in the boxes are contrast contributions or contrast-reserve factors. The above is calculated for 4 λ/D, λ = 600 nm, D = 8 m.

Error Budget Validation

Given the critical role of the CEB, it is necessary to validate that the budget is properly constructed and captures all the important errors and interactions. The error budget is based on linear sensitivity matrices, meaning that the contrast contribution caused by errors from each source can be added directly to calculate a total error as described below. This approach allows straightforward scaling and modification, and is chosen because of its simplicity and suitability for sensitivity analysis. It remains to be validated through end-to-end models designed to capture the non-linear effects arising from propagation of diffraction. The error budget is finalized and validated before the end of Phase B through a combination of testbed results and end-to-end system models that address each item in the error budget tree. The level and method by which each item or set of items is to be addressed is determined by the end of Phase A.

Error Budget Structure

The TPF coronagraph contrast error budget comprises the static (initial wavefront setting at the start of an observation) and dynamic (any changes to the wavefront during an observation) terms that contribute to image plane contrast. Static terms include wavefront sensing and control (WFSC), stray light, coronagraph mask imperfections, and polarization leakage. Dynamic terms include motion of an optic or bending of an optic due to vibrations or thermal effects. Figure 2-2 shows the structure of the error budget including reserve factors, mean image plane contrast, and the standard deviation of contrast as detailed below.
Initial work has focused on the dynamic part of the error budget. It was assumed based on

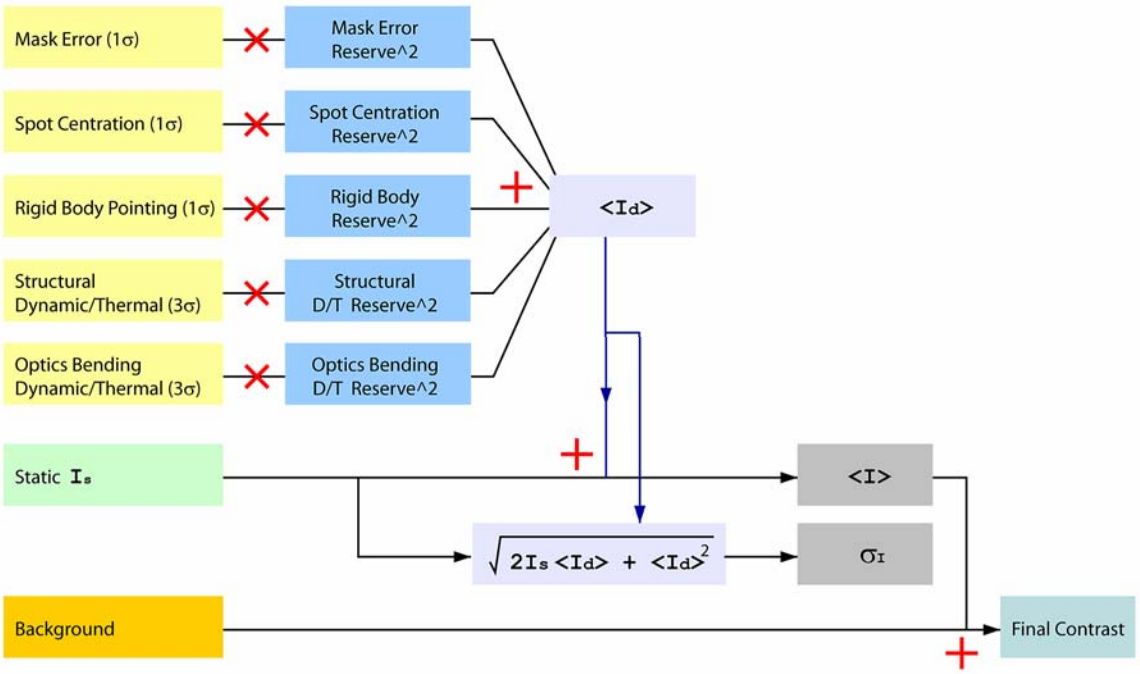

Figure 2-2. Error Budget Tree

existing proof-of-concept budgets developed during the TPF Industry Studies and early success on the HCIT that the initial wavefront sensing and control and background stray light levels meet the static requirements as allocated. Consideration of dynamic errors was given highest priority due to the implications for mission design, such as mass, stiffness, and thermal requirements; that is, dynamic errors place more limitations on design options. Static requirements drive the wavefront sensing and control approach, contamination requirements, baffling and optical surface quality among other things. Detailed modeling of static wavefront contributors, namely polarization leakage, coating uniformity, optical surface shape power spectral density, and surface contamination, is now in work and will be folded into the error budget studies.

Dynamically induced errors include optical aberrations, beam walk, and mask leakage. Aberrations arise as the system is perturbed from its ideal design, independent of the quality of the optics. Aberrations result from bending of optics (the primary mirror is of greatest concern), as well as from structural deformation. When the structure deforms, the secondary mirror moves relative to the primary mirror, as do downstream optics. This introduces low-order aberrations that scatter light near the inner edge of the coronagraph 'dark hole.' The effect places stringent requirements on the relative motions of the optics during an observation as errors are proportional to the square or 4th power of the optic displacements. Beam walk is the motion of the beam across the optics. Both rigid body pointing errors and structural deformation cause the beam to be deflected from its initial state at the beginning of an observation. When the beam reaches the DM, it is sheared relative to the compensating DM surface which was set prior to the observation. A corrugated wavefront results, adding to the scattered light level. The amplitude of the uncompensated wavefront varies linearly with displacement and spatial frequency, while the scattered energy varies as the square of the wavefront error. In addition to aberrations and beam walk, one other dynamic term contributes to image plane contrast. This term is labeled "image position" and is the energy that leaks around the mask when the beam is not perfectly centered on it. For all coronagraphs considered, the mask leakage is proportional to the 4th power of wavefront tilt.

The error budget keeps track of contrast error (energy) contributions from many sources. A memo by S. Shaklan, dated May 20, 2004, derives the equations for combining terms in the error budget; results are briefly summarized here. Assuming a set of random, uncorrelated complex field amplitudes in the Lyot plane of a stellar coronagraph, the summed variance of the contributions at a point in the image plane is equivalent to the sum of the intensity (contrast) contributions from each field component weighted by their variances. That is, given an aberration $\phi(\vec{x},t)$ defined as the sum of time-varying orthogonal modes $a_i(t)\phi_i(\vec{x})$,

$$\phi(\vec{x},t) = \sum_{i=1}^{N} a_i(t)\phi_i(\vec{x}) \qquad (1.1)$$

where the variance of the amplitudes is $\sigma_i^2 = \left\langle a_i^2 \right\rangle$, it can be shown that the mean intensity in the image plane is given by

$$\left\langle I(\vec{n}) \right\rangle = \sum_{i=1}^{N} \sigma_i^2 I_i(\vec{n}) \qquad (1.2)$$

where $I_i(\vec{n})$ is the intensity at an image point $\vec{n}$ for the *i*th aberration. In other words, *contrast terms sum linearly; they are not combined as the root-sum-square of contrast values*. (Although from Eq. 1.2 it can be shown that the wavefront errors do combine in a root-sum-square sense.)

Further, it is shown that in the presence of both static contrast I_s and dynamic contrast I_d, the mean contrast level (ignoring incoherent scatter) is the sum of these terms,

$$\langle I \rangle = I_s + \langle I_d \rangle \tag{1.3}$$

while the variance of the contrast includes static and dynamic cross-terms and is given by

$$\sigma_I^2 = 2I_s \langle I_d \rangle + \langle I_d \rangle^2 \tag{1.4}$$

The TPF-C science requirements are tied to the engineering requirements by both $\langle I \rangle$ and σ_I. The mean intensity level, $\langle I \rangle$, determines the instrument contrast and the standard deviation, σ_I, determines the stability of the contrast. Detecting a planet having 10^{-10} contrast with a signal-to-noise ratio of 4 requires the stability to be $\sigma_I < 2.5 \times 10^{-11}$, while integration time requirements and stability requirements (through the cross term of Eq. 1.4) require the mean coherent background level to be ~5×10^{-11}.

Error Budget Models

The error budget is built upon several models, as shown in Figure 2-3. Static models describe the optical performance of various algorithms and optical effects (e.g., stray light) that are independent of dynamic effects. Dynamic models describe the change in wavefront and leakage that occurs when the state of the system changes. Dynamic models used to compute the error budget include:

- Frauhnofer pupil-to-image plane model used for calculating image plane contrast as a function of wavefront components. The wavefront components are decomposed into Zernike polynomials that are orthogonal over circular and elliptical apertures. This is called the 'diffraction aberration sensitivity' model.

- MACOS-based aberration sensitivity model that determines the Zernike mode amplitudes when any optical component is moved over 6 DOF. This model is the 'Zernike sensitivity matrix.'

- 'Beam walk sensitivity matrix' based on the 'power spectral density (PSD) models' of the optics. To compute the beam walk contribution at a specific point in the image plane, the PSD is filtered by the spatial frequency corresponding to the image plane position (e.g., at 3 λ/D, the relevant frequency is 3 cycles/aperture). The amplitude of the filter is set by the lateral beam walk amplitude, which is determined by a MACOS ray trace (the "structural model"). The PSD function is flat below a turnoff spatial frequency and decreases as f^{-3} above that frequency, following the TDM specification. The PSD amplitude and turnoff frequencies are selected for the primary, secondary, small flat, and small powered optics. The PSD of the DM is the summed PSD of the other optics in the system in front of the mask (for the critical spatial frequencies comprising the "dark hole") since its wavefront is set to be equal and opposite to the summed wavefronts of the other optics.

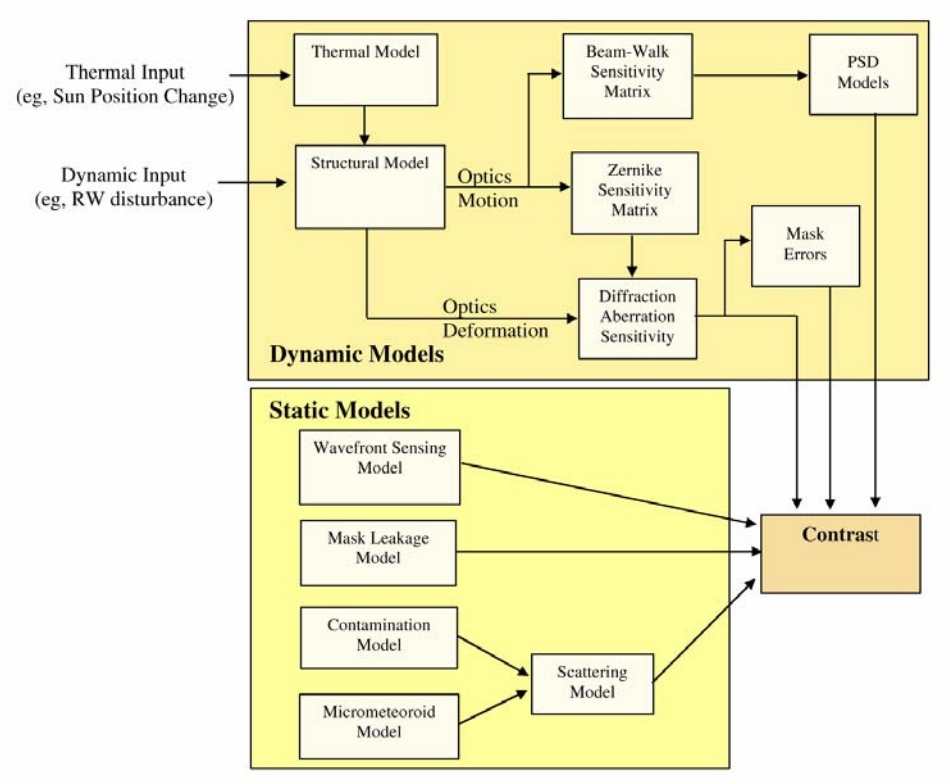

Figure 2-3. Models used to create the TPF-C dynamic and static error budget.

Performance Implications

The error budget enables the calculation of contrast at selected points in the image plane (e.g., 3, 3.5, and 4λ/D). This approach has allowed us to determine that the dynamic part of the budget is dominated by beam walk. Both throughput and low-order aberration stability considerations lead to a practical limit to the inner working angle (IWA) of the coronagraph. Contrast stability requirements applied to the IWA then determine the dynamic engineering requirements (e.g. mirror shape stability, pointing stability, secondary mirror position stability). Within the target angular range in the image plane (i.e., between the IWA and the outer working angle), the achieved stability will improve as we move outward from the IWA.

The TPF error tree depicts the quantitative contrast contributions and margins for a given image plane point with the contrast requirements appearing at the top level, as shown in Figure 2-1. In this case the image is evaluated at an angle of 4 λ/D, where λ is the wavelength of the light and D is the length of the long axis of the telescope. The baseline 8-m version of TPF must achieve the required contrast working as close in as 4 λ/D to provide an adequate IWA no larger than 62 milli-arcsecs (mas) at λ=600 nm.

Thermally induced deformations of optical surfaces must meet the requirements shown in Table 2-1. The allowed structural motions of the secondary mirror relative to the primary are shown in Table 2-2. Recognizing that the required relative stability of their positions along the line of sight to the star is sub-micron, we plan to implement a laser metrology truss between them to control a hexapod mounted on the back of the secondary mirror. The metrology system has a resolution and stability of ~200 pm, but it responds slowly (<1 Hz). It can be used to

Table 2-1. Requirement on Stability of Thermal Deformation of Optical Surfaces (Angstroms)

Zernike	Primary	Secondary	Small Flats	OAPs	DM
4	8.0	2.0	1.0	1.0	1.0
5	8.0	2.0	1.0	1.0	1.0
6	8.0	2.0	1.0	1.0	1.0
7	4.0	1.0	0.5	0.5	0.5
8	8.0	2.0	1.0	1.0	1.0
9	6.0	1.5	0.75	0.75	0.75
10	8.0	2.0	1.0	1.0	1.0
11	0.1	0.025	0.0125	0.0125	0.0125
12	0.1	0.025	0.0125	0.0125	0.0125
13	0.1	0.025	0.0125	0.0125	0.0125
14	0.1	0.025	0.0125	0.0125	0.0125
15	0.1	0.025	0.0125	0.0125	0.0125

eliminate thermally induced motions of the secondary tower, but it is not designed to control vibration-induced motions. Thus for thermally induced motion, the primary-secondary positioning is controlled, independent of temperature. For vibration-induced motion, the vibrations must induce motions smaller than those given in Table 2-2.

Table 2-2 shows the allowed motion of secondary mirror relative to primary mirror. The "***dL***" line gives the motion consistent with a laser metrology truss with 27-nm rms measurement precision, while the "Frequency ***dF/F***" line indicates motion consistent with 1×10^{-9} relative frequency changes. "Fast changes" are not measured by the metrology system—these must be limited by proper design of vibration isolation and damping systems.

All other optics in the system up to the Lyot stop are required to be stable in position to 100 nm and 10 nrad 3σ rms. As with the secondary mirror, this is required to limit beam walk. The positional stability requirement also limits beam walk contributions.

Table 2-2. Motions of Secondary Resulting From Random Metrology Errors and Vibrations

Mirror	x-tilt (nR)	y-tilt (nR)	z-tilt (nR)	x-trans (nm)	y-trans (nm)	z-trans (nm)
Secondary (***dL***)	45	30	130	65	137	27
Secondary (Frequency ***dF/F***)	0	0.2	0	2	4	12
Secondary (Fast Changes)	2	1	5	2	5	1

There are two other critical terms in the dynamics error budget. They are rigid-body pointing and beam centration on the mask. Rigid-body pointing introduces beam walk but does not cause significant aberration because the telescope is well corrected over small pointing errors (a few mas). The required rigid-body pointing stability is 4 mas rms for high-resolution (8-m) axis. The rotation stability about the line of sight (about the z-axis) is on the order of arcminutes. Beam centration on the mask is much more stringent since it leads directly to leakage around the mask. The centration offset from the ideal on-axis point is required to be <0.3 mas rms. This is achieved with a steering mirror located near the deformable mirror.

The reserve factors on image motion and shape, laser metrology performance, spot centration on the coronagraph mask, and rigid body pointing are set to 2. For a given allocation of dynamic errors and a given contrast stability, the reserve factors increase as the IWA is pushed outward. In other words, the design has less margin for operation at 4 λ/D than 5 λ/D.

The reserve factors are equal to the product of performance margin, model uncertainty factors (e.g. missing or wrong physics) and model errors (e.g., incorrect damping factors). The uncertainty factors apply to the wavefront and/or motion or pointing requirements. Their effect on contrast contributes as the square or fourth power of the given value.

2.2 Throughput (Sensitivity) Budget

This section serves as a placeholder for the throughput (sensitivity) budget. This section will be added in the next yearly update to the plan scheduled for March 2006.

3 Optics and Starlight Suppression Technology

As a program matures, technology groupings grow to increasingly higher levels of integration. What began as individually identifiable component technologies naturally lead to subsystems and testbeds that are used to validate them. The development of TPF-C critical technologies can be understood in this framework. The bulk of the technology development effort has taken place at JPL. Unless otherwise noted, the component technologies and testbeds described below are JPL products.

3.1 Component Technologies

3.1.1 Apodizing Masks and Stops

Objective

The TPF coronagraph must suppress on-axis starlight, while passing light from off-axis planets that are many orders of magnitude dimmer. In order to meet the required contrast over the full bandwidth, the masks must be fabricated with extremely high optical density and controlled diffraction characteristics. This activity is aimed at developing the technology necessary to produce and test several types of high precision masks.

Approach

Several candidate technologies are being explored to demonstrate the feasibility of manufacturing various kinds of masks that would achieve the end goals for star light suppression. The two basic classes of masks are focal plane and pupil plane, as described previously in Section 1.6.3.

Focal plane masks: Apodizing occulting masks to be placed at a focal plane require a very high dynamic range in optical density (OD from 0 to 8) and smooth variations within that range. Such masks are very difficult to both make and measure, and are not used in existing applications. There are two fundamental approaches to designing such masks: analog (i.e., gray scale) and binary (opaque and transparent). Several manufacturing techniques will be examined for each approach. JPL is leading the effort in developing the technology for occulting masks in association with industry resources for materials development, fabrication and characterization.

Final performance of the masks will be evaluated in the HCIT at JPL. This activity will demonstrate that hardware can be manufactured to meet optical requirements of the coronagraph in space environment.

Pupil plane masks: A second approach for coronagraphy is to employ masks at a pupil plane that apodize the pupil so as to suppress and diffract away unwanted star light, thereby providing the required contrast between star and planet lights at the image. Several theoretical designs have been proposed for such masks with varying through-put efficiencies and system complexities, primarily at universities under JPL subcontract. Experimental demonstrations are aimed at discriminating between technologies to allow selection of those with the best system performance. To support and complement experimental work, teams at JPL (Hoppe et al.), Princeton (Kasdin et al.), UC Berkeley (Neureuther et al.), Ball Aerospace (Lieber et al.), and GSFC (Lyon) focus on incorporation of experimental results into the optical system model and validation of those models. The goal is to develop an understanding of the limits of the scalar diffraction theory for this application and determine whether any design modifications are necessary to achieve the desired coronagraph performance.

Progress to Date

Focal plane gray scale masks: Significant progress has been made in the past year in fabricating and testing focal plane masks at JPL. The first approach uses HEBS glass manufactured by Canyon Materials, Inc., San Diego, CA, and further modified for JPL to meet TPF-C requirements. HEBS glass will darken to different levels of absorption of visible light when exposed to different electron beam levels. This makes it possible to create controlled optical density profiles in the glass with each mask design. Masks with linear 1-sinc^2 patterns have been written in such glass with a state-of-the-art electron beam exposure system at the Micro Devices Laboratory (MDL) at JPL. Tests with such masks during the past year in the HCIT have shown average contrast of 0.9×10^{-9} in the dark field with 784 nm laser light[1] and more recently in the 5×10^{-9} level with about 40 nm bandwidth around 785 nm. Figure 3-1 shows a mask and a picture showing the dark region in the image plane when such a mask is employed. Further experiments

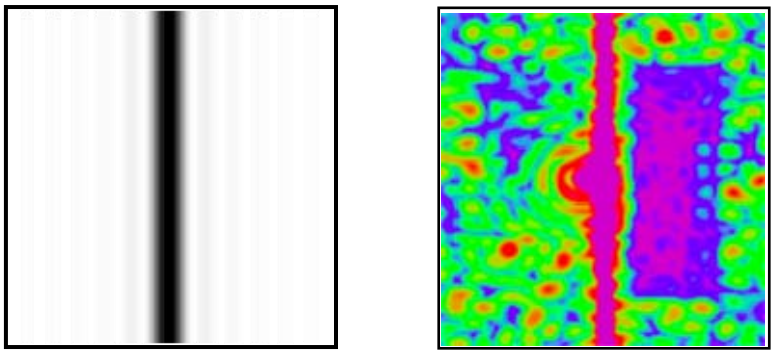

Figure 3-1. Mask (left) and image (right). The mask is included in the optical train of the HCIT where the corresponding image is recorded.

[1] Trauger et al., "Coronagraph contrast demonstrations with the High Contrast Imaging Testbed," *Proc. SPIE* V.5487, i.3, pp. 1330–36 (2004)

are in progress with continuous improvements in the mask material, fabrication progress, algorithms, and testbed optics. Initial radiation tests show minimal HEBS mask performance degradation for the expected environmental exposure over mission lifetime.

In addition to the HCIT implemented for evaluating mask performance and perfecting methodologies for star light suppression, an interferometer system has been developed at JPL to characterize HEBS mask material. This system, shown in Figure 3-2 incorporates 830, 785, 635, and 532 nm wavelength laser sources and a cooled CCD camera to capture interference fringe images. Algorithms have been developed to extract phase retardation/advance from such fringes from the various regions of different optical densities in the HEBS mask. This information is fed into models to validate experimental results. Reduction of error bars in measurement is an ongoing activity. Additionally, precision spectrophotometry and spectroscopic ellipsometry are employed to measure optical density and optical constants of the material as a function of wavelength.

More recently Kuchner, Crepp, and Ge[2] have proposed replacement of the linear sinc^2 mask with an eighth order mask which is predicted to yield better tolerance to pointing instabilities and low order aberrations[3].

Focal plane binary masks: Focal plane masks of opaque and transparent regions lithographically formed on a metal film on glass are predicted to perform similar to the gray scale masks described above. Patterns of 1-sinc^2, continuous sin^2, and discontinuous sin^2 have

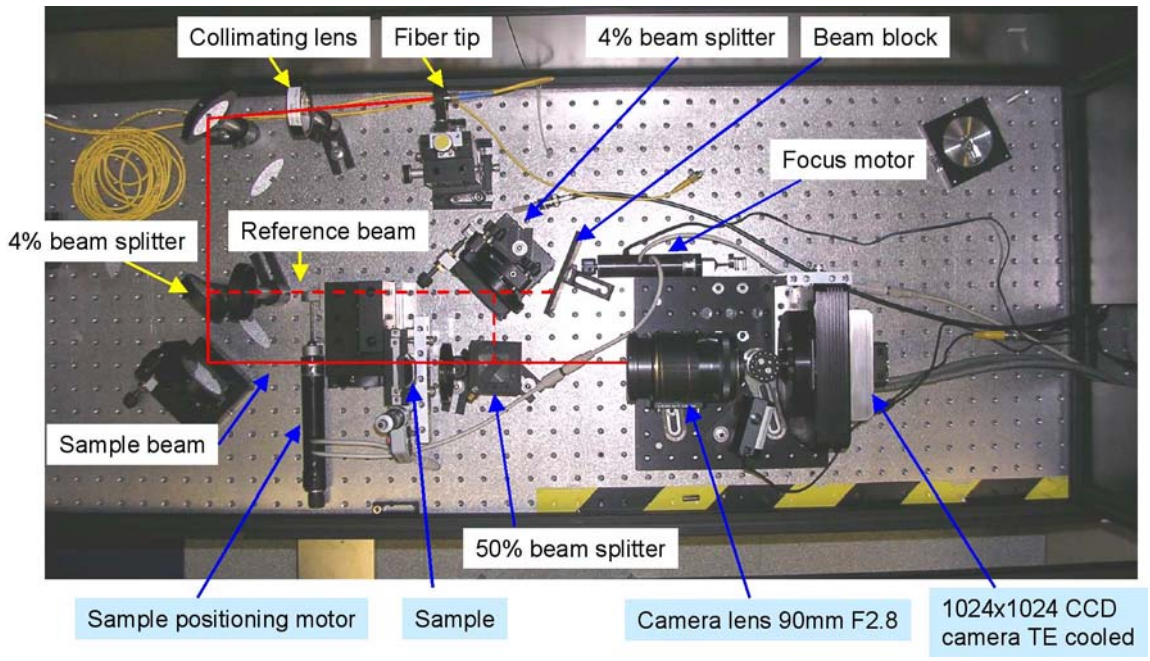

Figure 3-2. Interferometric characterization of mask phase retardance.

[2] M.J. Kuchner, J. Crepp, and J. Ge, "Eighth-Order Image Masks for Terrestrial Planet Finding," *Ap.J.* 628, pp. 466–73 (2005).

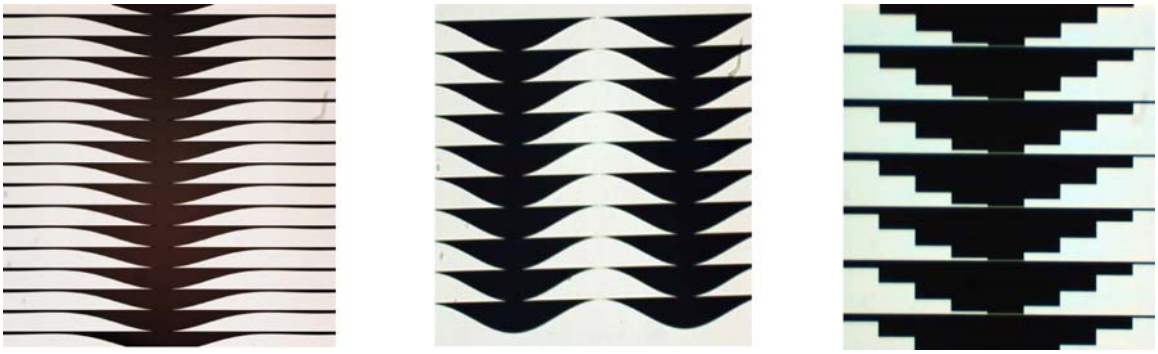

Figure 3-3. Binary 1-sinc^2 mask (left) produced by e-beam lithography of aluminium on glass for f/28.55 and a wavelength 785 nm, binary continuous sin^2 mask pattern (middle), and binary discontinuous sin^2 mask pattern (right).

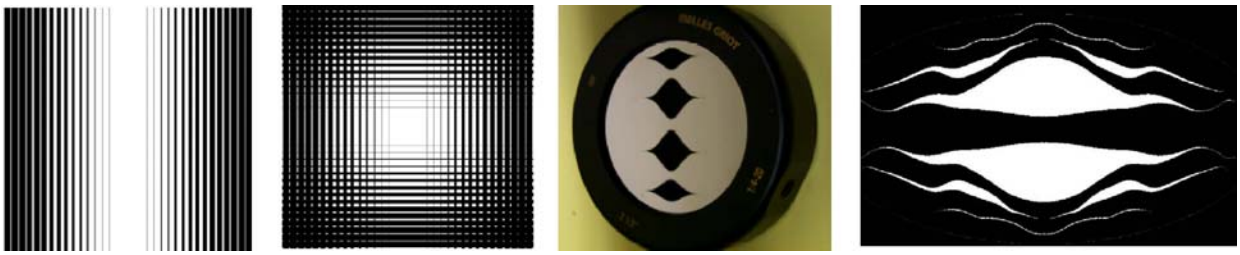

Figure 3-4. Bar code masks and shaped elliptical masks. From left to right: 1-D bar code mask; 2-D bar code mask; four-aperture mask elliptical mask; multi-aperture elliptical mask.

been designed and fabricated at JPL. Figure 3-3 shows optical microscope images of such patterns in a mask that is currently under test in the HCIT for direct comparison with the HEBS mask.

Pupil plane masks: Pupil masks of various designs are being studied theoretically and experimentally, primarily at Princeton University by a group headed by Professor Jeremy Kasdin under JPL subcontract. A parallel effort is also underway for accurate vector diffraction modeling of the system by a group headed by Professor Andy Neureuther at UC Berkeley[4] and in association with Ball Aerospace. Figure 3-5 shows the modeling approach used at Ball Aerospace to integrate numerical results into an end-to-end performance prediction model. Several mask designs are being explored and reported[5,6]. A few examples of such pupil plane masks are shown in Figure 3-4.

---

[3] Shaklan S.B. and Green J.J., "Low order Aberration Sensitivity of Eighth-Order Coronagraph Masks," *Ap.J.* 628, pp. 474–77 (2005).

[4] D. Ceperley et al., "Vector Scattering Analysis of TPF Coronagraph Pupil Masks," *Proc. SPIE* 5526B pp. 228-239, SPIE Denver Annual Meeting, 2004.

[5] Kasdin, N.J., R. J. Vanderbei, M.G. Littman, M. Carr, and D.N. Spergel, "The Shaped Pupil Coronagraph for Planet Finding Coronagraphy: optimization, sensitivity, and laboratory testing," in

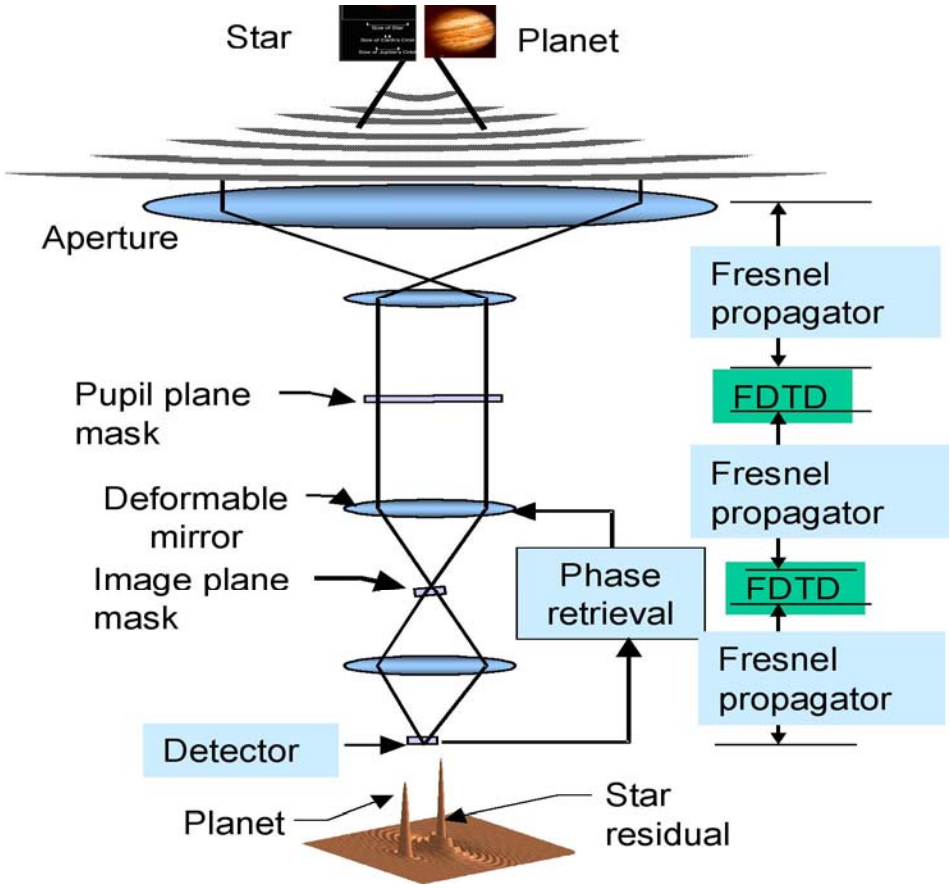

Figure 3-5. Coronagraph system model with pupil plane and focal plane masks.

Initial experiments at Princeton have yielded contrast in the 10^{-7} scale at 632.8 nm in their lab. Further experiments with improved masks and testbed optics are expected to provide pathways to reach the final goals. Some of these masks will also be fabricated at JPL with precision e-beam lithography and tested in the HCIT at JPL.

Silicon based masks: To take advantage of the advanced and mature technology of silicon processing and deep etching, masks based on silicon are also being considered as candidates for development.

Proceedings of SPIE conference on Astronomical Telescopes and Instrumentation, 5487(63) pp.1312-1321, 2004.

[6] Vanderbei, R. J., Kasdin, N. J., Spergel, D. N., "Rectangular-Mask Coronagraphs for High-Contrast Imaging", *The Astrophysical Journal*, Vol. 615 pp. 555-561, November 1, 2004.

3.1.2 Technology Demonstration Mirror

Objective

The TDM is a 1.8-m mirror that will demonstrate mirror technology required for the primary mirror (PM). The static error budget for the entire system requires sub-nm wavefront quality, and the dynamic error budget is two orders of magnitude more stringent for TPF-C. For both static and dynamic errors the PM is expected to be the largest error contributor. Errors on the primary mirror must be within the capture range for the wavefront sensing and control system. Control of the deformable mirror is then relied upon to reduce the WFE to the required sub-nm level. The technology necessary to control these errors for the large TPF-C can be demonstrated on a 1.8m sub-scale mirror if it is a light-weighted, off-axis optic like the PM. For both the TDM and TPF-C static errors will be driven by the structural design, figuring and polishing techniques, coating process, and the sensitivity of the metrology to these errors. Dynamic errors like the static errors are driven primarily by the structural design but also by material characteristics and fabrication processes. Timing of the TDM is very important so that technology risks are reduced before the fabrication of the TPF-C PM. Due to the long lead time for fabrication of the PM, it must be procured early in the formulation phase if TPF-C is to meet its launch readiness date. TPF-C performance requires that mirror technology sufficient to achieve the required levels, as outlined in Table 3-1, is demonstrated early in the program.

Table 3-1. TDM Performance Requirements

Parameter	Range	Requirement	Goal
SURFACE ERROR REQUIREMENTS			
Low Spatial Frequency (LSF)	<0.025 cycles/cm	10 nm rms	5 nm rms
Mid Spatial Frequency (MSF)	0.025 – 0.5 cycles/cm	5 nm rms	2.5 nm rms
High Spatial Frequency (HSF)	0.5-10 cycles/cm	1.4 nm rms	0.7 nm rms
Micro-roughness	>10 cycles/cm	10 Å rms	5 Å rms
COATING RESIDUAL REFLECTANCE REQUIREMENTS			
Mid Spatial Frequency	0.025–0.5 cycles/cm	<0.3% rms	≤0.1% rms

Approach

TDM requirements were based on coronagraph mirror requirements that emerged from the TPF Architecture Studies by Ball Aerospace and Boeing-SVS as presented at the December 2001 Final Architecture Review (http://planetquest.jpl.nasa.gov/TPF/arc_index.cfm). Their study showed that the addition of a DM for wavefront correction would relax the PM surface error requirements from an unheard of ~100 pm rms to a challenging but achievable level.

When evaluating the state-of-the-art, it must be remembered that TPF-C requires a large, light-weight, off-axis primary mirror. The PSD of surface errors for several state-of-the-art, large

(though not light-weight or off-axis) optics are compared in Figure 3-6 and fitted with a third order function given by

$$PSD(k) = \frac{A}{1+\left(\frac{k}{k_0}\right)^3}, \text{ where } k = \sqrt{(k_x)^2 + (k_y)^2}, \quad A \approx 6\times10^5 \text{ Å}^2\text{cm}^2, \text{ and } \quad k_0 = 0.025\text{cycles/cm}.$$

The TDM is to be manufactured with a PSD amplitude a factor of 2.5 below the fitted curve. For the TDM, $k_0 = 0.04$cycles/cm and $A \approx 2.4\times10^5 \text{ Å}^2\text{cm}^2$ are required with a goal of $A \approx 6\times10^4 \text{ Å}^2 cm^2$. The performance requirements vary with spatial frequency as summarized in Table 3-1. Manufacturing process development for the TDM will address materials effects, structural integrity, thermal impacts, and measurement and test methods; coating process development will address spatial reflective uniformity and experimental determination of coating performance. Going through the process of fabricating and testing the TDM will provide insight into achievable performance for the TPF-C PM and SM.

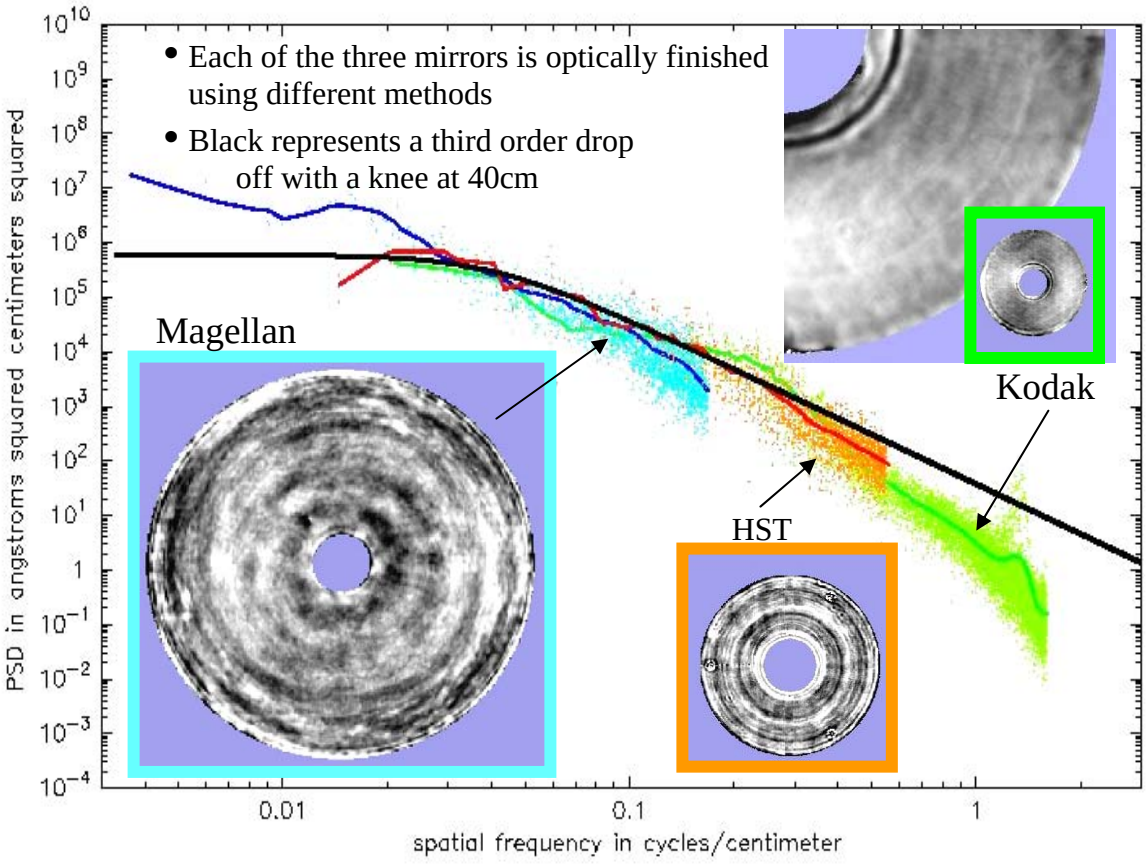

Figure 3-6. Power spectral density for three mirrors: Magellan (left) 6.5 m and made at the University of Arizona Mirror Laboratory for ground-based astronomy, HST (middle), and a 1.5-m development optic made at Kodak (right). PSD for the TDM is 2.5 times lower.

Table 3-2. ITT Design Parameters

Parameter	Description
Material/construction	ULE/LTF/LTS
Finished plate OD: back plate	1900 mm
Finished plate OD: front plate	1875 mm
Core OD (plano blank)	1880 mm
Core depth	114.3 mm
Core cell geometry (hex, flat-flat)	127.3 mm
Initial plate thickness	12.7 mm
Front-plate final thickness	9.3 mm
Back-plate final thickness	5.1 mm
Core strut thickness: Interior	1.4 mm
Core strut thickness: Edge walls	1.9 mm
Core strut thickness: Mount	2.8 mm
Best fit ROC	7837.3 mm
Mount pad location	665 mm
Midspatial gravity quilting	3.6 nm-rms
Number of cells	273

Progress to Date

The TDM effort started with a three-month design effort by four large mirror companies, Brashear, Goodrich, ITT, and SSG. A careful review of the proposed designs led to award of the contract for the fabrication of the TDM to ITT.[7] ITT proposed a closed back, ULE mirror that will be slumped to near net shape, polished with a full tool active lap, and ion beam figured. A drawing of the ITT mirror and mounting struts with the core structure exposed is shown in Figure 3-7. The important design parameters for the ITT mirror are given in Table 3-2.

Currently ITT is completing the design of the mirror, bipod supports, strongback, and handling equipment. Six boules of ULE have been produced and their coefficient of thermal expansion (CTE) uniformity has been measured. The ULE for the cores has been surfaced in preparation for water-jetting the core cells. The boules for the faceplates have been flowed out from the standard 1.5-m size to 2 m. The CTE properties are critical if the TDM is to meet the stability requirements. Based on the thermal requirements, ITT derived CTE requirements that Corning, the manufacturer of ULE, must meet. Most critical is the weighted average of the mirror's CTE which must be between −10 and +10 ppb/ºC. It is also critical that the CTE for the same location on the front and back face sheet differ by no more than 5 ppb/ºC. The first critical specification

[7] Cohen and Hull, "Selection of Mirror Technology for the 1.8m Terrestrial Planet Finder Demonstration Mission," SPIE, Optical Fabrication, Metrology, and Material Advancements for Telescopes proceedings Eds. Eli Atad-Ettedgui and Philippe Dierickx, Volume 5494, pp. 350-365.

Table 3-3. ITT Metrology Error Budget compared to TDM Requirements and Goals

Spatial Frequency	ITT Estimated Errors (nm rms)	TDM Requirement (nm rms)	TDM Goal (nm rms)
Low Spatial Frequency (LSF)	2.8	10	5
Mid Spatial Frequency (MSF)	1.6	4.8	2.4
High Spatial Frequency (HSF)	0.03	1.4	0.7
Micro-roughness	0.2	1	0.5

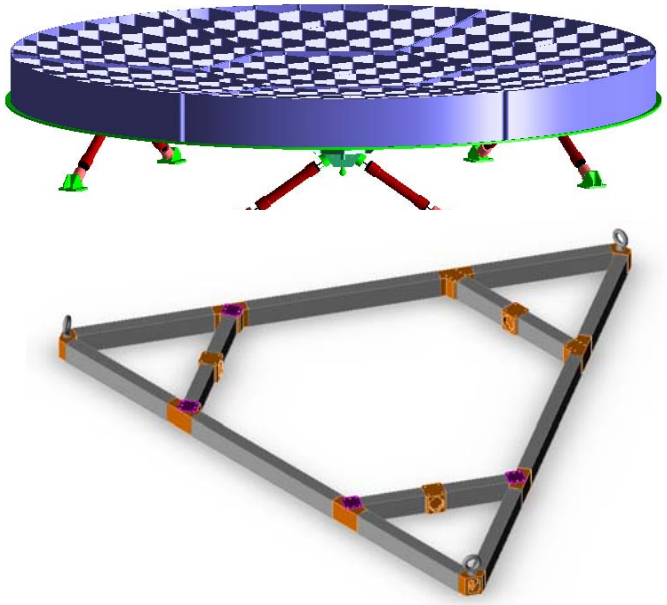

Figure 3-7. ITT's TDM concept with the core structure exposed. Also shown is the strongback on which the mirror will be mounted.

should easily be met since Corning's measurements show that the volumetric average CTE for each boule varies from −3 to +2 ppb/ºC. Radial CTE measurements for each plate will be completed in late winter of 2005.

ITT will use a center of curvature test with a 2-element Offner null lens, to be calibrated using computer generated holography (CGH), for the low and mid-spatial frequency measurements and a Chapman MP 2100 line scan profilometer for the high spatial frequencies and micro-roughness measurements. All hardware for these tests is on order, and the CGH calibration concept has been demonstrated. ITT's metrology error budgets are compared to the TDM requirement and goal in Table 3-3. All hardware for these tests is on order or has been received. In particular, the MP 2100 was received in late December '04. Calibrating the Offner with a CGH is a technique that has been used before at ITT. This calibration technique has been developed by Jim Burge of the University of Arizona (U of A) and the TDM CGH work is a joint effort of ITT and U of A. Demonstration CGHs have been built and tested and have demonstrated that the ITT CGH related errors are realistic.

3.1.3 Wavefront Sensing and Control

Objective

Imperfections in the optical surfaces and coatings create starlight speckles over the field of view. To enable the planet detection and characterization objectives of TPF, these speckles must be sensed and controlled to the 10^{-10} level as compared to the brightness of the parent star. For the planet detection objective, this speckle suppression must be achieved over the entire controllable field of view as defined by the actuator geometry of the deformable mirrors, and this suppression must be achieved over an optical bandwidth of up to 25%. For planet characterization, the speckle suppression need only be achieved over a smaller range of field angles about the planet but maintain a suppression that enables the planet spectral reflectivity to be measured over a substantial portion of the overall TPF sensitivity range.

Approach

Deformable mirrors are an integral part of the speckle control methodology. The density and geometry of the DM actuators define the ultimate extent and shape of the "dark hole" where the speckles are suppressed and planets can be detected and characterized. The resolution at which the actuators are controllable (and remain stable) together with the actuator density define the ultimate suppression level that can be achieved. In fact there is an inverse relationship to the actuator density and actuation resolution that can be traded-off to specify the level of achievable speckle suppression. A higher density of actuator reduces the level of actuator command resolution required and reduces the surface figure requirements of the optical elements in the telescope.

The optimal arrangement of multiple DMs is a major consideration for wavefront control system architecture. A single DM at pupil (such as on the High Contrast Imaging Testbed) is capable of controlling conventional phase errors over the entire controllable field of view, however amplitude errors are only controllable over half the FOV. More complex schemes that involve interferometric[8,9] or multi-conjugate DM arrangements are currently being evaluated for their ability to enable full control speckles over the entire FOV in the presence of broadband illumination. Having a full-field discovery space is vital for the overall survey completeness required for TPF-C.

In addition to the deformable mirror technologies described previously, wavefront sensing and control algorithm development is key to achieving the required contrast. The primary function of wavefront sensing on TPF-C is to establish optimal settings for the DM surfaces such that the intensity level of the stellar speckles is reduced to the 10^{-10} contrast level over a suitable field of view and optical bandwidth. This process of determining beneficial updates to the optical degrees of freedom must take place in short time spans as compared to the stability of the system, and in general it must enable a substantial portion of the operation time for science

[8] M. G. Littman, M. Carr, J. Leighton, E. Burke, D. N. Spergel, and N. J. Kasdin, "Phase and Amplitude Control Ability using Spatial Light Modulators and Zero Path Length Difference Michelson Interferometer," *Proc. SPIE Int. Soc. Opt. Eng.* 4854, 405 (2003).

[9] C. W. Bowers, B. E. Woodgate, and R. G. Lyon, "Novel method of high-accuracy wavefront-phase and amplitude correction for coronagraphy." *Proc. SPIE Int. Soc. Opt. Eng.* 5170, 292 (2003).

observations. The time it takes to sense and null the speckles must take no longer than the time it takes to detect a planet.

Typically a sequence of images is taken with a camera to observe residual light from the on-axis source in the presence of a known induced diversity. For example, on HCIT the DM actuators are moved in a predetermined way while a series of images is collected at either the post-coronagraph pupil[10] or post-coronagraph focal plane.[11] Other approaches have considered using phase-retrieval using imagery collected about the occulter focal plane,[12,13] by inducing diversity through the optical element alignments or by the introduction of a coherent reference beam to conduct direct interferometry on the speckles.[14]

Ultimately the wavefront sensing schemes must be well matched to the wavefront control and coronagraph architectures in a way the enables efficient and reliable high contrast imaging.

Progress to Date

Experiments on the HCIT are in part the demonstration of a single-DM-based wavefront sensing and control architecture. Aside from having a single DM at a pupil, the HCIT employs a Lyot coronagraph that has a HEBS glass occulting spot. The camera at the final focal plane represents the science camera. Using a phase-retrieval approach at the HCIT occulter focus, it has been demonstrated that the testbed is stable to the l/10000 level.[13] Using a focal-plane speckle nulling approach[11] the residual light from the on-axis source has been suppressed to levels approaching 10^{-9} over a portion of the controllable field of view. See Section 3.2.1 for recent HCIT experimental results.

3.1.4 Deformable Mirrors

Objective

Unlike adaptive optics systems designed for correction of atmospheric seeing in ground based observatories, the active optical system for a space telescope needs only to correct for wavefront errors created in the telescope itself. The magnitude of wavefront errors is reduced to the magnitude of errors expected in a diffraction-limited optical system, and the bandwidth required to follow significant wavefront drift is reduced from kHz rates to the time scales associated with mechanical and thermal stability of spacecraft systems. The accuracy with which the wavefront can be corrected is fundamentally limited to the accuracy of wavefront error information that can

[10] S. B. Shaklan, D. Moody, and J. J. Green, "Residual wave front phase estimation in the reimaged Lyot plane for the Eclipse coronagraphic telescope," *Proc. SPIE Int. Soc. Opt. Eng.* 4860, 229 (2003).
[11] J. T. Trauger, C. Burrows, B. Gordon, J. J. Green, A. E. Lowman, D. Moody, A. F. Niessner, F. Shi, and D. Wilson, "Coronagraph contrast demonstrations with the high-contrast imaging testbed," Proc. *SPIE Int. Soc. Opt. Eng.* 5487, 1330 (2004).
[12] J. J. Green, D. C. Redding, S. B. Shaklan, and S. A. Basinger, "Extreme wave front sensing accuracy for the Eclipse coronagraphic space telescope," *Proc. SPIE Int. Soc. Opt. Eng.* 4860, 266 (2003).
[13] J. J. Green, S. A. Basinger, D. Cohen, A. F. Niessner, D. C. Redding, S. B. Shaklan, and J. T. Trauger, "Demonstration of extreme wavefront sensing performance on the TPF high-contrast imaging testbed," *Proc. SPIE Int. Soc. Opt. Eng.* 5170, 38 (2003)
[14] R. Angel, "Imaging Extrasolar Planet From the Ground," ASP Conference Series, Vol. 294, (2003).

be collected on time scales short compared to the stability of the optical system. The stability of a space environment provides the opportunity for extremely high-order wavefront correction.

Deformable mirrors are a critical component of speckle control methodologies for all wavefront control architectures under consideration. The deformable mirror must have sufficient control authority to correct the wavefront phase as commanded to ~1 Å accuracy. The objective is to develop DMs that are reliable and robust to support the TPF-C/High Contrast Imaging Testbed with the goal of demonstrating contrast performance of 1×10^{-10} or better at angular separations of 4 λ/D or greater from the central point source.

Approach

Two current technologies are viable for the DM; one is made by Xinetics, and the other is a MEMs device made by Boston Micromachines. The MEMs device capabilities are a lower TRL than Xinetics, as seen in Table 3-4. The Xinetics mirrors are being developed for use in the HCIT and they compose the bulk of this discussion.

Ongoing development at Xinetics will provide the next generation modular mirror technology, including refinements in material processing, larger module dimensions, larger actuator count per module, and more efficient and compact low-power actuator driver systems. The procured components from Xinetics will be integrated on the testbed in order to continue establishing a path of technology advancement for the TPF-C High Contrast Imaging Testbed.

The DMs are built up from 32 × 32 mm electroceramic blocks, each delineated with 1024 actuators arrayed on a 1-mm pitch. Single-module 1024-actuator mirrors, and a four-module assembly with 4096 actuators driving a single 64 × 64 mm mirror facesheet, as shown in Figure 3-8, are currently available for HCIT experiments. These are an outgrowth of seven years of development of modular PMN actuator technology at Xinetics Inc., a research effort initiated in 1997 within NASA's small business innovative research (SBIR) program. The DM actuators are driven by a multiplexed voltage supply with 100 volt range and 16-bit voltage resolution. A

Figure 3-8. Xinetics Deformable Mirrors, 32x32 and 64x64.

vacuum-compatible, low-power 64-channel multiplex switch ASIC has been developed at JPL to distribute the voltage settings while minimizing the number of control wires that must pass through the vacuum chamber wall.

The products to be developed are 32 × 32, 48 × 48, 64 × 64, and 96 × 96 deformable mirrors leading toward technical hardware that are reliable, large enough, and robust enough to support flight performance levels required by Sept. 2008. Module development and combinations will enable a best understanding of last path for flight hardware development.

In addition, Boston Micromachines is providing DMs for the GSFC Michaelson testbed, Princeton pupil plane testbed, and NOAO PIAA testbed with a similar architecture to the DMs required by HCIT. Boston Micromachines also provides the Visible Nuller (VN) with segmented DMs. The alternative approach and supplier represented by these MEMS DMs provide risk mitigation.

Progress to Date

Xinetics has delivered five 32 × 32 actuator DMs and two of four 64 × 64 actuator DMs. The 32 × 32 DMs have been used in HCIT to achieve suppression approaching 10^{-9} with speckle nulling. Work is currently progressing on the 48 × 48 DM 2,304 channel single module manufacturing pathfinders, including module development, actuator machining and delineation pathfinder, interconnect evolution pathfinders, and facesheet development.

Table 3-4. Deformable Mirror Specifications

Deformable Mirror Property	State of the Art - MEMS*	State of the Art - Xinetics	TPF-C Flight Baseline
Actuators across aperture	32 actuators/pupil	64 actuators/pupil	96 actuators/pupil
Actuator spacing	3.3 actuators/mm	1 actuator/mm	≥ 1 actuator/mm
Command resolution	~5 Å surface/step †	< 0.10 Å surface/step	< 0.05 Å surface/step
Actuator stroke	~20000 Å surface ‡	> 2000 Å surface	> 2000 Å surface
Actuator position stability	TBD	< 0.20 Å surface/hour (includes effects of 10-mK thermal stability)	< 0.02 Å surface/hour
Actuator thermal stability	TBD	~ 3.5% of stroke / K	TBD
Mirror surface quality at uncontrollable spatial scales	~10 nm surface §	< 10 Å surface	TBD

* Based on Boston MicroMachines Devices

† Command resolution is currently limited by the precision of the high voltage drivers with an average step size of ~10 nm/V; with custom 16-bit electronics, an average 0.3 Å/step is expected. Current devices on order are expected to achieve up to 12-13 bit resolution or 4.9-2.4 Å/step.

‡ Nominal actuator stroke is ~20,000 Å (2 μm), however usable stroke over full aperture is limited by unpowered, surface curvature to somewhat less than this.

§ Small area, periodic deviations at actuator frequencies (2x outer working angle frequency) in unpolished devices. Devices on order are being polished to reduce this level.

3.1.5 Transmissive Optics

Objective

The minimum mission design incorporated two features that make use of large (greater than 10-cm clear aperture) transmissive optics. The first is a polarizer assembly consisting of a polarizing beam splitter (PBS) and two additional cubes required to achieve the required extinction while compensating for the chromatic dispersion. The polarizer assembly serves to give two separate paths for two orthogonal polarizations, each with its own set of deformable mirrors and downstream optics. The second feature is a Michelson assembly, chosen over the Mach-Zehnder due to its compactness, which accommodates wavefront control via the two DMs in each path. The total path in the glass for each sub-system is on the order of 25 cm.

The objective of this effort is to identify and, if necessary, address materials issues involved in the fabrication of large transmissive optics to the required tolerances, such as the uniformity of the glass, stress birefringence, scatter and depolarization, and the chromatic variation of these.

Approach

The preferred approach to addressing this technology risk is to develop design options that bypass entirely or reduce the dependence on transmissive optics. Several trades are still open in the coronagraph design and may result in the elimination of the two separate polarization paths or modification of the interferometric configuration. There are two main options. The first one is to control polarization through special coatings on the mirrors along with design changes that will allow elimination of the second polarization beam path. The second one is the introduction of a non-interferometric DM arrangement, thus removing another large transmissive optic. Polarization control through mirror coating is an ongoing effort. Concepts for polarization-insensitive occulting masks are also being considered.

However, if it is decided that a configuration similar to that of the minimum design mission is needed, the technology development will be planned and initiated in Phase A.

Progress to Date

Progress to date has consisted solely of initial investigation into the state-of-the-art; detailed requirements have not yet been developed for transmissive optical elements.

Homogeneity

Published data for fused silica[15] show homogeneity values in the range of 0.5 ppm. These were assessed with blanks ~200 mm in diameter and ~50 mm thick. Wavefront error of less than ~0.007 waves rms is achievable with blank selection. Homogeneity is determined from the p-v net wavefront error upon transmission for any given blank. It therefore leaves unanswered the question of spatial distribution, which would need further study. For other optical glasses, the Schott glass catalog shows values of 1 ppm as achievable depending on the type of glass and

[15] J. L. Ladison et al., "Achieving low wavefront specifications for DUV lithography; impact of residual stress in HPFS® fused silica," *Proc. SPIE* **4346**, 1416-1423 (2001).

blank size. Westerhoff et al.[16] show a considerable improvement in homogeneity of FK5 glass, making 0.5 ppm values achievable. The specific glass type decided upon for the polarizer will need to be evaluated individually.

Stress birefringence
Typical values for optical glass show a birefringence level of not much less than 4 nm/cm after selection. These values are measured again through the entire length of a blank and give no information about spatial distribution. However, the Corning fused silica samples of Ladison et al.[15] were found to exhibit much smaller values, as little as 0.07 nm/cm with an average of 0.26 nm/cm over fifteen samples. Marker et al.[17] studied the effect of annealing on BK7, and were able to demonstrate a value as low as 0.52 nm/cm with very slow annealing (0.3 K/hr). This clearly shows that the relatively high published birefringence values for optical glass are subject to significant reduction, a conclusion hopefully applicable to the glass selected for the polarizing beamsplitters. The wavelength dependence of the stress-optic coefficient for fused silica has been studied by Priestley.[18] This variation is an inherent material property not subject to reduction, hence it will need to be modeled accurately. Birefringence may be manifested as a wavefront error but also as a polarization error, and the two are not necessarily correlated. The wavefront error may be correctable through a specially fabricated compensating plate, as has been demonstrated in the case of CaF_2 lenses.[19] This was shown to remove a low order (radial) wavefront error resulting in halving of the overall error.

Scatter
At 633 nm, internal scatter (transmission loss) in fused silica has been measured to be just over 10^{-5}/cm.[20] This is likely tolerable with appropriate stray light reduction design. The same study includes some depolarization information, but it is not easily comprehensible. This is primarily Rayleigh scatter. In optical glasses, bulk scatter can also be caused by bubbles. Special glass selection can substantially decrease the bubble content. Class "0" glass has less than 0.03 mm^2 of area per 100 cm^3 of glass occupied by bubbles greater than 50 μm (or ~0–5 individual bubbles). There are glass types within the LaK/SK group in the 0–1 bubble class.

3.1.6 Coatings

Objective

Coating performance of the TPF-C reflective optics can critically affect the achievement of the TPF-C goals (ability to detect and characterize terrestrial planets). Some general coating requirements that TPF-C shares with similar telescopes include high reflectance consistent with the overall throughput budget, operation over the required bandpass of 500–800 nm (goal 500–

[16] T. Westerhoff, K. Knapp, and E. Moersen: "Optical materials for microlithography applications," *SPIE Proc*. **3424**, 10-19 (1998).
[17] A. J. Marker, III, B. Wang, and R. Klimek: "Effect of residual stress in optical glass on the transmitted wavefront," *Proc. SPIE* **4102**, 211-218 (2000).
[18] R. Priestley: "Birefringence dispersion in fused silica for DUV lithography," *Proc. SPIE* **4346**, 1300-1305 (2001).
[19] J.E. Webb: "In search of the optimal objective for 157 nm," *Photonics Spectra*, pp. 94-98, Dec. 2003.
[20] S. Logunov and S. Kuchinsky: "Light scattering in CaF_2 and fused silica for DUV applications" presented at SPIE 2003.

1060 nm) and suitability for large area application on the primary and secondary mirrors. The objective of this task is to design a coating material and application process and verify through a combination of analysis and test that it will meet TPF-C requirements.

Approach

The coatings have several challenging requirements TPF-C must achieve but that are not normally placed on similar coatings for ground or space use. The system amplitude and phase uniformity must be very high, of order 10^{-4}, over the relevant spatial frequencies. This may be correctible to some degree with the deformable mirror downstream, but the overall uniformity requirements of each component will still be very high; this is not normally a consideration for instruments in which only the total, integrated reflectivity is important. System level polarization must be minimal, preferably small enough that we can dispense with large polarizing beam splitters that would be required to work with each polarization component independently. The thickness of the metallic coating is required to be uniform to within a few percent on each optic, including over the 8-m primary, in order to maintain the figure specifications. Each of these characteristics must be stable from coating application through observatory lifetime.

Particularly challenging are the coatings for the primary and secondary mirrors. For these the angle of incidence varies over the aperture from about 1 to 12 degrees, causing non-uniform phase and amplitude and small but significant polarization. Figure 3-9 illustrates these variations for a *single element* using a candidate, protected-Ag coating at 650 nm. The overall variation in phase (~0.006 λ) can be removed using a deformable mirror corrector, however this still leaves a residual error (due to the two polarization components) of about 5×10^{-4} λ. The form of this polarization error (a smooth, low order polynomial can represent the effective figure error) will reduce contrast most significantly near the inner working angle. For the multi-element TPF-C design, the total residual polarization will likely be larger than this single surface result; designs which produce compensation will be considered. Ongoing design work will determine the specific contrast sensitivity of such candidate coatings when applied throughout the entire TPF-C optical path. Using prescribed coating designs for specific mask and wavefront corrector

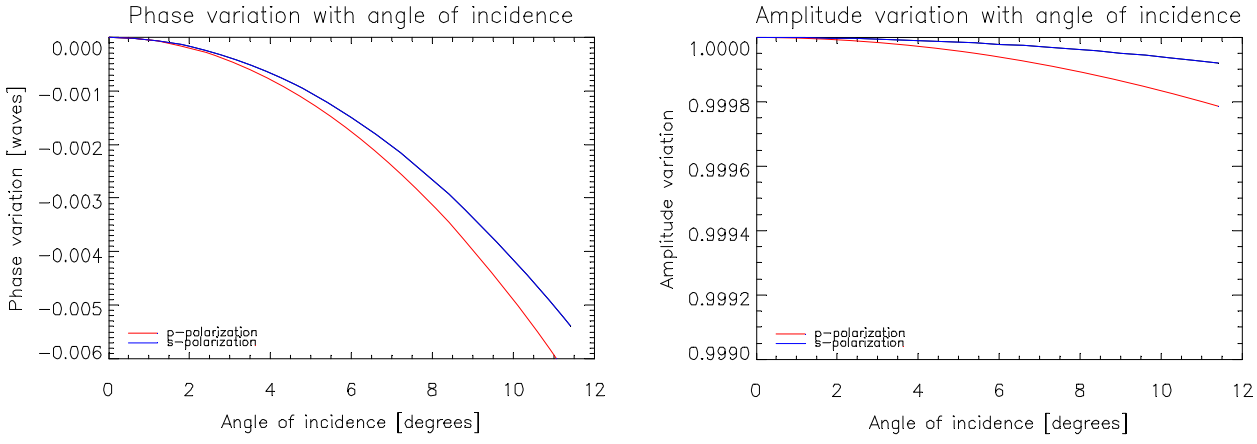

Figure 3-9. Variation of phase (left panel) and amplitude (right panel) with angle of incidence for a coating of Ag+SiO_2 (124 nm) at 650 nm for both s- and p-polarizations.

configurations, performance will be assessed for sensitivity to polarization and phase and amplitude uniformity. Each parameter must be analyzed over the nominal and goal bandpass and allowable performance degradation (contamination effects) budgeted to assure satisfactory performance over the observatory lifetime. For components other than the primary and secondary mirrors, the variations of angle of incidence are much reduced, so their performance will be more nearly constant over the aperture, but they must also be well controlled and stable at the particular angles of incidence used and over the full bandpass

This activity will develop the coating designs and determine the overall system contrast performance when they are incorporated. Small test samples of critical coating candidates will be obtained for evaluation and comparison to the predicted performance during pre-Phase A. One source is a Phase II SBIR by Surface Optics Corporation which will seek to produce uniform thickness (<2%), protected-Ag coatings over an aperture of about three meters. Witness samples can be positioned at various positions within the coating chamber to simulate coating performance of a larger optic. Measurements of such samples can be compared with the predicted variations of phase, amplitude, and polarization at various spatial frequencies to validate the coating design models. The results of this activity will provide a first look at the particular problems of protected-Ag coating large apertures along with the witness samples for measurement and comparison with TPF-C requirements. Currently measurements on these samples are planned from various facilities including: ellipsometry (from Woollam Co.), spectral reflectivity (GSFC), and high precision relative reflectometry (GSFC).

During pre-Phase A, the project will investigate the effects of various types of coating contamination, begin to define required cleanliness levels to prevent lifetime degradation of coatings, and initiate tests to determine coating stability of the most promising samples. During Phase A and B, the processes for producing such coatings, particularly on the large primary and secondary mirrors, will be developed, and measurement techniques beyond the use of surrogate witness samples will be investigated. The Technology Demonstration Mirror (TDM) will serve as a coating pathfinder for these large optics.

Progress to Date

Initial studies have focused on (1) improved understanding of the system polarization effects, (2) reflectivity and polarization analysis of various over-coated metals to identify potential candidate coatings, (3) initial sensitivity analysis of coatings in terms of system contrast, (4) preparing computational tools for full system coating and polarization analysis, and (5) initial ellipsometric testing of a sample coating currently used in the HCIT.

Initial analysis of candidate coatings for large optics included designs for protected-Ag , bare Au, and protected-Al. Bare Au has poor performance below 600 nm and so cannot be used over the nominal bandpass. Protected-Al has inferior polarization and lower reflectance than protected-Ag, which appears to be the best candidate coating. Protected-Ag coating of comparably large optics was achieved with the Gemini 8-m telescope mirrors during 2004. These coatings were successful, although the requirements, consisting of integrated reflectance and emissivity, are much less stringent than those for TPF-C.

A particular design for protected-Ag was developed by Balasubramanian. By adjusting the thickness of the protective overcoat, a coating can be designed that has no polarization at two

wavelengths in the bandpass and very low polarization elsewhere. Figure 3-10 shows the performance of this coating design and a similar design based on the original protected-Ag designs of Hass et al.[21] Sensitivity analysis of these low polarizing designs is underway to confirm that their use will allow TPF-C to achieve its required contrast level. Further work by Balasubramanian has also shown that modifications of these basic designs may allow for some polarization compensation, further improving the overall system performance. Integration of these designs with the capabilities of the DM based corrector is also underway to assure that the necessary bandpass for TPF-C and overall system performance can be achieved with such coatings.

3.1.7 Scatterometer

Objective

The scatterometer testbed provides laboratory testing for model validation of stray and scattered light effects. These effects must be better understood on TPF-C than on prior observatories if the desired contrast is to be achieved. The coronagraph contrast is degraded by diffraction effects, optical surface scatter (e.g., PSD modeling), contamination (particulate and hydrocarbon), and stray light multiple scattering off of baffles, stops, etc.

Stray and scattered light are not easily separable. One description attributes stray light to such elements as optical baffles and baffle design (specular effects, bidirectional reflectance distribution function modeling, etc.), while scattered light is composed of diffraction, non-specular, near- and wide-angle scatter, and contamination. All of these must be modeled and well understood to ensure the required contrast. This testbed provides checks on how the physics of these effects are handled in various engineering codes, judges impacts to the project, and informs the selection of a code for use during baffle design.

Approach

The scatterometer testbed at GSFC[22] will allow testing of precision laboratory optics against modeling codes. Capabilities within the testbed allow surface testing to levels comparable to the TDM tests across the relevant range of spatial frequencies and coupling of this metrology data to deep scattered light measurements. We will test the modeling of the physics of scatter from surface roughness and contamination. In the past, near-angle scatter measurements have been

[21] G. Hass, J.B. Heaney, H. Herzig, J.F. Osantowsky, and J.J. Triolo, "Reflectance and durability of AG mirrors coated with thin layers of Al203 plus reactively deposited silicon oxide," *Appl. Opt.* 14, 2639-2644 (1975) and G. Hass, J.B. Heaney, and J.J. Triolo, "Evaporated AG coated with double layers of Al203 and silicon oxide to produce surface films with low solar absorptivity and high thermal emissivity," *Opt. Comm.*8, 183-185 (1973).

[22] I. Kuznetsov, D. Content, R. Boucarut, and T. Madison, "Design, performance, and reliability of a high-angular-resolution wide-angular-range large-aperture fully-automated UV scatterometer," *Proc. SPIE Int. Soc. Opt. Eng.* **4485** p. 417-428 (2002).

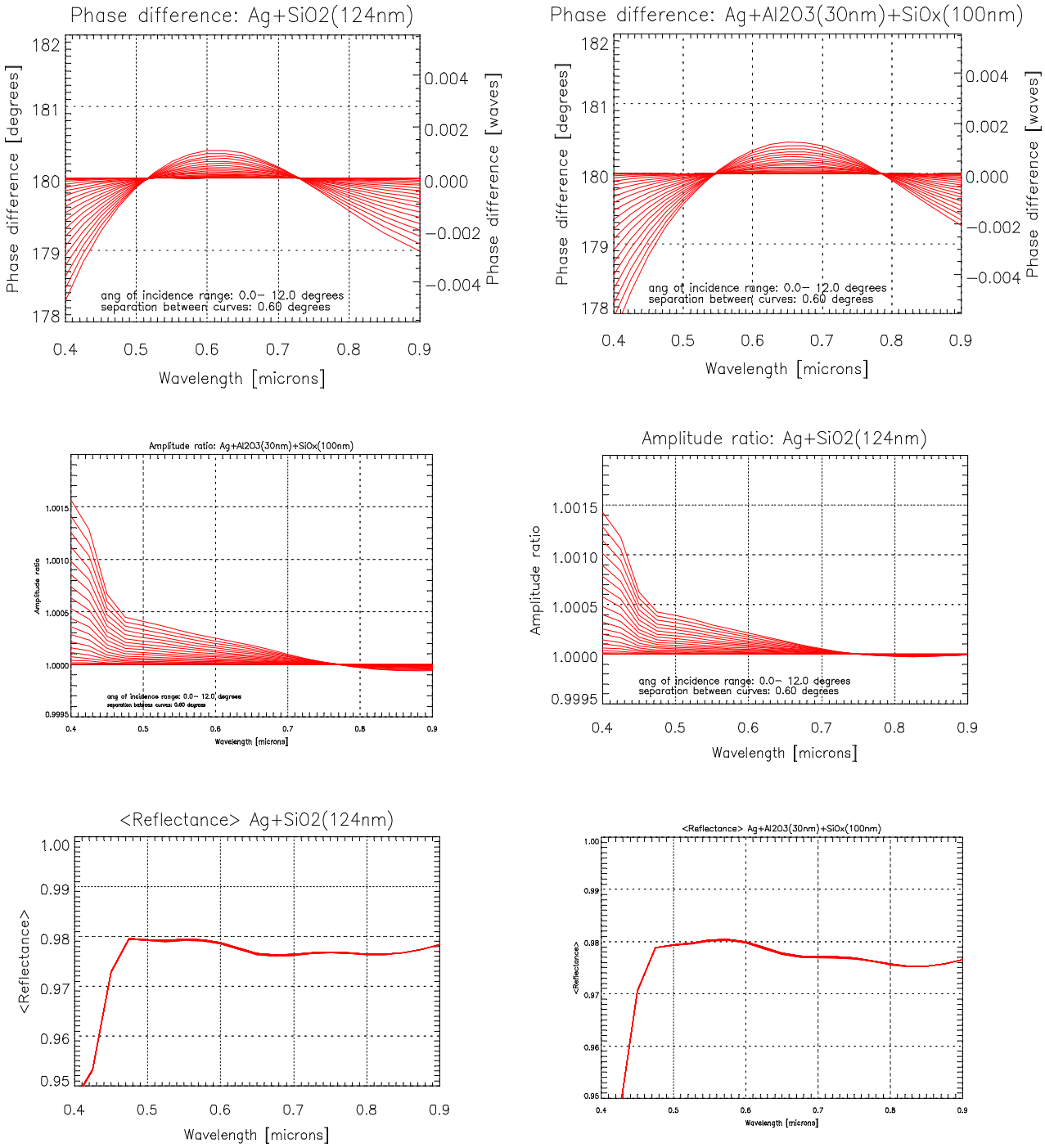

Figure 3-10: Plots showing the performance of two similar candidates for the primary and secondary telescope mirrors. The left panels show the phase difference, relative reflected amplitude and reflectivity for Ag+SiO_2 (124 nm) design by Balasubramanian et al. The right panels show similar performance by Bowers of the design of Hass et al. (1973) incorporating Ag+Al_2O_3 (30 nm)+SiOx (100 nm). Both designs have very similar performance with low polarization over the full bandpass and high reflectivity.

accurate to only ~<5% (HST[23], SUMER[24], FUSE[25]). This experiment will shed light on the state-of-the-art in scatter measurement and modeling and determine required improvements, potentially by orders of magnitude. We will set up a simple scatter test in the Diffraction Grating Evaluation Facility (DGEF)[26] chamber using TPF-C-like optics (a pair of known high quality off-axis parabolas of ~30–50 cm diameter) to measure near- and wide-angle scatter. We will compare laboratory data to model predictions from various codes including the Optical Surface Analysis Code (OSAC), Fred (Photon Engineering), Advanced Systems Analysis Program (ASAP), TracePro (Lambda Research), and Optical Systems Characterization and Analysis Research (OSCAR).

Progress to Date

Initial work will compare measurements and models of diffraction and near angle scattered light. A pair of known high quality off-axis parabolas at ~30 cm aperture size has been identified. Surface comparison against prior data is being made to ensure that the archival surface data is still representative. The existing scatterometer hardware based on ~15 cm optics will be reused for these larger optics. A 6 × 3.5 m vibration-isolated optical bench in a cleanroom is to be used for stability and to limit air scattering from dust. Initial work will use rectangular or square baffles at 45° to minimize diffraction. These baffles will be replaced with apodized masks in future upgrades.

In the longer term the facility will be used to measure near and far angle scattering from baffle materials to increase precision in the models for baffles, light traps, etc. This will allow more detailed comparisons of stray light models with measured data.

3.1.8 Small Precision Optics

Objective

The TPF-C baseline design has several small optics of size 10–20 cm, including flats, off-axis parabolas, and cylindrical mirrors. The surface flatness of these optics directly impacts the structural stiffness, thermal deformation, and rigid body pointing requirements related to beamwalk (lateral shear of the optical beam across imperfect optics). The stiffness, thermal, and rigid-body pointing requirements can be relaxed by employing high quality small optics between the secondary mirror and the fine-guiding mirror inside the coronagraph.

---

[23] P. Glenn, "Space Telescope performance prediction using the OSAC code," *Proc. SPIE Int. Soc. Opt. Eng.* **571** pp 164- (1985).

[24] T. T. Saha, D. B. Leviton, P. Glenn, "Performance of Ion-figured SiC SUMER Telescope Mirror in VUV," *Applied Optics*, **35**, 1742 (1996).

[25] R. G. Ohl, T. T. Saha, S. D. Friedman, R. H. Barkhouser, H. W. Moos, "Imaging Performance of Telescope Mirrors for Far-Ultraviolet Astronomy," *Applied Optics* **39** pp. 4513-4523 (2000).

[26] R. Boucarut, F. Bush, D. Content, D. Leviton, T. Madison, L. Miner, et al., "Ultraviolet-Optical Instrument development in the Diffraction Grating Evaluation Facility," in "UV-Optical Astronomy beyond HST," *Astron. Soc. Pacific Conference Series* **164** pp. 446-452 (1999).

The wavefront quality of the occulting mask substrate must also be considered. Mask errors drive the requirement for spot centration. Mask substrate errors also impact the static error budget because the errors can be compensated by the DM for only a single spectral wavelength.

Approach

The small optics are reflective and coated with protected silver. The contribution of the coating to the surface quality must be considered. The incident angle on most of these optics is near normal incidence, thereby minimizing coating effects. Two folding flats are at 45 degrees, but will pair-wise cancel each other's polarization effects. To meet the beamwalk requirements, the surface flatness of these optics must be <1 nm rms over 3 to 5 cycles/clear aperture (2–7 cycles/cm). These specifications can be met by the state of the art used in manufacturing optics for lithography.

The occulting mask must be superpolished and rest on or in a homogeneous substrate. At the occulting mask, the f/60 beam is 1 mm in diameter and has a depth of focus of 1.8 mm. The substrate for the mask should be thinner than the depth of focus. The required wavefront quality is 0.40 Å rms at a 30-μm spatial scale.

Progress to Date

Superpolishes have achieved a surface roughness of 0.5 Å rms over 1-μm scales by using 50-layer ion beam-sputtered coatings, as seen in Figure 3-11.[27] These superpolishes need to be evaluated on spatial scales of 30 μm.

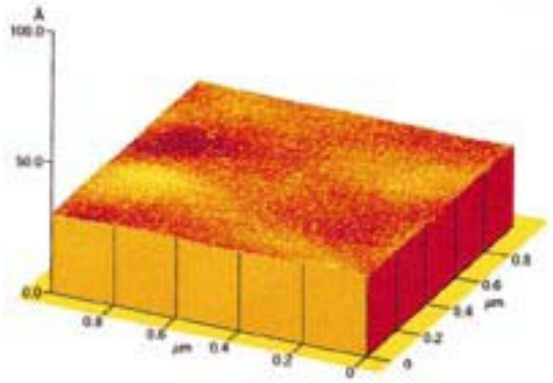

Figure 3-11. Superpolish using a 50-layer ion beam-sputtered coating achieving 0.5 Å rms surface roughness.

EUV lithography is driving the precision of small reflective optics to 0.25 nm rms over spatial frequencies of 1 cycle/clear aperture to 10 cycles/cm.[28] A four element system has been assembled that achieved 1-nm rms wavefront quality.[29]

[27] Charles Langhorn and Arthur Howe, "Optical Morphology: Just How Smooth Is That Surface?" June 1998 *Photonics Spectra*.

While the TPF requirements are challenging, they are either within the state-of-the-art or a factor of a few beyond the state-of-the-art.

3.2 Subsystem and System Testbeds

The subsystem and system level testbeds are intended to validate, at higher levels of integration, the contrast error budget for TPF-C.

3.2.1 High Contrast Imaging Testbed (HCIT)

Objective

The High Contrast Imaging Testbed (HCIT) is an adaptable testbed located at JPL, established to validate the high-contrast coronagraphic technology fundamental to direct detection of extrasolar planets from a spaceborne observatory. The optical layout of HCIT is shown in Figure 3-12 and

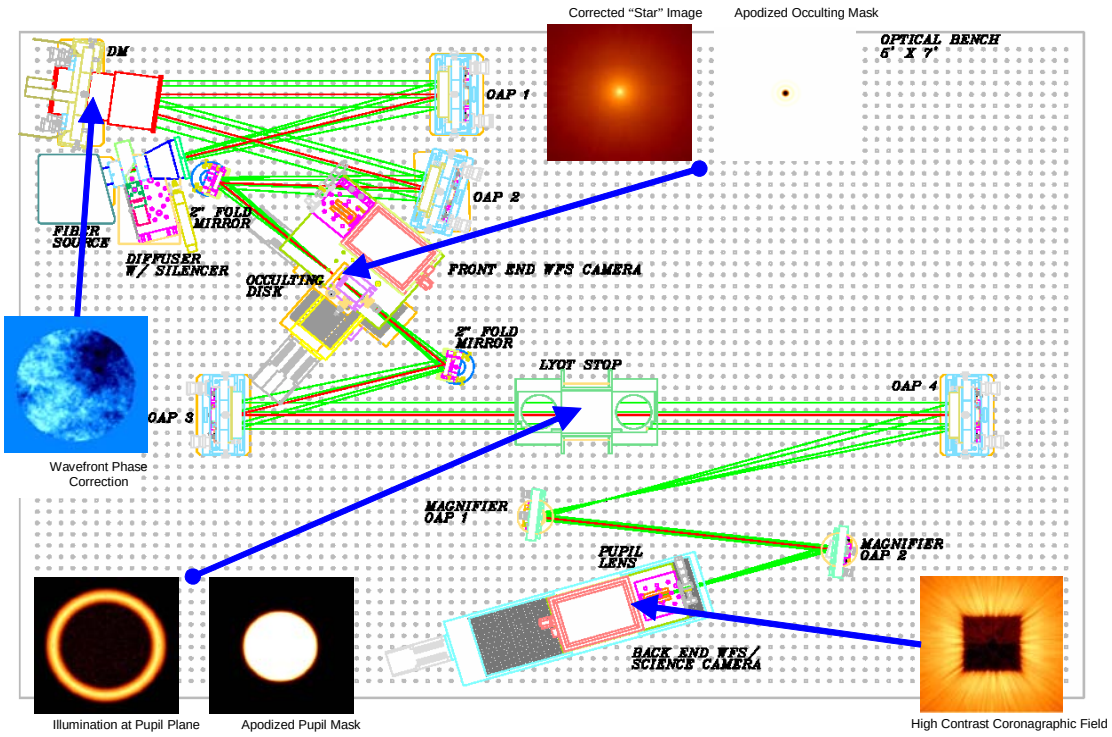

Figure 3-12. Layout of the HCIT with insets of focal and pupil planes.

---

[28] John S. Taylor, Gary E. Sommargren, Donald W. Sweeney, and Russell M. Hudyma, "The Fabrication and Testing of Optics for EUV Projection Lithography," Proceedings of SPIE -- Volume 3331 Emerging Lithographic Technologies II, Yuli Vladimirsky, Editor, June 1998, pp. 580-590

[29] Kenneth A. Goldberg, Patrick Naulleau, Phillip Batson, Paul Denham, and Erik H. Anderson, Henry Chapman, Jeffrey Bokor, "Extreme ultraviolet alignment and testing of a four-mirror ring field extreme ultraviolet optical system," Journal of Vacuum Science & Technology B: Microelectronics and Nanometer Structures -- November 2000 -- Volume 18, Issue 6, pp. 2911-2915

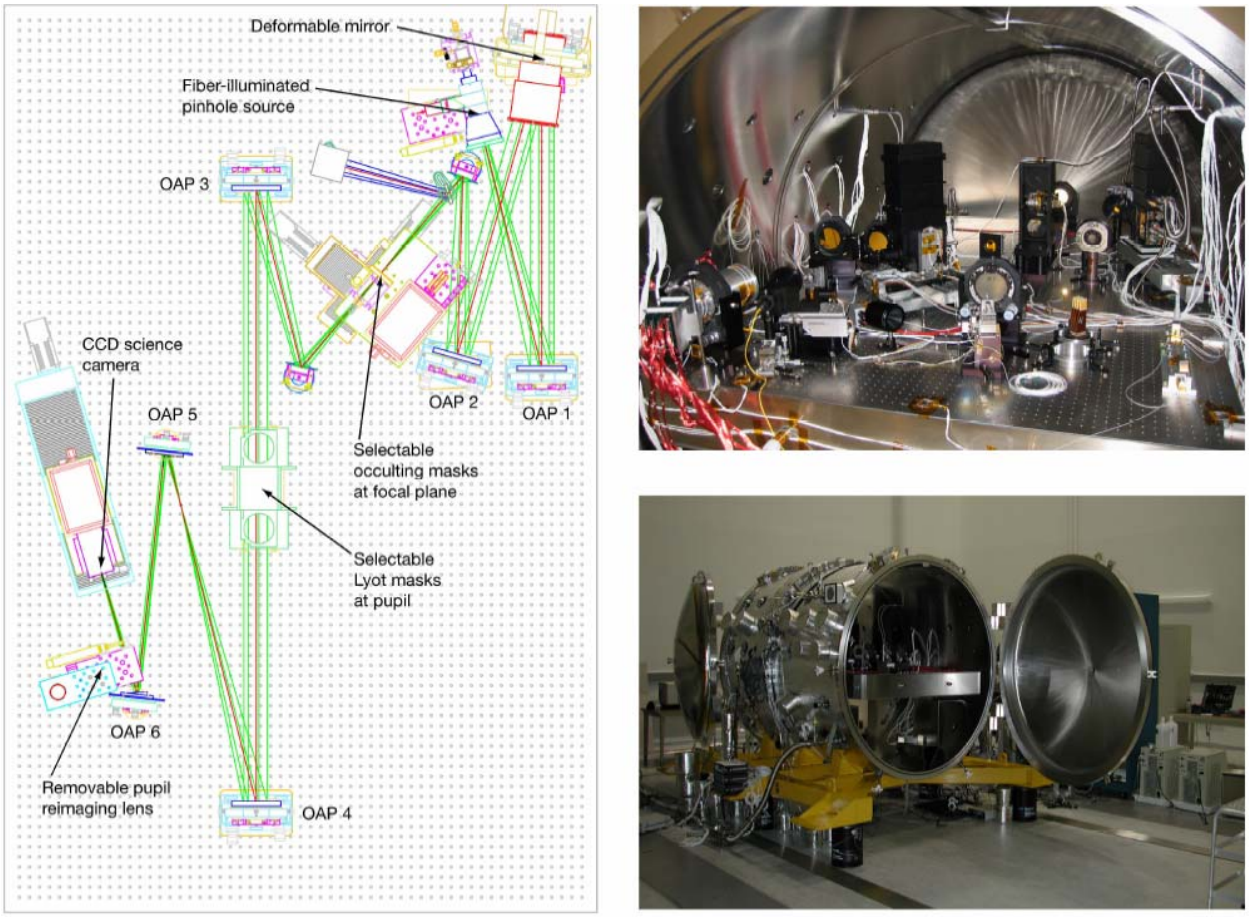

Figure 3-13. Optical layout and views of the High Contrast Imaging Testbed (HCIT).

a side view of the testbed is shown in Figure 3-13. This facility is modular, allowing for integration of modules from a variety of sources and designed for remote observing, so that users from many institutions can be supported. JPL will schedule and support guest users commencing in 2005.

Approach

Empirical investigation and validation of core coronagraph technology is practical with HCIT. This testbed represents two essential subsystems of a high contrast instrument: wavefront retrieval and correction and coronagraphic control of diffracted light. The testbed will validate that an instrument can achieve and maintain contrast beyond 10^{-10} (10^{-9} in pre-Phase A) at the required inner working angle of the TPF coronagraph telescope. This constitutes a fundamental confirmation that phase and amplitude errors can be sensed, corrected, and held for the time period of extrasolar planet detection. Furthermore, it will validate software, diffraction models, and an error budget necessary to construct and operate a flight instrument.

The HCIT development will consist of the following hardware thrusts: continued improvement in the deformable mirror and its performance; continued demonstration of wavefront sensing and control; and testing of apodizing masks and Lyot stops provided by government, industry, and

academic sources. The testbed has been designed to accommodate a suitable subscale telescope and associated masks and stops such as those planned to be developed as part of the Industry Coronagraph Technology thrust. In addition, the HCIT can be used to correlate analyses provided by outside sources and can accommodate possible additional back-end subsystems. The testbed is in operation and has achieved contrasts in a half dark hole of better than 10^{-8}. The testbed status and mapping to the technology gates is shown in Table 3-5.

Table 3-5. TPF-C HCIT Testbed status and mapping to the technology gates

Objectives	Metric	Status	Planned Completion Date	Tech Gate
Demonstrate starlight suppression	1×10^{-9} (goal 1×10^{-10}) at a 4 λ/D inner working angle, at λ≈785 nm, stable for 1 hr	A 9×10^{-10} average contrast was achieved over the half-dark hole, including the 4 λ/D inner working angle, at λ=785 nm; measurement was repeatable; stability of the measurement better than 1×10^{-10}/hr.	Q3 FY05	1
Demonstrate broadband starlight suppression	1×10^{-9} (goal 1×10^{-10}) at a 4 λ/D inner working angle, over a 60 nm bandpass (goal 100 nm) with center wavelength between 0.5–0.8 µm	A 5×10^{-9} average contrast has been achieved over the half-dark hole, including the 4 λ/D inner working angle, over the wavelength band 800±20nm; repeatable measurement	Q3 FY06	2
Validate optical modeling approach	Starlight suppression performance predictions are consistent with actual testbed measurements	An error budget of the HCIT is being developed. This will guide the plan for experimentation to support development of a deterministic model.	Q4 FY06	3a
Demonstrate mission feasibility	Demonstrate through modeling that TPF-C can achieve the required contrast over the required optical bandwidth	The next iteration of the flight baseline design concept is due on January 28. Modeling and analysis is due to be completed by the end of April.	Q1 FY07	3b

Progress to Date

The testbed was aligned in a clean tent and became operational in ambient conditions in October 2002. Experiments with a 1764-actuator deformable mirror yielded contrast on the order of 10^{-5}. Modeling suggested that better contrast was not attainable given the imperfections in this DM.

In April 2003 the testbed was moved to a vacuum chamber. Wavefront sensing experiments commenced in June 2003 using a flat mirror as a surrogate for the DM. The first fully-functional 1024-actuator DM was installed in October 2003. Initial experiments using phase retrieval, a phase-only method, to sense and correct the wavefront, immediately yielded contrast of 2×10^{-6}.

Speckle nulling experiments commenced in December 2003. This technique, which uses science camera images to calculate the DM control, has the ability to compensate for amplitude errors over half the field. These experiments quickly drove the contrast to 7×10^{-9}. In addition to the speckle nulling technique, two Lyot plane algorithms have been developed and tested. These

algorithms have limitations in achievable contrast, but they provide useful tools for diagnostic and error modeling experiments. Combining speckle nulling with one of these approaches has yielded improved control of the DM and better contrast. Other algorithms under development in the TPF community will eventually be tested on the HCIT.

Illumination has been improved in the last year. Amplitude uniformity was improved significantly by changing the input source from a fiber to a pinhole (by imaging the fiber onto a pinhole inside the vacuum chamber). Increased efficiency in the illumination has made white light operation more practical. Stability of the source has been studied, identifying the need to carefully calibrate contrast measurements and to make further improvements to the illumination design.

DM calibration was identified as an impediment to achieving convergence of the speckle nulling algorithm. Due to the construction of the DM, the actuator gains differ slightly depending on whether a single actuator or a group of adjacent actuators is moved. Experimentation using the surface gauge, a Michelson interferometer in vacuum used to calibrate gains of the actuators, has yielded a way to separate these effects and improve control of the DM in the testbed. Testbed experiments have also led to improvements in the DM manufacturing process, notably in the requirements on mirror polish.

Initial speckle nulling performance was limited by the 12-bit digitization used by the multiplexed driver electronics that control the DM. An improved 16-bit multiplexer (MUX) was completed in early 2004. The new MUX uses high voltage Application Specific Integrated Circuits (ASICs – chips) situated in the vacuum chamber, simplifying cabling to the DM and replacing a large rack of electronics with a compact system on the path toward a flight qualified MUX. With the MUX no longer a limiting error source, contrast was improved to near its current levels.

Examples of laboratory results from the HCIT are shown in Figure 3-14. The HCIT has now achieved a contrast of 0.9×10^{-9} for laser light ($\lambda = 785$ nm), as shown in Figure 3-15.[30] This contrast is an average measured in the half dark hole over a range of angles from 4 to 10 λ/D. At the innermost speckle of interest (4 λ/D), the contrast is 3×10^{-9}. Experiments in white light (40-nm bandpass) have yielded an average contrast over the half dark hole of 5×10^{-9}.

3.2.2 Planet Detection Simulator (PDS)

TPF-C is planning to add an industry-built planet detection simulator (PDS) to the HCIT. The PDS will allow simulation of a variety of error sources expected in the flight telescope, including phase, amplitude, polarization, and beam walk. The initial TPF-C plan was to let three study contracts in FY04 with a downselect for hardware construction at the end of the fiscal year; due to budget uncertainties, this was delayed. Current thinking has a single study contract starting at the beginning of Phase A, followed by hardware design and fabrication. Delaying this activity to Phase A ensures that the PDS will have an architecture similar to the baseline TPF-C design.

[30] J. T. Trauger, C. Burrows, B. Gordon, J. J. Green, A. E. Lowman, D. Moody, A. F. Niessner, F. Shi, and D. Wilson, "Coronagraph contrast demonstrations with the high-contrast imaging testbed," in *Optical, Infrared, and Millimeter Space Telescopes*, J. C. Mather, ed., *Proc SPIE* **5487**, 1330-1336 (2004).

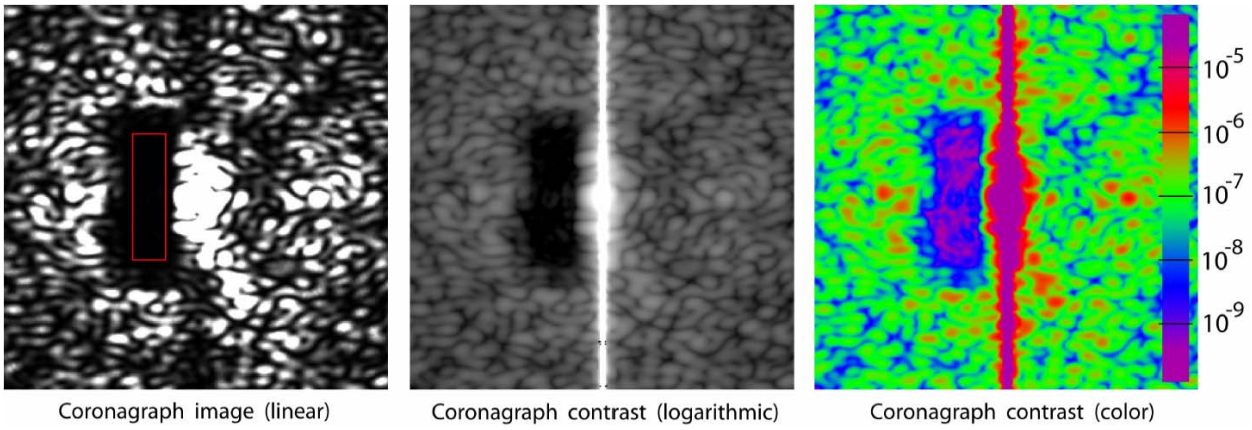

Figure 3-14. Laboratory results from the HCIT showing an average contrast of 1.2×10^{-9} for laser light, as measured in the half dark hole over angles from 4 to 10 λ/D.

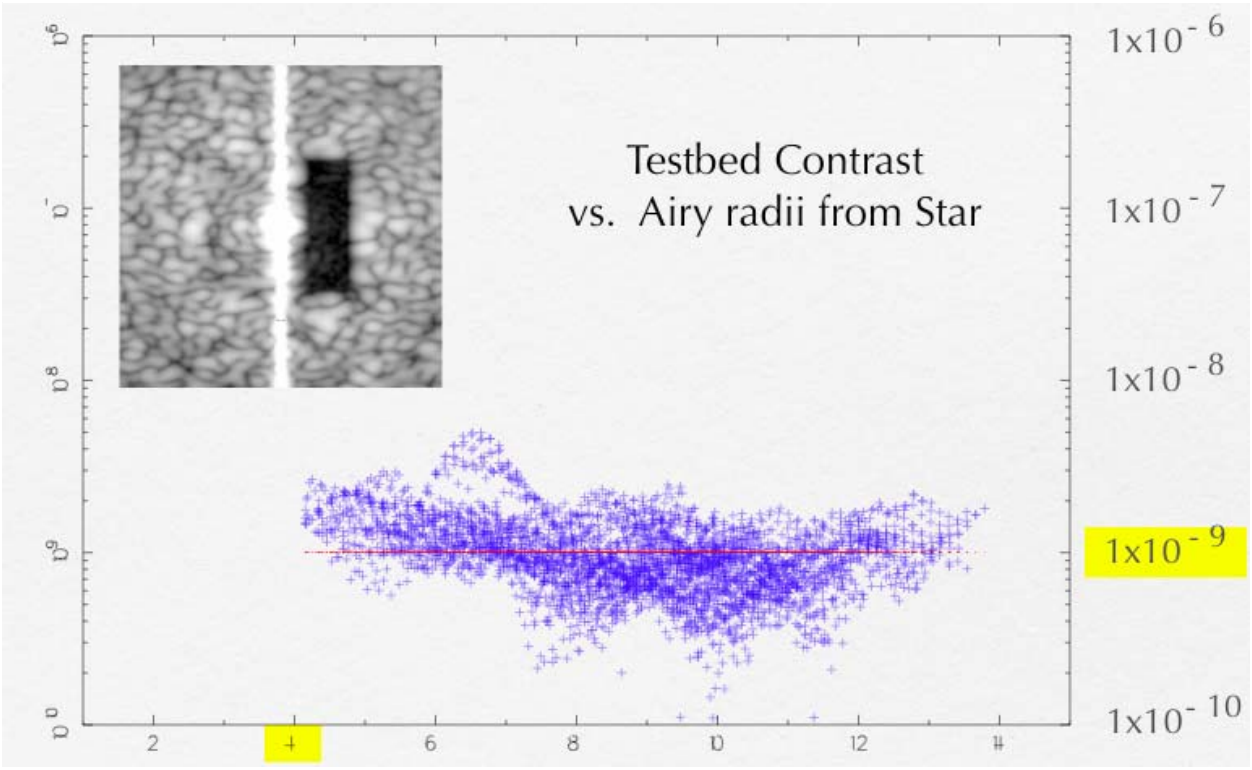

Figure 3-15. Laboratory results from the HCIT showing an average contrast of 0.9×10^{-9} for laser light, as measured in the half dark hole over angles from 4 to 10 λ/D.

Details of the error sources, including whether individual errors will be introduced at fixed or variable levels, will be determined during the study phase.

The PDS is also expected to include a planet simulator. Current experiments on the HCIT demonstrate starlight suppression by comparing the intensity of a dark hole image to the original source. The planet simulator would provide a weak source of calibrated intensity alongside the simulated star source; the weak source could then be directly observed in the HCIT when the

simulated star source is suppressed to the appropriate contrast level. The requirements for the PDS have yet to be developed regarding spectral and polarization properties. Similarly, the need for the PDS mirror to duplicate aspects of the planned TPF-C primary mirror fabrication approach have yet to be considered.

4 Structural, Thermal, and Spacecraft Technology

4.1 Components Technology

4.1.1 Metrology Components

Objective

The extremely high contrast ratio requirement of the TPF coronagraph requires in turn that the telescope secondary mirror be positioned with respect to the primary with a precision of 50 nm over time scales of up to 24 hours. This level of position control demands precision metrology to measure the variation in position of the secondary. The adoption of the 8^{th} order mask design has significantly relaxed this requirement from the previous requirement of 300 pm with the 4^{th}-order design. This activity is aimed at providing the technology necessary to measure the relative SM-PM position.

Approach

The baseline approach is to adapt the SIM external metrology truss, based on common path heterodyne interferometers (COPHIs), to TPF-C. The sensing scheme provides the secondary mirror position in all 6 DOFs as shown in Figure 4-1. This involves splitting the beam into a number of components, directing it along paths between the primary and secondary, and interfering the outgoing and returning beams to extract the variations in distance between the two mirrors. Key components are beam launchers, fiducials, and sources. A beam launcher is a compact interferometer that sends a laser beam on a path whose length is being monitored. Metrology fiducials are retro-reflectors which don't change the path length of the beam being reflected and must be mounted to give a stable reference for the measured path. Metrology sources consist of two lasers, acousto-optic modulators (AOM) for frequency shifting and power switching systems. Various associated optical components may be employed, including fiber beam positioners, corner cube reflectors, and low loss optical cavities.

SIM metrology requirements exceed those of TPF-C in all areas with the single exception of the frequency stability of the laser, which is required to be $\sim 10^{-9}$ over a 24-hour timescale. Components SIM will develop and flight qualify include beam launchers, metrology fiducials

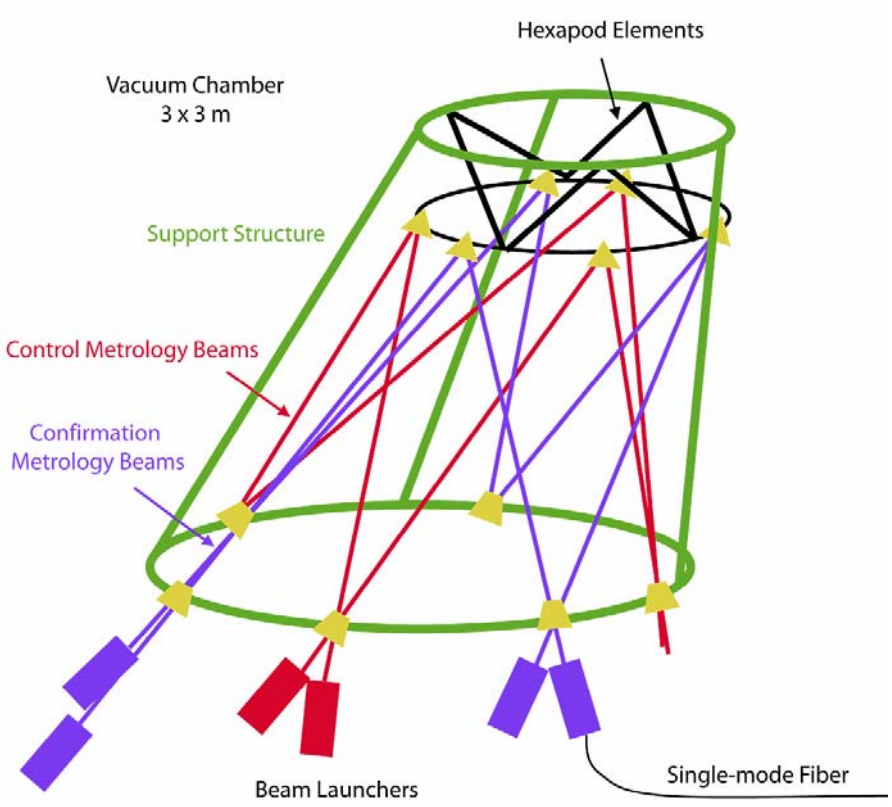

Figure 4-1. Overview of the metrology beam arrangement for secondary mirror position sensing and hexapod control.

and fiducial mounting techniques and metrology sources. The extension of the technology to achieve the frequency stability is expected to be relatively straightforward.

Progress to Date

SIM has demonstrated the required displacement and angular sensitivity on the KITE Testbed with SIM Milestone #4, although at much shorter timescales. Much of the additional attention to date has focused on demonstrating the laser frequency stability to address the previous stability requirement of ~10^{-11} over a 24-hour timescale, associated with the 4th order masks and now considerably relaxed.

4.1.2 Precision Hexapod

Objective

The TPF Coronagraph instrument requires that the Optical Telescope Assembly deliver a wavefront of extraordinary quality and stability. One of the key parameters contributing to the quality and stability of the wavefront is the absolute position of the secondary mirror relative to the primary mirror in 6 DOF. The current TPF architecture and error budget envisions a system in which the relative position of the secondary mirror (SM) to the primary mirror is held on the order of 25 nm. A 6-DOF laser metrology system is envisioned to provide feedback to a 6-DOF

mechanism that supports the secondary mirror. The precision hexapod test-bed will be used to investigate actuator and sensor designs and mechanism concepts and ultimately will prove the feasibility of developing a 6-DOF mechanism that meets the TPF-C OTA wavefront quality requirements.

The objective of this testbed is to demonstrate the capability of meeting the stringent positioning requirements placed on the relative orientation between the secondary and primary mirrors and to develop a facility which can be used to verify the engineering test unit and flight secondary mirror mechanism performance.

Approach

The testbed will be developed in three stages. The first stage is the development of a facility capable of measuring the orientation of an object in 6 DOF down to the sub-nanometer level. In stage two, specific candidate actuators will be investigated and compared to derived engineering requirements developed for the mechanism. Stage three involves the measurement and verification of a prototype and engineering unit secondary mirror mechanism, which will also be used to verify the flight mechanism.

This testbed will be a setup with which GSFC can accurately characterize sub-nanometer level actuators, sensors, and hexapod systems. It will be used in conjunction with an actuator qualification program including performance, environmental, and life testing. It will be used to characterize the motion and stability of the hexapod system with both fine and course actuators under loads (static and dynamic). The testbed would simultaneously measure 6 DOF over a range of at least 5 mm. Commercially available interferometers, from Zygo for example, have measuring capabilities down to 0.15 nm under ideal conditions. However, arranging them in a quiet, turbulence and vibration free environment and including temperature stability and laser wavelength compensation will require significant design effort.

The testbed consists of the following components as depicted in Figure 4-2:

- Vacuum enclosure with ion pump (no vibration) to maintain vacuum
- Vibration and acoustic isolation system
- Temperature stability system
- Measurement in 6 DOF.
- Data acquisition and processing hardware and software
- Stable optical bench
- Various candidate actuators and hexapod systems which can meet or show promise of meeting the spaceflight requirements developed for the TPF-C mechanisms

Progress to Date

This activity is currently in the requirements definition, conceptual design/formulation, and planning stage of development. No other resources have been allocated for this particular testbed activity up to this time, although other technology developments currently being investigated will feed into this activity either directly or indirectly. For instance, characterization of the micro-dynamics of mechanical attachments, material characterization, stable thermal

enclosures, and stable laser metrology systems will all be key activities leading to the development of this testbed.

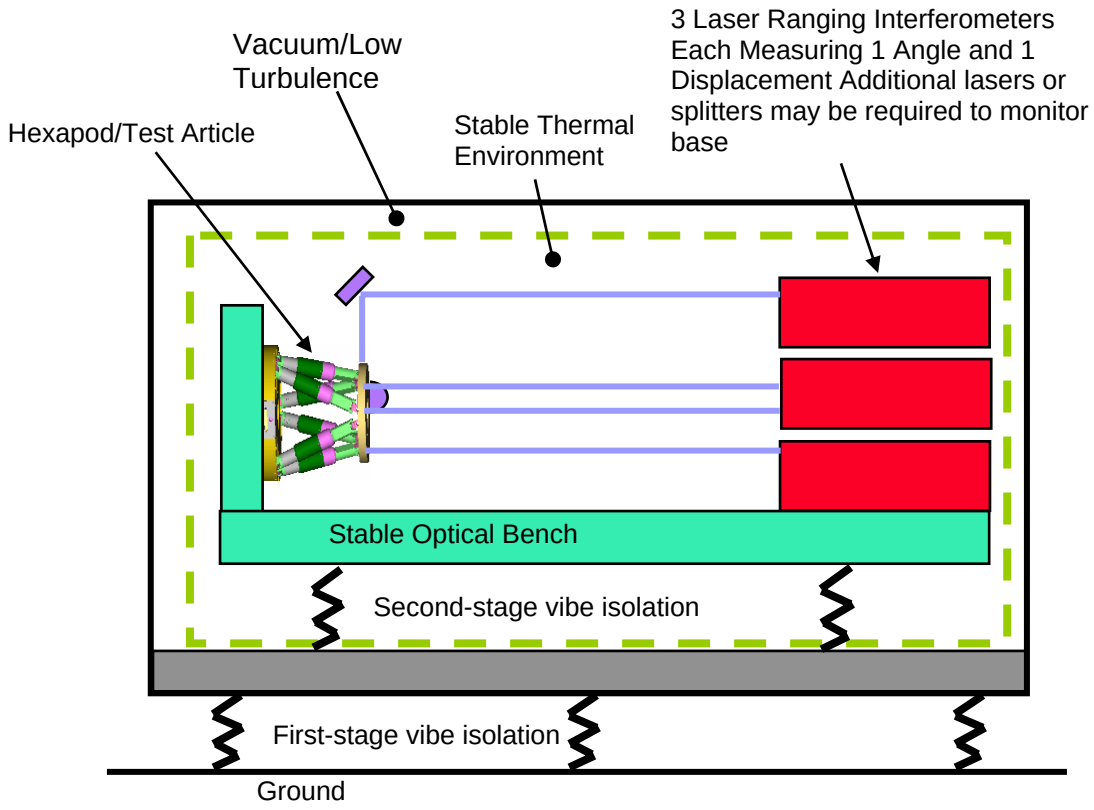

Figure 4-2. Schematic of the Precision Hexapod Tesbed.

4.1.3 Precision Structural Stability Characterization

Objective

The TPF Coronagraph will have to rely on extreme structural and thermal stability to achieve its performance goals. The objective of this work is to determine, with the high degree of precision necessary, the material and sub-component characteristics necessary for accurate modeling of the thermal and dynamic stability of the TPF-C telescope performance. Most importantly, the thermo-mechanical linear and non-linear characteristics and their scatter need to be tested and identified to levels consistent with the error budget.

At present, the error budget for the TPF-C concept at 4λ/D with an 8-m PM requires that the rigid-body position of the PM relative to the SM be better than 25 nm over the 10-m separation, and that the RMS PM surface figure over the first 15 Zernicke modes be better than about 300 pm during the course of an observation, which entails a 36 degree dither and approximately 2 hours of data collection at station. This activity will assure that material properties and models of critical sub-components are characterized to levels of precision commensurate with the mission requirements, which in many cases is at or beyond the current state-of-the-art.

Approach

This activity will develop several experimental test facilities contributing to improved knowledge of precision stable structures, as described below. Note that since the facilities described herein are for the purpose of material characterization and model validation only they are not associated with any TRLs.

Precision Dilatometer Facility

We take advantage of the (Cryogenic) Precision Dilatometer Facility (PDF) developed at JPL for JWST to characterize the thermal strains, material variability, and long term dimensional stability of relevant precision optical materials, at any temperature between 305 K and 20 K. The facility is shown in Figure 4-3, along with an example of measured data in Figure 4-4.

This facility is now being calibrated, and recent data shows that the error in the instantaneous coefficient of thermal expansion is approximately 2 ppb/°C, at least an order of magnitude better than other existing test facilities in the United States typically used for this kind of measurement. Preliminary sensitivity analyses on mirror CTE variations for the TPF-C Minimum Mission configuration have shown figure requirements were achieved with variations of 5 to 15 ppb/°C, representative of ULE fabrication capabilities. This implies that the PDF has sufficient precision to characterize material CTE to tolerances required for TPF-C analyses. Examples of materials to be tested include ULE and Zerodur for optical mirrors, PMN for the deformable mirrors, and titanium and various metals for mechanical components or flexures. Other mechanical and thermal properties will also be gathered from the literature or tested when necessary. It will be important to also capture the accuracy with which this data has been measured, so as to propagate the measurement uncertainties within the analytical predictions. This implies that all

facilities from which data is collected will require a validated error budget. Note that test repeatability only highlights random errors and does not evaluate systematic errors.

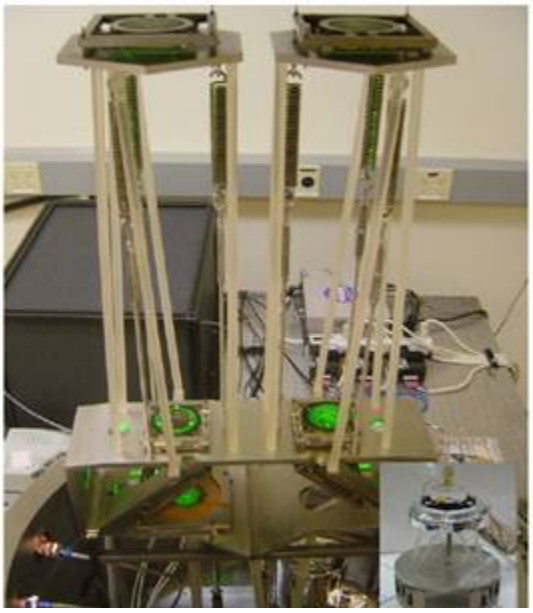

Figure 4-3. JPL Precision Dilatometer facility, with depiction of sample test configuration.

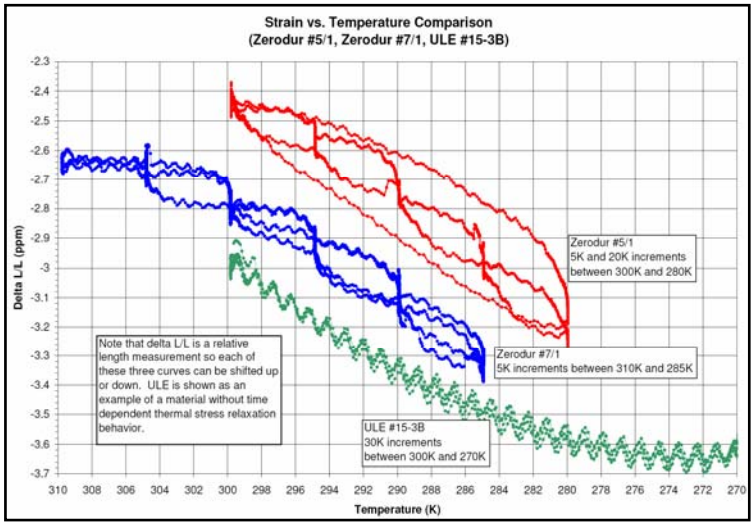

Figure 4-4. Preliminary thermal strain data obtained on the JPL Precision Dilatometer for Zerodur and ULE.

Material property measurements will not be limited to CTE alone. The Project will establish a list of all material properties required for assessing performance stability using the integrated thermal, structural and optical models. Included in this material property list are all elements in the dynamic and thermal load paths, including joints, cables, etc. Data will be needed for these properties as a function of temperature, wavelength, frequency, and load cycle as appropriate. Published literature data will be reviewed, and if it is established that the quality of the published data does not meet TPF-C accuracy requirements, then additional materials testing will be performed. Accuracy requirements on material property data will be defined later as more analysis is performed to understand the sensitivity of material data error on predicted performance. Allocations for material data error will eventually be folded into the Modeling Uncertainty Factor allocation. Ultimately, all material property data assembled under this endeavor will be gathered within a Project-controlled database for use on all TPF-C modeling activities.

Microslip Tribometer Characterization Facility

The (Cryogenic) Microslip Tribometer Characterization (MTC) facility will measure the coefficient of friction in the microslip regime well below the onset of gross Coulombic slip. This information is required as a physical parameter within established microslip hysteresis model forms which combine both stress-induced and roughness-induced microslip. Data will be collected for representative materials of frictional interfaces, such as hinges and latches, with varying surface roughness specifications and over the temperature range of 305 K and 20 K to investigate thermal sensitivities. The MTC, shown in Figure 4-5, is designed, built, and calibrated in air by Dr. Jason Hinkle at the University of Colorado. The apparatus will be delivered to JPL to be placed within a thermally controlled cryogenic vacuum chamber. Representative data sets are shown in Figure 4-6. Data collected on this facility will be enclosed in the TPF-C Project Material Database.

Precision Sub-Structure Test Facility

The Precision Sub-Structure (PSS) test facility will be developed at JPL to characterize the thermo-mechanical stability of composite materials, composite structure sub-assemblies, and eventually actual flight hardware including hinges and latches. The facility will derive experience gained on the Precision Dilatometer test facility to incorporate a sub-nm interferometric metrology system within a thermally controlled vacuum chamber to enable distortion and strain measurements for these mechanical sub-assemblies. The current testbed goal is to achieve better than 1-nm measurement accuracy over a 1 minute time interval, which is consistent with current requirements on the SM tower stability. Better measurement performances have already been achieved on the Precision Dilatometer test facility and the SIM Thermo-Optical Mechanical testbeds, so the measurement capability itself is not seen as a risk.

The immediate goal will be to collect property data for non-optical materials. The focus will be on measuring and understanding the thermal strain, CTE, material variability, microdynamics, and dimensional stability of proposed composite materials on TPF-C. Of special interest are the materials forming the PM support structure, the SM tower, and the coronagraph optical bench.

Over time the facility will be used to investigate the dimensional stability and thermal sensitivity of critical sub-assemblies such as bonded composite parts, bearings, hinges and latches, and

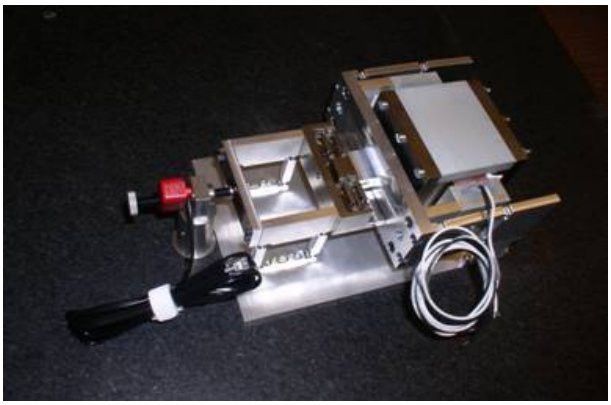

Figure 4-5. Microslip Tribometer Characterization (MTC) apparatus.

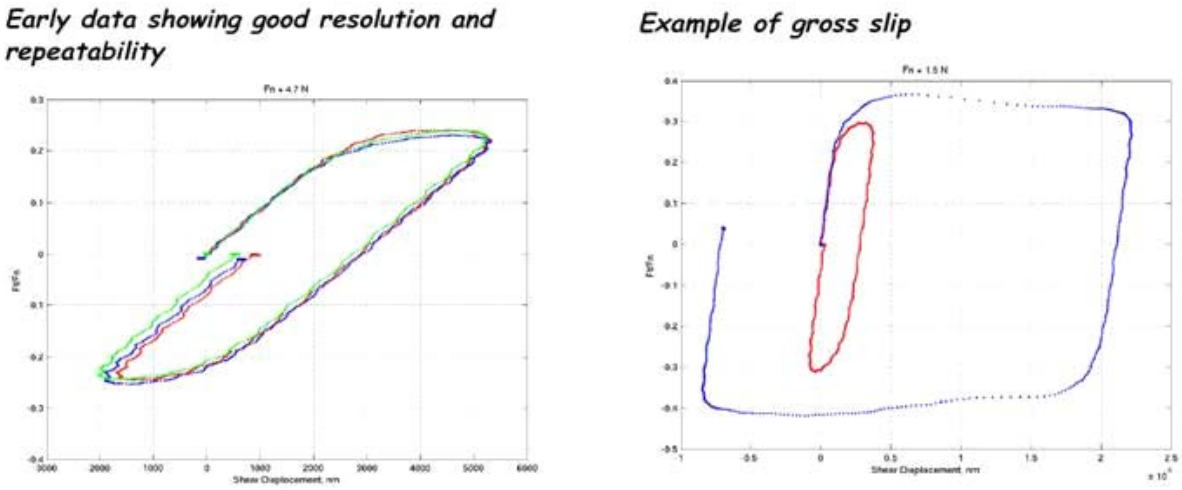

Figure 4-6 Representative data obtained from the Microslip Tribometer Characterization (MTC) facility.

parasitic effects of cables through pivot or latch joints. Other areas of potential concern include micro-cracking and residual stress behavior of ULE segments joined through a low-temperature fusion process, especially as they relate to non-recoverable launch-induced deformations, or geometric misalignment of sub-assembly elements due to initial fabrication imperfections. This testbed could also be used to investigate active or passive structural damping technologies, should there be a need in the future. Details and test plans for the sub-assembly test articles will be developed as the design and analysis of TPF-C mature and as the understanding of these risks with respect to the error budget improve.

The test facility will be multi-functional and will be capable of measuring nm-level motions due to thermal or mechanical disturbances. Tests will range from long-term stability observations to high frequency measurements, all of which are required to investigate a variety of nonlinear mechanical physics. For instance, test articles will be tested for quasi-static thermal or mechanical cyclic loads to identify hysteresis, and for steady-state dynamic loads to characterize harmonic distortion of the frequency response. When testing hinge and latch assemblies, the specimens will be turned around in various orientations to investigate and model the effects of 0-gravity. Alternatively, means to artificially change the pre-load on the frictional interfaces will

be implemented. The facility will be required to provide extreme thermal stability and control, as well as accurate means to decouple the response of the test article itself from external error sources such as those typically attributed to instrument misalignment, load path parasitics, and nonlinear interactions with mounting the hardware.

Material data and validated models gained from this activity will be collected within the Project controlled Material and Model Databases and used by the modeling team for prediction of flight performance.

Frictional Stability Characterization Facility

The Frictional Stability Characterization (FSC) facility will be developed at the University of Colorado by Prof. Lee Peterson and Dr. Jason Hinkle to evaluate, on a generic frictional interface, the various parameters contributing to microdynamic stability. The facility will be a simplified representation of the PM to SM telescope assembly with an inter-changeable frictional interface whose parameters, such as preload, stiffness, and surface roughness, can be varied to study the impact of the microdynamic stability at the simulated optics positions. These parameters are those included in existing models for frictional nonlinearities, and the measurements will be used to validate the sensitivity of these parameters to the microdynamic requirements on TPF-C, (e.g., less than 300 pm PM to SM position stability). In particular, performance analysis models that bound the microdynamic performance will be developed and validated, and nonlinear analysis tools to model localized nonlinear behavior of hinges and latches will also be validated. A secondary goal of this test facility is to define the parameters and mechanical performance requirements of hinges and latches that will be levied on the actual TPF-C flight mechanisms.

Progress to Date

Progress has only been made on the Precision Dilatometer Facility (PDF), since its development has been funded by JWST, and some material information has already been collected. Of particular interest is the calibration that is currently being performed on a sample of single crystal silicon, shown in Figure 4-7. The CTE data collected on the sample matches almost exactly, to within 5 ppb/°C, the data measured on another extreme precision facility in Australia by K. G. Lyon over 30 years ago.

Preliminary data has been obtained on a representative Zerodur sample. Very intriguing nonlinear effects have been characterized, the behavior of which has been confirmed by the vendor, Schott, in Germany. Figure 4-4 shows hysteresis in the material, as well as thermal relaxation at constant temperature. Being able to maintain temperature anywhere between 305 K and 30 K to within 10 mK is a unique capability of the PDF. Similar tests were performed on a ULE sample, which did not display hysteric behavior, also shown in Figure 4-4. Additional tests on Zerodur and ULE will be performed using annealing and surface treatments on the samples consistent with mirror fabrication standards to obtain data more relevant to TPF-C analysis needs. Several ULE samples will be extracted from the TDM (Technology Demonstration Mirror) material to directly correlate the TDM test results with its analytical predictions.

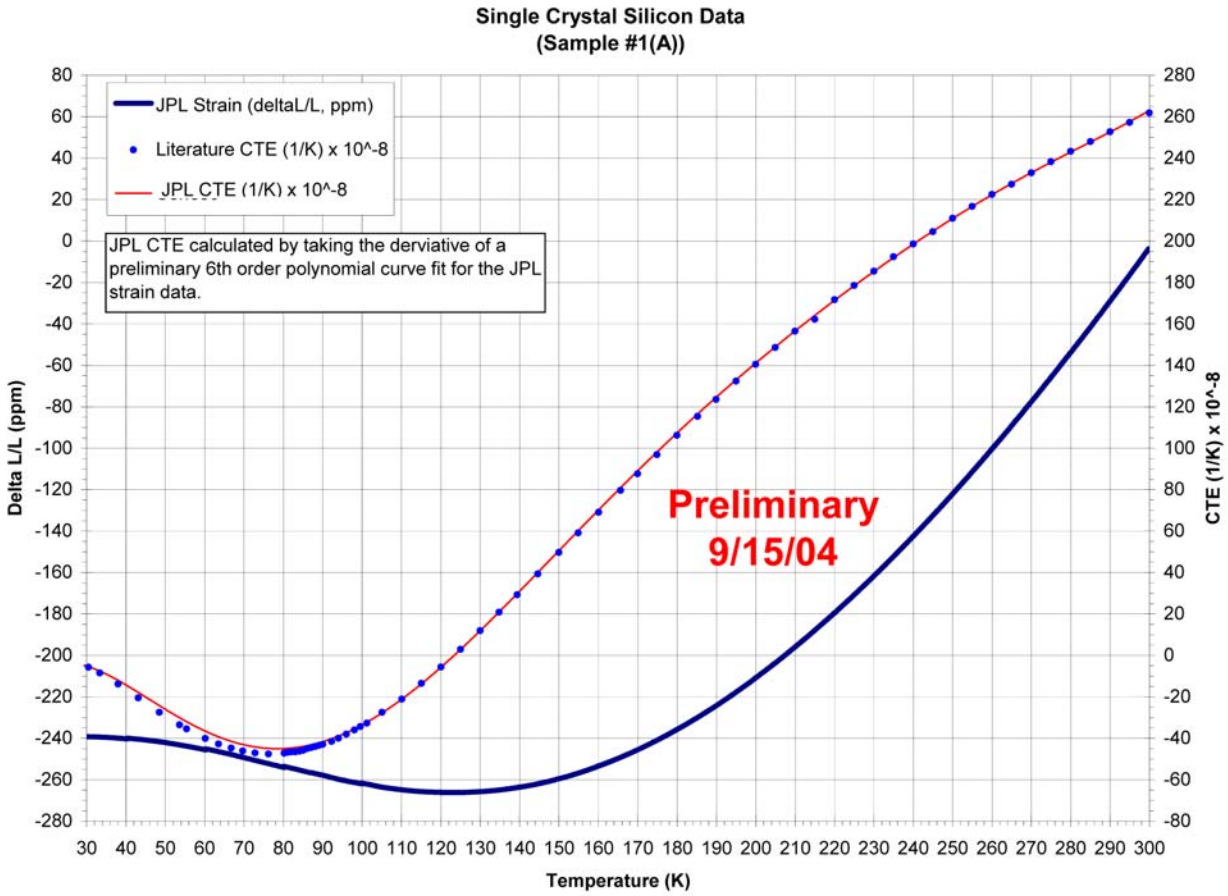

Figure 4-7. Calibration of the JPL dilatometer using Single Crystal Silicon showing good reproducibility with literature data.

The design, fabrication and assembly of the MTC facility was completed by CU (University of Colorado) in FY04, and calibration of the experimental accuracy is underway. Preliminary data have been obtained that show the test capability to measure microslip hysteresis, as shown in Figure 4-5.

The funding for the two other test facilities, the PSS and the FSC, has just now been made available in FY05, and there is no progress to report at this time.

4.1.4 Vibration Isolation Testbed

Objective

To reject the star flux and detect the planet flux in the visible light range, TPF-C must achieve a rejection ratio of better than a billion to one. Dynamic jitter, introduced by environmental and on-board mechanical disturbances, degrades the optical performance (image quality) and the capability to reject starlight (contrast ratio). TPF-C must maintain the dynamic stability of its instrument to the sub-mas and sub-nm level in order to successfully perform contrast imaging required for planet detection. Meeting these stringent stability requirements in the presence of

dynamic jitters poses great challenges to the vibration isolation system. The objective of the vibration isolation activity is to create viable passive and active isolation designs for TPF-C and ultimately test and verify the performance of the selected isolation system.

Approach

Since TPF-C has dynamic stability requirements tighter than most current and planned missions, it will be critical to ensure that the isolation system can reduce vibrations sufficiently. Two fundamental approaches to vibration reduction are passive and active isolation systems. Passive isolation uses a soft suspension to limit the transfer of disturbance energy across an interface. Passive isolators have a significant flight heritage, and are lower risk (with relatively fewer components and no chance of instability of the feedback loop). However, the performance is fundamentally limited by static displacement constraints, parasitic stiffness, and high frequency isolator modes. An active isolation system requires additional sensors and actuators to suppress vibration based on real-time measurement feedback. A combined active isolation and spacecraft pointing approach separates the payload pointing and vibration isolation mechanisms through a non-contact interface between the spacecraft and payload, and non-contact sensors and actuators at the interface. Both the pure and hybrid active approaches may potentially offer higher levels of vibration reduction than a passive isolation design, but with additional risk and a shorter flight heritage.

Currently there are two concepts under consideration: (1) a three-stage passive isolation system and (2) a hybrid pointing and isolation system. The passive isolation design includes a passive isolation stage between the spacecraft and the payload, another stage that isolates the entire reaction wheel assembly, and a third stage that provides isolation to each of the reaction wheels. The current hybrid design chosen as a baseline is called the disturbance free payload (DFP), under development by Lockheed Martin. The DFP architecture involves the nearly-complete mechanical separation between the telescope and the spacecraft, non-contact interface actuators that allow precision inertial control of telescope pointing, and non-contact relative position sensors for spacecraft attitude control to maintain the proximate angular separation. In this architecture, spacecraft vibration isolation is achieved through mechanical separation, and is thus independent of sensor characteristics, while stable telescope pointing is achieved through non-contact actuators. [31]

Integrated models, combining structural, optical, control, and isolation models, are used to evaluate each of the isolation designs and provide end-to-end performance predictions. The analytical work will help identify the best or most appropriate isolation design that leads to mechanical development of the chosen design. This activity will demonstrate or verify the isolation system performance by combining analysis efforts and hardware testing.

Progress to Date

Preliminary performance analysis of the two concepts has been completed, and the results are discussed in this section. To compare the two isolation designs, an integrated model was created to take reaction wheel disturbances as inputs and line-of-sight (LOS) and Zernike amplitudes as

[31] Pedreiro, N., "Spacecraft Architecture for Disturbance-Free Payload", *AIAA J. Guidance, Control and Dynamics*, v.26, No.5, pp. 794-804 (September 2003).

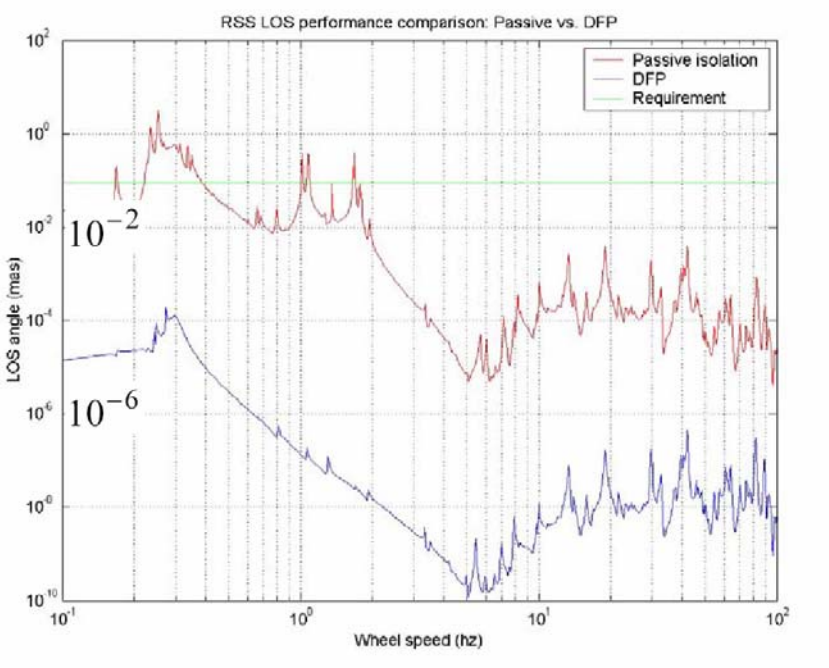

Figure 4-8. Comparison of passive isolation performance versus DFP performance for line-of-sight stability requirement.

outputs. In this analysis, two reaction wheels were assumed to spin at the same speed with random phasing, the structural damping ratio was assumed to be 0.1%, and model uncertainty factors were also added to increase conservatism.

Figure 4-8 illustrates the LOS performance for the passive isolation design (red line) and DFP (blue line), as well as the requirement (green line). The passive isolation design cannot alter the system response for frequencies below the isolator break frequency, typically ~2 Hz, but can achieve 40–60 dB attenuation per stage at frequencies sufficiently above the break frequency. Although the passive isolation design does not meet the LOS requirement at low wheel speeds, it is simple to limit wheel speeds to above 2 Hz where passive isolation can meet the requirement with a large margin. The DFP, on the other hand, does not have a theoretical limit in rejecting vibrations at low frequencies. As a result, the active DFP design can meet the LOS requirement for all wheel speeds and demonstrate vibration reduction about two orders of magnitude better than the passive isolation design.

The wavefront error (WFE) due to telescope deformation, expressed in terms of the first 15 Zernike amplitudes, is plotted in Figure 4-9. The top graph shows the margin in dB for each Zernike amplitude:

$$-20\log\left(\frac{\max Z_i(\omega)}{R_i}\right), i = 4...15$$

where Z_i is the amplitude of Zernike mode i versus wheelspeed, and R_i is the requirement for mode i. The bottom graph shows the peak Zernike amplitude from the passive isolation and DFP designs as blue and green lines, respectively, along with the requirement for each mode in

nanometers shown in red. The insets show the deformation pattern for each of the Zernikes. The legend indicates the frequency at which the peak response occurs. For this analysis, the passive isolation design is sufficient to satisfy all Zernike amplitude requirements, and the DFP performance exhibits between 1 and 2 orders of magnitude margin on all requirements. The up-to-date analysis shows that a three-stage passive isolation design is sufficient to meet requirements with wheel speed limitation or damping augmentation. The active DFP design seems to demonstrate even greater vibration reduction capabilities but carries additional risks as mentioned above.

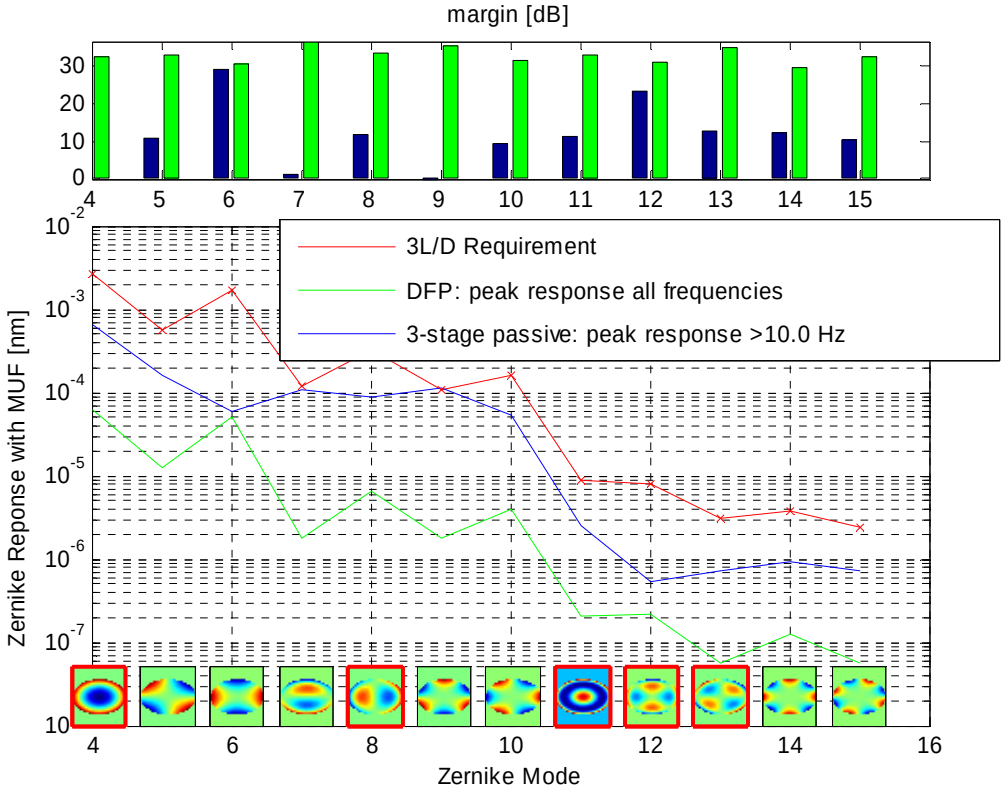

Figure 4-9. WFE due to telescope deformation for 3-stage passive isolation (blue) and for DFP pointing/isolation system with conservative assumptions on cable stiffness and residual coupling (green): top graph, dB margin for each Zernike mode; bottom graph, peak Zernike amplitude from 10-100 RPS wheelspeed plotted along with the requirement.

4.2 Subsystem and System Testbeds

4.2.1 Closed-loop Secondary Mirror Position Control

Objective

The TPF telescope requires very high stability to enable transmission of a wavefront to the coronagraph meeting the requirements for planet finding. A critical aspect of the telescope stability is the position of the secondary mirror with respect to the primary. The TPF requirements allow for no more than 26-nm variation in the piston and transverse directions, and 100-nrad variation in the tip and tilt directions, over a timescale of 24 hours. This level of control cannot be maintained passively, but must be provided with an active feedback correction system.

The feedback system will include two main aspects: an error signal that will indicate the deviation of the secondary mirror from its nominal operating point, and an actuator to correct the mirror positioning so that the error signal is driven to zero. The error signal will be provided by the laser metrology system described earlier. The actuation system will incorporate a hexapod, a high precision positioning device with six actuator legs (described above). The hexapod allows for 6-DOF positioning and possesses a high degree of stiffness that can provide relatively fast (>1 Hz) control.

The objective of this activity will ultimately be the development and test of a sub-scale secondary mirror position control system, which will include primary and secondary mirrors and a support tower for the hexapod. The activity will proceed in the stages described below.

Approach

A testbed designed for the study of closed-loop interferometric control at low frequency is now operational at GSFC, as in Figure 4-10. The testbed contains a vacuum system housing two hexapods, which in turn will support a small, simple model of the TPF telescope optics. Two frequency-stabilized lasers are used in the testbed. One utilizes the metrology scheme to measure the variation of position of the secondary optic, and then feeds this signal back to the hexapod to stabilize the optic position. The second laser system is used to independently confirm that the residual noise in the motion of the model telescope is at the level required by TPF. The testbed will operate in the presence of laboratory seismic and thermal disturbances (of order 10^{-6} m over 1 hour), which is much larger than the disturbance expected in space. However, the stability of the testbed is limited only by the sensitivity of the metrology system, thus control of the model telescope at the 10^{-10} m level will be possible. In fact, the development of this level of control in the presence of environmental disturbances will allow the design of future larger-scale prototypes that can be useful for end-to-end telescope testing in the laboratory.

This testbed will allow for the study and characterization of many elements that will be critical to designing a realistic control system, including: testing of the metrology system, including its sensitivity to motion in all 6 DOF; measurement of non-linear behavior and hysteresis in the hexapod PZT actuators; the effect of the hexapod internal resonances on the control system; and overall performance of the control system in real time. The insights gained from this testbed will allow for the design of a realistic, full-size secondary mirror positioning system with a high

degree of confidence, as the scaling of the control system with regard to the full telescope length and optic weight will be straightforward.

Progress to Date

The field of precision control is extensive and well documented, including the use of the hexapod for 6-DOF control. The challenge for TPF is to extend the hexapod control system to the sub-nanometer level; this necessitates the use of laser interferometry to provide the control signal. The most relevant area for the work described here is the ground-based gravitational wave field, where laser interferometry is used to measure and control disturbances at the sub-picometer level. For example, the Laser Interferometer Gravity Wave Observatory (LIGO) interferometer has achieved control of the 30 cm diameter optics forming its resonant cavities (10 – 4000 m in length) at the level of 10^{-13} m over several tens of minutes[32]. In the LIGO case a frequency stabilized laser is used to measure deviations of the cavity length from its nominal operating position, and magnetic actuation is used to force the cavity deviations to zero. While there are obvious differences between the LIGO and TPF configurations, the many similarities between the two systems (stabilized laser for position error measurement, high gain control system, precision mechanical actuation) give confidence that the TPF secondary mirror position control requirements are achievable.

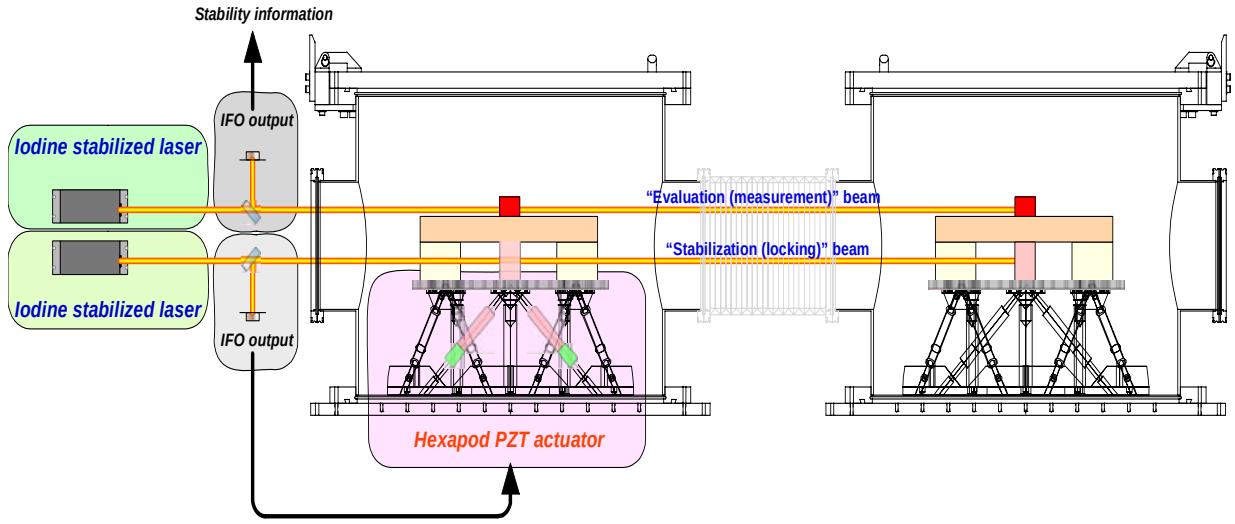

Figure 4-10. GSFC hexapod closed loop control testbed, showing vacuum system, hexapod platforms, optics supported by hexapods, stabilized laser for error signal readout, and independent stabilized laser to read out final residual noise.

[32] P. Fritschel et al., "Readout and control of a power-recycled interferometric gravitational-wave antenna", *Applied Optics* 40, 4988-4998 (2001).

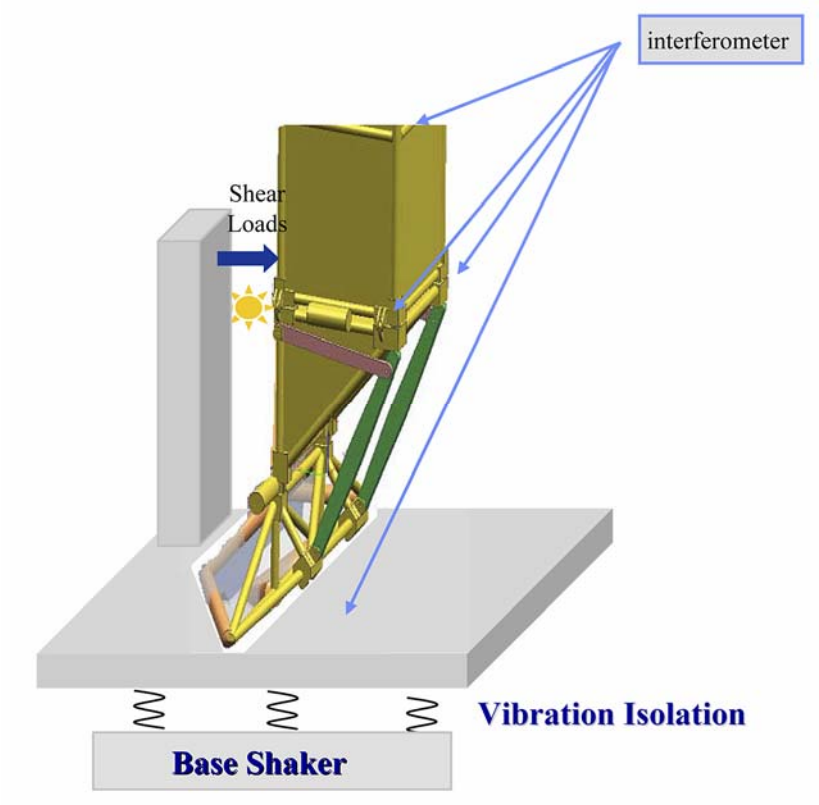

Figure 4-11. Schematic of the Secondary Mirror Tower Structure Testbed.

4.2.2 Secondary Mirror Tower Partial Structure Testbed

Objective

The objective of this testbed is to characterize, with participation of industry, the instabilities and nonlinear dynamics of mechanisms on a full scale hinge/latch assembly with flight-like interfaces to a truncated SM tower, and in an environment representative of the TPF-C operating conditions. The main concern is the existence of dynamic instabilities above 1 Hz that would jeopardize the 300 pm SM position stability requirement. This includes sudden and repeated energy releases (a.k.a. “snap, crackle and pop”), as well as harmonic distortions of sinusoidal waveforms propagating through the nonlinear mechanisms. The primary objective is to validate bounding analysis models for microdynamic behavior due to stored strain energy release at the hinge/latch assembly. This testbed will also be used to validate analytical models of the SM tower sub-assembly, especially with regard to the nonlinear representation and impact of the hinge/latch, and to characterize scalability of the response to various thermo-dynamic inputs. It is envisioned that the mechanisms, materials, and architecture of this testbed will be traceable to the actual TPF-C flight design.

Approach

A schematic of the test facility is shown in Figure 4-11. The testbed will be housed within a thermally controlled vacuum chamber, and vibration isolation will be provided to minimize jitter

noise from the laboratory environment to much better than 1 mg. Using the Lockheed Martin DFP is a possibility since it is capable of at least 40 dB of vibration attenuation, and as an active system can be used to simulate the input of RWA disturbances through the telescope system. Other disturbances can be incorporated to drive the microdynamic instabilities such as base shakers, heaters, and shear loading devices near the hinge/latch interfaces.

The test article itself will be appropriately mass loaded so as to provide the same inertia to the truncated tower as would the full-length flight tower. The primary goal is to exercise the mechanisms in the right frequency regimes and inertial loading configurations.

The position stability of the assembly will be monitored through a suite of precision instruments such as a displacement interferometer, micro-g accelerometers, nano-strain gauges, eddy current sensors, temperature sensors, and load cells. This instrumentation suite will enable the high-frequency measurements of relative tower motions, harmonic distortions, hysteresis, modal frequencies and damping, and acoustic emissions—all phenomena that can adversely impact the SM stability requirement.

Materials and testbed sub-components are expected to be tested individually prior to testbed assembly. The testbed data will then be used to validate the assembled testbed model, focusing primarily on the interface models and nonlinearities. Material and sub-component testing can be performed as part of the Precision Structural Stability Characterization activity at JPL and/or at the contractor facility. In any case, although the contractor will be responsible for delivering validated models of the testbeds, NASA will conduct an independent modeling activity for verification.

Progress to Date

This activity is currently in the requirements definition and planning stage. No other resources have been allocated for this particular testbed activity up to this time. Other technology developments currently being investigated will feed into this activity, in particular the Precision Structural Stability Characterization testbed suite.

4.2.3 Pointing Control Testbed (PCT)

Objective

TPF-C faces challenging pointing requirements. The major pointing requirements are (1) maintain stability of the telescope pointing to 4 mas 1σ /axis, and (2) direct the star light to the coronagraph mask to an accuracy that maintains an “acceptable” contrast ratio that results in a trade between jitter and offset requirements, as shown in Figure 4-12, which refers to the previous pointing requirement. Currently, if there is a pointing offset (bias) of 0.3 mas, the pointing jitter can be up to 0.3 mas 1σ, RMS. This fine pointing mode was recently relaxed by a factor of nearly 8 from what is shown in Figure 4-12. The objective of the pointing control testbed is to demonstrate the required sub-mas pointing.

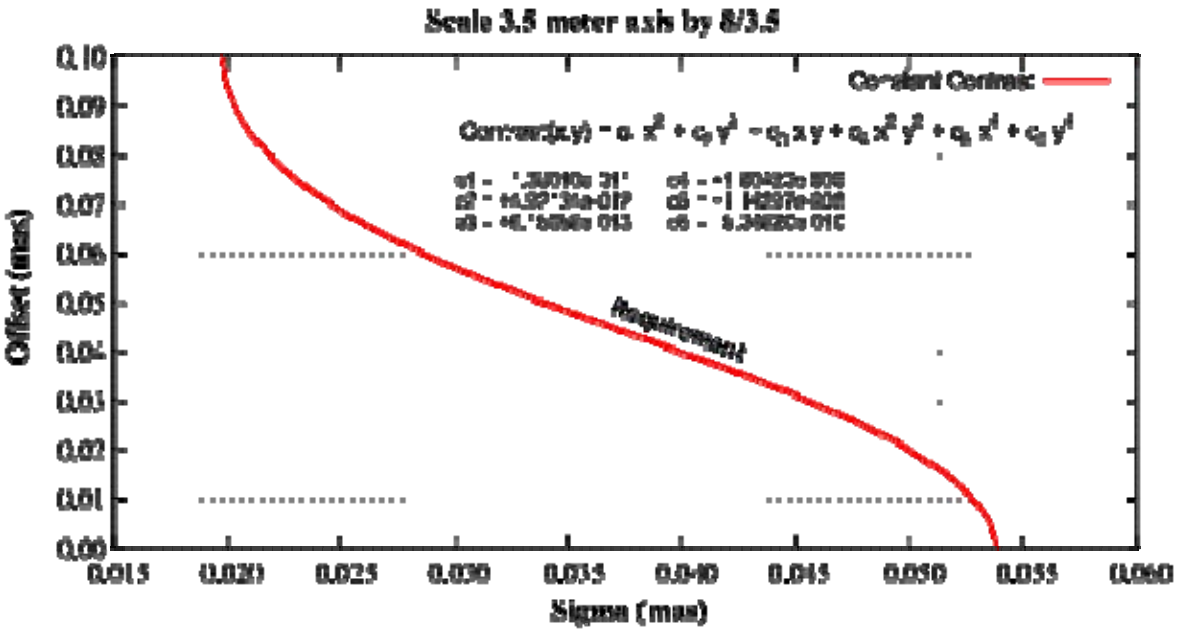

Figure 4-12. Fine guiding sensor offset versus jitter required for an 8 m TPF-C. Using the 8th-order masks, the pointing requirement is relaxed by roughly a factor of 8 from what is shown in this figure.

Approach

Both the first and second requirements are very challenging, and the verification is also difficult—0.3 mas (or 1.44 nanoradians) is a length of 1.5 μm seen from 1 km. This pointing requirement results in the corresponding testbed requirements:

(a) Demonstrate capability to perform S/C rigid body stability to 4 mas 1σ /axis
(b) Demonstrate control to met the jitter and offset pointing capability

Both a physical testbed, shown in Figure 4-13, which is needed to demonstrate the capability of the components, and a high fidelity simulation that models the expected environment are necessary to develop and demonstrate the needed flight capability. The simulation testbed would also then be responsible for the generation of models for inclusion into any more extensive S/C system model. The critical testbed components include disturbance models and disturbance inducing mechanisms.

The TPF-C pointing and control hardware testbed must allow demonstrations of sub-mas pointing capabilities while undergoing spacecraft-equivalent vibration and other disturbances and using "reference stars" and ACS sensors for measurements. While the TPF-C has a space environment, the PCT will be operated in a ground facility where external disturbances such as acoustics, air disturbances (at least when not in vacuum), and ground transmitted vibrations are very difficult to eliminate. A list of key testbed components, disturbance sources, and comments follow.

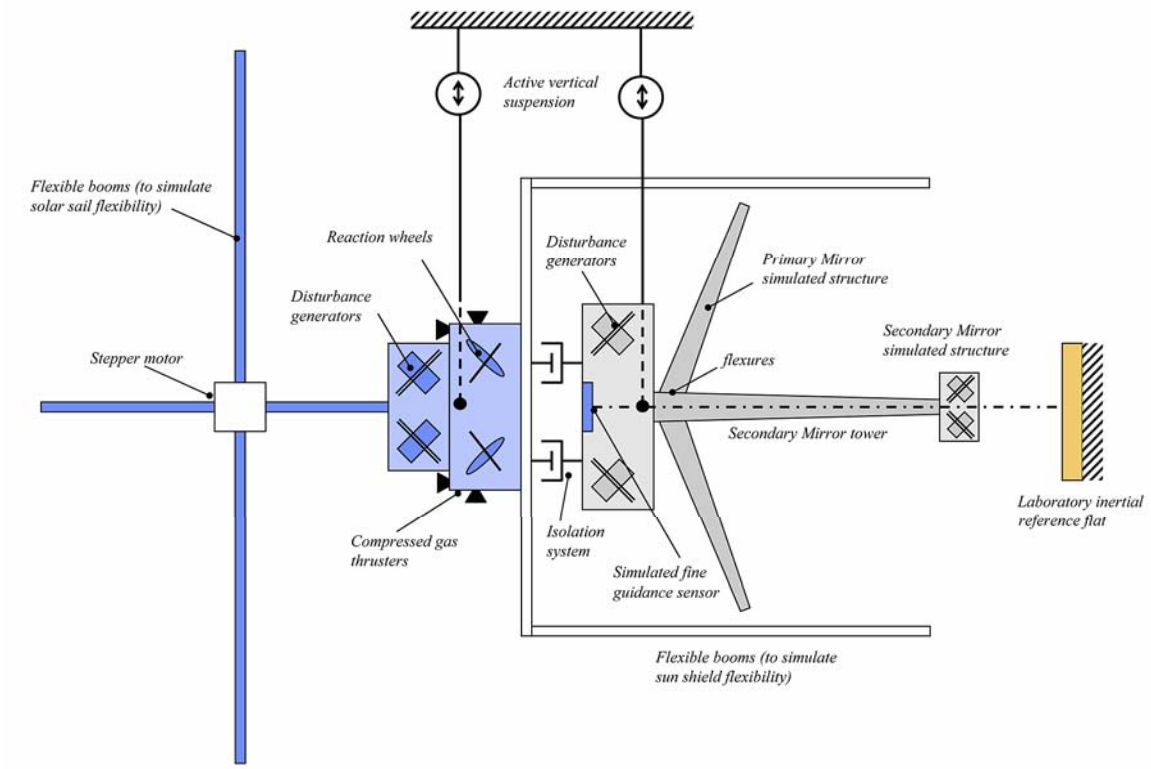

Figure 4-13. Schematic of the Pointing Control Testbed.

Critical Testbed Components

(1) RWA disturbances on the S/C. The reaction wheels assembly (RWA) will induce vibrations on the S/C. There is a separate structures testbed that will perform detailed evaluation of the induced vibration and allow the creation of a vibration model. This model will then be used to simulate the disturbances at the isolation interface. Additional disturbance models will include the unloading of RWA.

(2) A model of the disturbances of the S/C transmitted to the telescope as a function of the disturbance into the isolator. The testbed will require an isolator or isolator simulator with the characteristics of the flight system (or an appropriate model of the performance) and a computer controllable vibration inducing system, which can induce disturbance onto the testbed.

(3) A number of additional sources of disturbance are present on the telescope. These include those caused by cryopumps, steering mirror actuation, secondary mirror actuation, and science shutter actuations and disturbances transmitted through the cabling between the spacecraft and payload.

(4) The acquisition camera will be part of the testbed. The acquisition camera is required to have highly accurate measurements over up to a 60 arcsec FOV to provide for handoff and pointing to the coronagraph. The acquisition camera design is not yet made final, but a simulated acquisition camera will be included in the testbed.

(5) The Fine Steering Mirror (FSM) and Fine Guidance Sensor (FGS) are key to the pointing. The FSM will demonstrate small angle jitter reduction and high accuracy pointing control, in tandem with the FGS focal plane detector measurements and centroiding algorithm. The focal plane is included for demonstration of centroiding accuracy, bandwidth (frame rate), and measurement noise characteristics. The end-to-end performance of the FGS/FSM will need to demonstrate the centroiding algorithm. The focal plane can demonstrate separately centroiding accuracy, bandwidth (frame rate), and measurement noise characteristics. The end-to-end performance of the FGS/FSM will need to demonstrate ~1/300 λ/D centroiding performance as defined by contrast requirements.

(6) Because of the reliance on image shape, a simulation of FGS optical path will be used to produce a simulation of the "spot." This includes the key reference surfaces (such as the reflection off the coronagraph spot), or diffraction pick-off locations used to pick off the science reference star signal. This will be used as part of the test with the FGS. This test may require copies of particular surfaces, including any substrates used as reflecting surfaces.

(7) Isolation of testbed from acoustics and external vibration. This will require both a vacuum and isolation of key testbed components for full demonstration, which may be too expensive for this size testbed; a reduced approach would test the FSM and FGS separately in an isolated vacuum chamber and use measured performance to evaluate overall performance.

The entire spacecraft would be required for full testing. Since this is not feasible, individual components will be tested in a reduced testbed. The ACS of the S/C and coronagraph is as shown in Figure 4-14. The testbed, shown in figures 4-13 and 4-15, introduces realistic disturbances and incorporates key components and measurement (for performance validation) devices.

Progress to Date

This testbed is currently in the requirements definition and planning stage. No other resources have been allocated for this particular testbed activity up to this time. Detailed design work for the testbed is scheduled to begin near the end of Phase A.

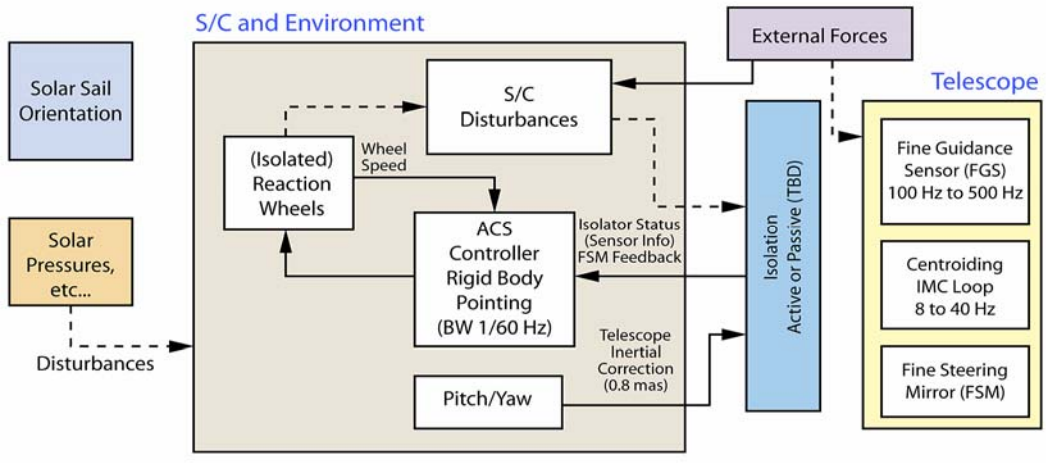

Figure 4-14. Simplified ACS diagram.

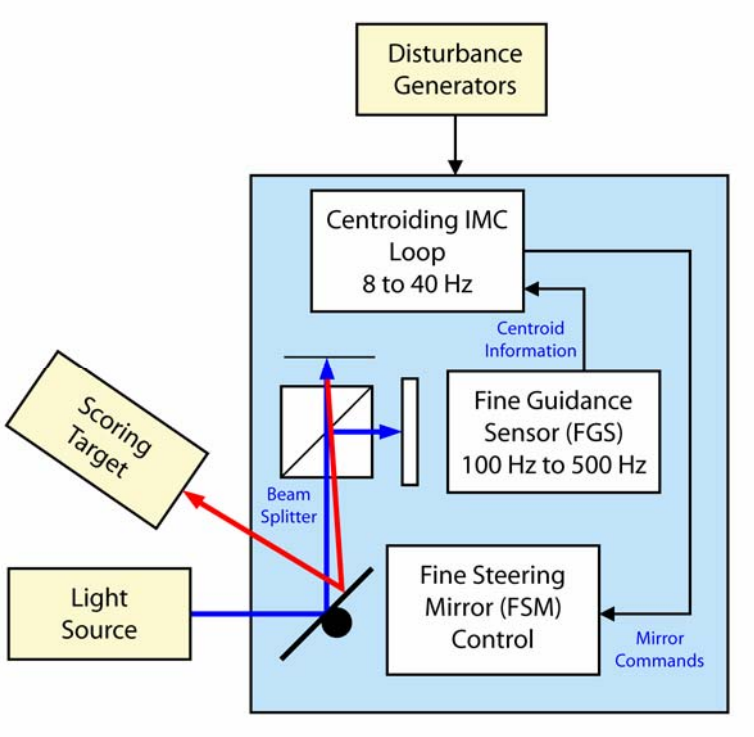

Figure 4-15. Fine Steering Mirror / Fine Guidance Sensor testbed block diagram.

4.2.4 Sub-scale Engineering Model (EM) Sunshield and Isothermal Enclosure

Objective

Successful observations with TPF-C require extreme stability of the wavefront during multi-hour observations. A major source of wavefront instability is thermally induced changes in the optical surfaces and in the structure linking these surfaces together. For example, temperature changes in the PM in excess of 1 mK during an observation are prohibited given the previous error budget, though this is likely to relax by an order of magnitude due to the adoption of the 8^{th} order mask. In order to provide the required thermal stability, a three-fold thermal design approach is taken.

Approach

First, the PM, the SM and the metering structure between them, all of which comprise the OTA, are decoupled from solar radiation by a multi-layered V-groove sunshield surrounding the telescope.

Second, two isothermal enclosures, one of which blocks direct thermal inputs from the Sun and the spacecraft and controls the temperature of the Payload Support System, one of which radiatively bathes the back of the PM with a constant background flux and isothermalizes the PM aft metering structure (AMS), and one of which bathes the back of the SM with a constant background flux, are provided and controlled to the required precision.

Third, precise thermal control of all critical conductive and radiative paths between the spacecraft and the PSS, between the PSS and the AMS, and between the AMS and the SM tower is maintained.

Thermal control of an optical system in a space telescope of the TPF-C size with the required precision has never been attempted, and thermal modeling accuracy is insufficient to eliminate the risk inherent in the thermal design. In addition, it is very unlikely that at the full-scale OTA/Payload protoflight level adequate thermal stabilities can be maintained to allow verification by test/analysis of the thermal system. To retire this risk an approximately $1/4^{th}$ scale testbed is designed (the smaller size permits the external vibration and thermal disturbances to be much better controlled) incorporating the main elements of the thermal design. The intent is to directly demonstrate that the absolute magnitude and stability of the thermal gradients on the PM meet specification in the presence of flight-like thermal loads. However, if local disturbances and test instrumentation result in too much sensor noise to allow flight level performance to be directly measured, the thermal model could be correlated with responses produced by overdriven levels of simulated solar illumination and the flight response levels analytically predicted using this correlated model. Another way of addressing concerns regarding system response below measurement noise floor would be to modulate the thermal disturbance such that the system response could be extracted from the noise and allow model performance to be correlated at flight-level precisions even in the presence of a relatively noisy background. However, the likely relaxation in the required temperature stability due to the use of the 8^{th} order mask makes the need for this test complication much less probable. A diagram of the proposed testbed is shown in Figure 4-16.

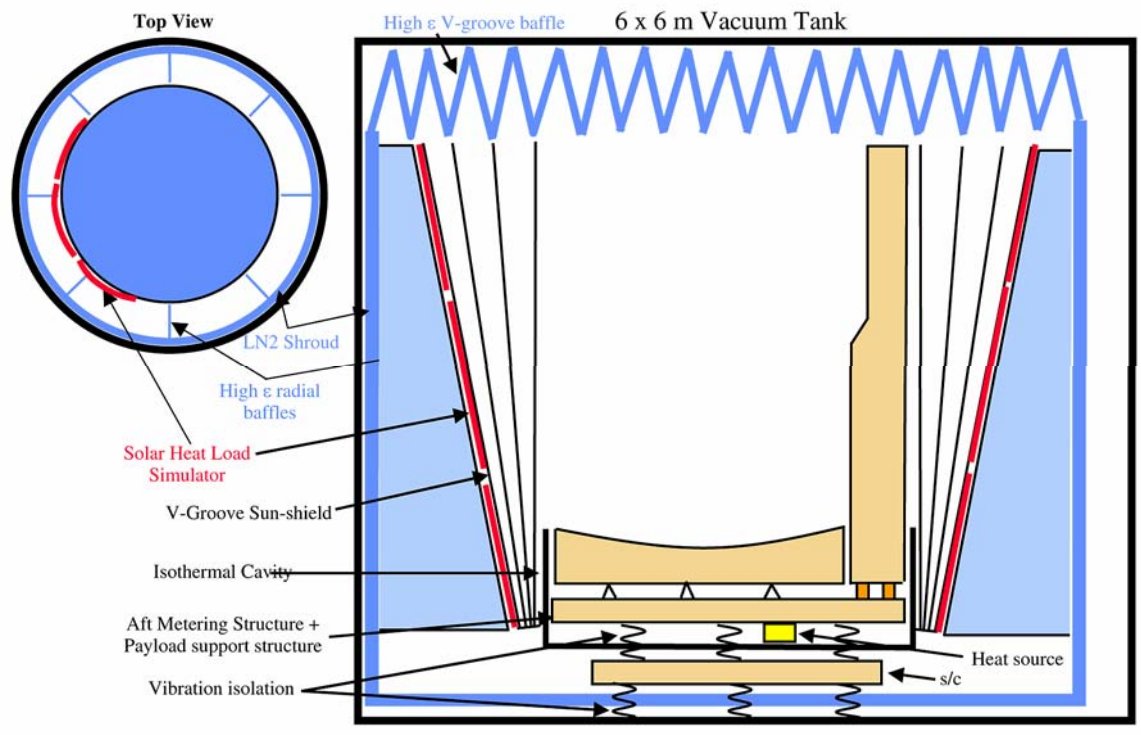

Figure 4-16. Conceptual diagram of testbed to validate the TPF-C Sunshield and Isothermal Cavity thermal design. The object is to determine if, under flight-like thermal loads, the mirror temperatures can be maintained stable to within the required sub-milli-Kelvin limits.

The testbed is located inside a large ~6-m wide, ~6-m high thermal vacuum chamber. The sunshield is simulated by conically symmetric and concentric sheets of material of high specular reflectivity with an opening angle between each sheet of ~3 degrees. The inner surface of the inner sheet is a high emissivity surface (black) which serves an additional purpose as a visible light baffle. If additional optical baffling is added to the design in the future, it would be included in the testbed. The PM is simulated by an approximately 2-m circular mirror with a structural design similar to the PM. It is not required to be figured, but may need to be polished and coated. The simulated mirror is instrumented with temperature-measuring devices with tens of micro-Kelvin precisions. Thermal simulations of the spacecraft, AMS, and payload instruments are included, as are their thermal enclosure and relevant conduction paths. This package is surrounded by cold shrouds intended to simulate as well as possible the cold heat sink of space. Etched foil Kapton film heaters are attached to the outer surface of the outer most sheet, which can be controlled to simulate solar heating at differing spacecraft angular orientations with respect to the sun.

Figure 4-17 shows the modeled steady-state thermal distortion response of a 6 m × 3.5 m PM to a 20-degree rotation of the telescope around the z-axis (the dither maneuver). The displacements are 0.53 pm rms and 1.9 pm peak-to-valley. The corresponding total range of all temperature changes in the PM is approximately 0.26 mK. These displacement levels are characteristic of those that must be maintained during exposures ranging up to 24 hours. It is not clear that system noise can be made low enough to detect temperature variations of this magnitude.

The components needed to build the Isothermal Cavity portion of the testbed (thermometry systems good to a precision of ~0.01 mK and PID controllers good to ~0.05 mK) are felt to be in the 4-5 TRL range based on an initial industry survey. The Microwave Anisotropy Probe (MAP) flew sensors with precisions of 0.1-0.2 mK based on integrations times of less than one second,

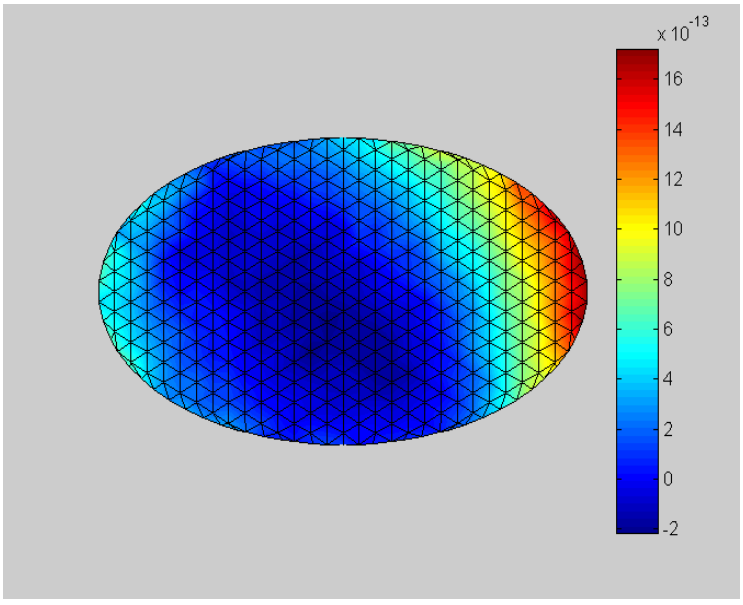

Figure 4-17. Steady-state thermal distortion response of the primary mirror to a 20 degree dither.

giving confidence that flight temperature sensors in the precision range needed are likely reasonable. Some level of flight qualification testing is likely to be needed on these testbed components during Phase A in order to reduce the risk of a problem being encountered during the later flight/protoflight unit qualification tests.

The V-groove sunshield will be fabricated from plastic (mylar or Kapton) film and overcoated with vapor-deposted pure aluminum or gold, such as has been used in flight thermal blankets for many years. The outer surface will most likely be a silver-Teflon second-surface mirror, which also has many years of spaceflight history. V-groove shielding is being implemented on the European Space Agency's Planck observatory, scheduled for launch into the L2 orbital environment. In this case, however, the individual shields are made from rigid aluminum honeycomb material, with the face sheets somewhat polished and coated with vapor-deposited aluminum. The closest technological neighbor to the TPF-C sunshield is that being developed for JWST. The deployment scheme for JWST has been developed and successfully tested at half scale. The primary differences between the JWST and TPF-C sunshields lie in their deployed shapes and number of layers. The TPF-C has more layers and is deployed into a basically conical shape. The deployment challenges are considerable and are the subject of study on several fronts.

4.2.5 Sub-scale EM Primary Mirror Assembly

Objective

This activity constitutes an extension of the testbed described above (Sub-scale EM Sunshield and Isothermal Enclosure). The object is to test for wavefront stability using representative optics in the Sunshield/Isothermal enclosure testbed and change the simulated solar illumination to approximate the dither maneuver. In this case the flat mirror is replaced by a high-quality (λ/100, TBD) spherical, ~f/1 mirror with construction similar to that of the flight TPF-C PM.

Approach

For this test the testbed in Figure 4-16 above is augmented by an interferometer placed at the mirror center-of-curvature with provision for isolation from the ambient vibration background, and by a laser metrology truss to measure displacements. This is done to eliminate vibration as a significant source of noise in the optical signal. The changes are shown in Figure 4-18. Again, all conduction paths must be simulated, including mirror actuators if these are included in the TPF-C design. Two stages of vibration isolation are provided to permit injection of a vibration signal equivalent to reaction wheel noise into the simulated science payload. Care is taken to minimize the heat entering the cold cavity from the interferometer in order to reduce thermally induced noise in the reflected wavefront. The interference pattern developed by the interferometer will measure the departure of the mirror surface from its ideal shape. The change in the pattern induced by changing the spatial distribution of the heat input to the simulated sunshield will be a measure of the effectiveness of the thermal design.

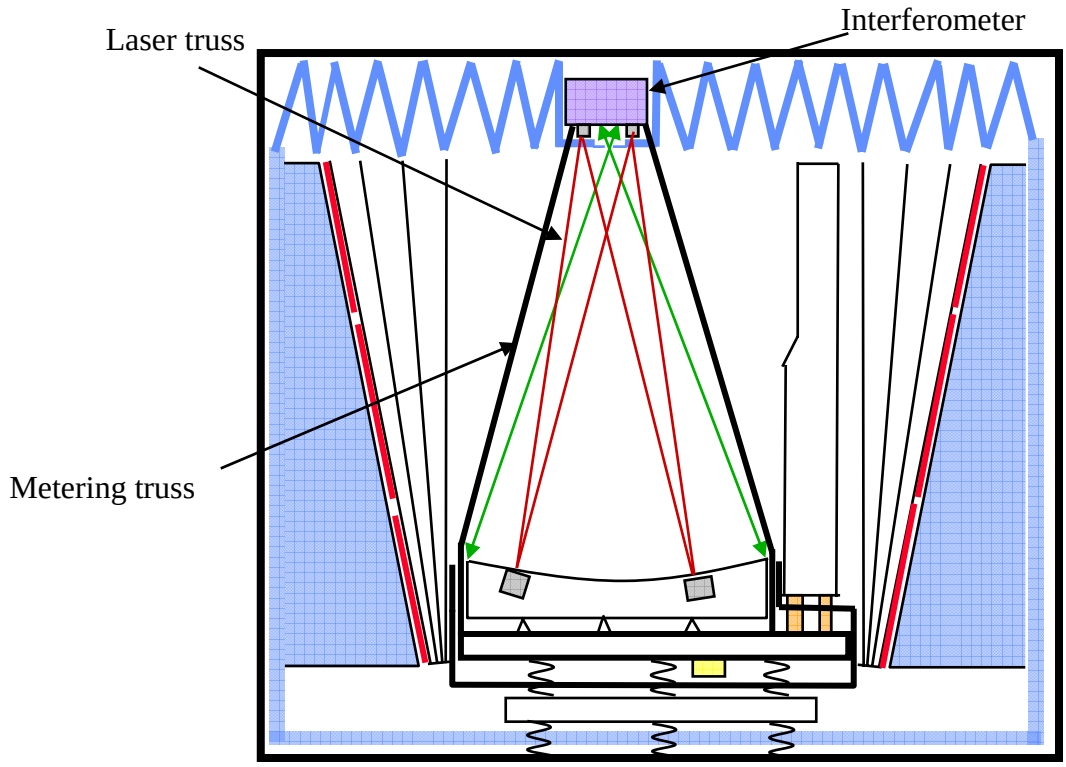

Figure 4-18. Sunshield/isothermal cavity performance testbed evolved to test the optical stability of a quarter-scale mirror representative of the TPF-C primary mirror.

Surface changes of 0.2–0.4 nm can be tolerated during an exposure, up to 24 hours and including a dither maneuver. The test will therefore be looking for thermally induced surface deformations of this size at low spatial frequencies. Relevant heritage for measurement accuracies of this level is only currently being established. Researchers at the National Institute of Standards and Technology have measured the surface of a 30-cm flat mirror at room temperature with an error of 0.2 nm (not yet published). Blake et al.[33] measured a 17-cm flat mirror at 30 K with an error of 1 nm. The test optics in these cases were comparatively small, allowing variables in the test to be tightly controlled. Measurements on a larger mirror (~1.4 m), the Advanced Mirror System Demonstrator (AMSD), at cryogenic temperatures, have error bars of 14 nm.[34] The test proposed here on a 2-m sphere represents a challenge to current measurement capabilities. We propose to largely eliminate noise in our measurements due to the support structure between the test mirror and the wavefront sensing device by employing a laser truss to control a hexapod support of the wavefront sensor. This technology is proposed to control the position of the secondary mirror in the TPF-C telescope. A subscale demonstration is discussed in Section 4.2.1. An independent laser system will measure the effectiveness of the truss. In addition tight thermal control of the wavefront sensor assembly and frequency control of the light source will reduce noise from these sources. Detector noise will be minimized. This test does not require a very accurate figure; $\lambda/20$ will suffice since the objective of the test is to track changes in the surface shape. However, good

[33] Blake, P. et al., "NIRSpec Mirrors Cryogenic Testing Final Report," Goddard Space Flight Center, 2005.
[34] Reardon, P.J et al., "Advanced Mirror System Demonstrator Cryogenic Error Test Budget," *SPIE Proceedings* 4850, 2003.

surface polish is nonetheless required to minimize fixed pattern noise. This test cannot measure thermally induced wavefront changes on the order of λ/10,000, (the magnitude of change that is relevant to successful coronagraph operation). If the spherical mirror is manufactured to λ/100 rms at MSF, then it is possible that thermally induced changes on the order of λ/1000 can be tracked. Thus, this test is a thermal "overdrive test," and the results can be correlated with the thermal system model. Likewise, simulated wheel noise excitation of the testbed can only be an overdrive test.

An alternative approach is to employ the TDM in a separate test that addresses mirror stability in a room-temperature vacuum chamber. The test (like the baseline approach) requires high-precision thermal control of the mirror and the ability to apply localized, measurable temperature gradients on it. The wavefront measurement interferometer/camera is placed at the center of curvature, and its position is monitored with laser metrology, as with the baseline. The advantage of this approach is that it separates the mirror stability test from the complications presented by the cold thermal-vac chamber and hardware in the Sunshield/Isothermal enclosure testbed. Testing would entail heating the mirror in a known, measurable way while monitoring the shape of the optic. Depending on camera-to-mirror metrology precision, focus may not be measurable, but other low-order aberrations (e.g., astigmatism, coma) can be measured and compared to model predictions. The test yields the sensitivity of the mirror to thermal deformations and validates our modeling approach. However, the advantages are somewhat offset by the long radius of curvature of TDM: 7.2 m. This means that the vacuum facility is an 8–9-m-long vertical vacuum chamber. This test also does not allow the mirror to see a cold background nor is it as highly integrated as the baseline test in the cold chamber.

Progress to Date

To date, work has resulted only in the definition of the measurement goals and the conceptual design of the testbed. See the Sub-scale EM Sunshield and Isothermal Enclosure discussion in Section 4.2.4 for information on the development of that portion of the testbed.

5 Integrated Modeling and Model Validation

5.1 Technology Rationale

Because of the size and complexity of the TPF-C design concepts, the end-to-end system will never be tested on the ground. The project will have to rely heavily on the use of engineering and science simulations to predict on-orbit performance requirements from the lowest level of assembly on up. Furthermore, current understanding of the system indicates that the 8-m class optical system needs to be as stable as picometers in wavefront and sub-milli arcsec in pointing. These extremely small requirements impose on the models a level of predictive accuracy heretofore never achieved, especially in the area of microgravity effects, material property accuracy, thermal solution convergence, optical diffraction and polarization effects, and all other second order physics typically ignored. This further imposes extreme challenges on the approach to experimental validation of models, since ground testing conditions and sensor accuracy will often exceed performance levels expected on orbit. The TPF-C technology plan will address the means by which models and analyses will be validated to meet the mission needs.

For full verification of the on-orbit performance, analyses will have to incorporate all the sub-system features leading to an end-to-end simulation as depicted in Figure 5-1.

Analyses will not be limited to predicting the end-to-end TPF-C system contrast, but will be extended to simulate the full planetary signal extraction process, incorporating planetary system models as well as the complete on-orbit observational maneuvers for speckle removal. This implies that new modeling tools and analysis paradigms, which emphasize computational accuracy, and fully integrated simulations will have to be developed.

The goal of the Integrated Modeling and Model Validation Technology is to develop and validate on testbeds a modeling methodology which authenticates the processes and models that will eventually be implemented for predicting the TPF-C flight performances. This will involve modeling the testbeds to the best of our ability by comparing measured and predicted performances, quantifying Modeling Uncertainty Factors (MUFs) to reflect where the agreement between the model predictions and measurements break down, incorporating the MUFs within the testbed requirements to validate the error budget allocation process, then incrementally implementing the same procedure to build up the flight system models starting with the flight materials characterization through to model validation of progressively higher levels of flight hardware assembly.

TPF-C is planning a suite of ground testbeds through which various aspects of the models and simulations will be verified and validated. Because it will be difficult, if not expensive or impossible, to duplicate the expected on-orbit environment, a large part of the technology development effort will be devoted to validating scaling and sensitivities of models. Technology developed on these testbeds will then be carried later into the ground testing activity of the actual flight system, as required by the Verification and Validation (V&V) process in Phase B and beyond.

Model validation needs will not push the performance levels of the testbeds beyond what is required from the flow down of the error budget. However, model validation will influence the design of the testbeds in that they will need a sufficient level of adjustability, modularity and testing flexibility to investigate the existence of the individual physics contributing to the analytical predictions, to their sensitivities, and to their scalability. Capabilities will be introduced in the applicable testbeds to investigate the modeling of the interfaces between components. It is also expected that these testbeds will be instrumental in uncovering "unknown unknowns" not initially anticipated in the models, and to that effect, there will be a continuous process within the model validation activity to re-evaluate what critical physics or assumptions have not yet been incorporated into the analyses.

Previous sections have outlined the link between the various testbed measurements and model validation. The exact details on the testing approach and performance levels required for model validation will be defined through a scheduled ongoing process of flowing down, through

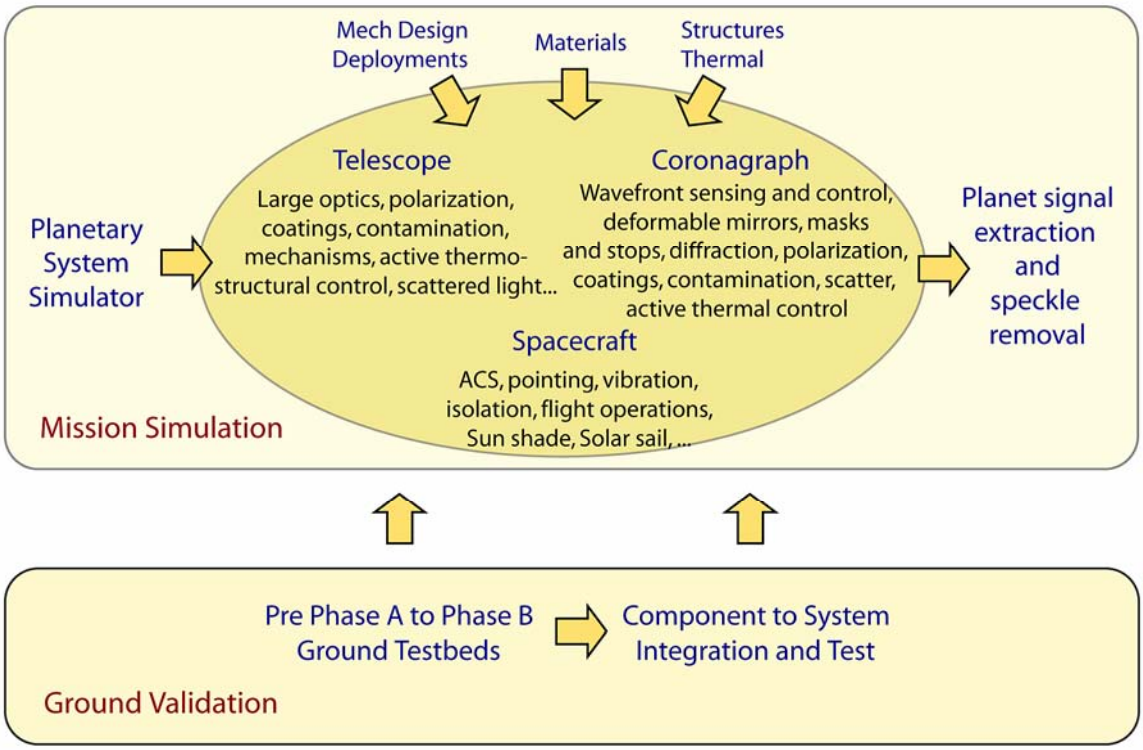

Figure 5-1. TPF-C Modeling and Simulation Roadmap.

analysis, the flight system requirements to the system testbed performance. This process is in progress. Some requirements are understood for the near-term model validation activities, e.g., limits on the variability of optical material CTE, and some are clearly less defined, e.g., larger testbeds planned for Phase A-B. The requirements for all the testbeds will be firmed up as soon as the flight design and flight performance requirements are formally established.

By the end of the project, the primary questions asked to the analysts will be, "Why do you believe the prediction?" To help achieve this challenge, a novel modeling strategy will be implemented on TPF-C. It is standard practice to include hardware fabrication tolerances as margins within the error budget. For TPF-C it is proposed to treat models as "software fabrication" by including additional margin in the error budget to account for modeling tolerances, *a.k.a.* modeling uncertainties. This implies that the accuracy of the prediction will be quantified by tracking contributions to the modeling errors during the project lifecycle.

Because the system performance objective now takes into account the predictability variances of the analysis, the design goal is no longer to select the design which meets the best nominal performance, but one that meets the best bounded performance including the modeling uncertainty. This means, for instance, that from the view point of predicting performance and meeting the error budget, a low CTE material having high variability and high uncertainty may not be as good a design choice as a higher CTE material with low variability and low uncertainty. Additional examples of modeling uncertainties include the nonlinear mechanics of hinges/latches, damping, etc.

The concern that arises from this new modeling paradigm is the issue of "over-designing" the system by imposing tighter nominal performance requirements to make up for larger margin allocations in modeling uncertainties. This unfortunately is inevitable when analysis is the only means to validate on-orbit system performance, as it will be for an increasing number of flight systems in the future. The best that can be done to alleviate this concern is to address the problem up front, and to devise means by which modeling uncertainties can be evaluated, tracked, and, especially, reduced to minimize its overall contribution to the margin. It is recognized that modeling uncertainties will be naturally reduced through the course of the Project as testbeds and design mature. Nonetheless, there will still be residual uncertainties in the prediction of those flight performances that can only be validated through analysis, and those need to be accounted for in the V&V process.

The overall margin allocation strategy is the responsibility of the Design Team and will not be discussed herein. At this time the design of the Baseline Mission concept is not mature and the margin philosophy has not yet been agreed upon. Nonetheless, eventually the Design Team will identify the required margin and levels of Modeling Uncertainty Factors (MUF) to achieve the mission. A future version of the Technology Plan will then be able to expand on how the required MUF levels will be validated. For now, the plan will focus on the approach and the testbeds planned for model validation. The current version of the error budget requirements will be used to illustrate the levels of magnitude expected from the model validation activity, but should not be considered as the definitive model validation technology requirements.

This paradigm is fairly new to NASA missions, with JWST and SIM using engineering judgment to define empirical uncertainty bounds through the mission lifecycle. Because the TPF-C requirements are in a realm where there exists no past experience from which to develop

engineering judgment (i.e., 10m class deployable structures, sub-mK thermal stability, pm mechanical stability, and sub-milli-arcsec pointing stability), the Project will devise a more rigorous approach to defining and reducing uncertainties. The plan is to:

1. Develop analytical techniques to propagate and evaluate uncertainties
2. Develop models and error budgets for each of the testbeds from which uncertainties are evaluated by comparing predicted results to experimental data – this implies that some testbeds will have to perform to flight levels if not better, or that scaling laws will have been defined
3. Most importantly, develop methods of reducing uncertainties by validating physics, by improving modeling tool accuracy and by proposing design options that minimize uncertainties

One such means of reducing modeling uncertainty is to allow on-orbit adjustments through control strategies, either active or passive. Current design features include the active deformable mirror for wavefront correction, active thermal control of the secondary mirror assembly and the aft-metering structure, active position alignment of the secondary mirror tower, and active vibration isolation of the reaction wheel disturbances. In these instances, the control errors will define the performance uncertainties. TPF-C will continue exploring, when necessary, other mitigating design solutions which implement control strategies for on-orbit adjustments. Other features that could be considered, but are not yet part of the baseline design of TPF-C, are active or passive structural damping, active wavefront control of the primary through mechanical actuators or distributed thermal control, or active wavefront control through a two-stage deformable mirror.

In effect, the TPF-C modeling challenge is now turned into validation of analysis bounds, whereby the uncertainty needs to be quantified and managed in the error budget by propagating error contributions from the lowest level of assembly on up. Another implication of this new modeling paradigm is that modeling margin allocations will be used to derive levels of accuracy required from the model validation, as well as the measurement accuracy of the test facility itself. Questions regarding what constitutes a validated model have plagued projects in the past. Through the use of the modeling error margins, we will now be able to derive rational and consistent acceptance criteria for the validation and delivery of models.

In summary, the most critical issues for modeling technologies on TPF-C include, in no particular order:

1. Development of multi-disciplinary integrated analysis tools with precision numerics
2. Precision measurements of material properties (thermal, mechanical and optical) including assessment of variability, wave length dependencies and dimensional/temporal stability
3. Validation of the physics described in models, such as mechanism frictional stability, scattered light behavior, contamination, sunshade thermal performance, polarization propagation, electromagnetic masks and stops models
4. Validation of scaling laws used to extrapolate results from the ground to flight:
    - Scalability to environment: 1-G to 0-G, thermal gradients, milli-G to nano-G jitter, air to vacuum

- Scalability to amplitude: link nm test validation to infer pm performance when ground disturbances or measurement sensors do not meet TPF-C performance specifications
- Scalability to size and geometry: partial or full-scale component testing
- Scalability to the level of assembly: validate component models on subsystem tests, and validate interface models at system tests.

5. Development and validation of multi-disciplinary model uncertainty propagation methods.

Testbeds and breadboards needed to validate these most critical modeling technology risks are defined herein. The testbeds will also be used to demonstrate the error budget allocation and validation process, including propagation of modeling uncertainties, and to refine test/analysis correlation techniques. As the design of TPF-C matures, test/analysis validation of the actual hardware and instruments will be defined in more detail in the V&V matrix, culminating with the final I&T at the highest level of assembly possible.

5.2 Technology Goals

The primary goal of the Modeling and Model Validation (M&MV) Technology element on TPF-C is to demonstrate the efficient and accurate end-to-end (e2e) predictive capability within prescribed modeling error tolerances (uncertainties). The main metrics of interest are contrast and WFE, and thus contributions from all subsystems and physics impacting the e2e prediction of these metrics are included in the technology development plan.

In demonstrating this goal, approaches will be developed and validated to scale and stitch together ground test results for e2e flight system performance prediction, and analysis tools will be developed which meet TPF-C specific needs.

The two derived goals of the M&MV technology development effort are: (1) to provide inputs to the system engineer/architect for acceptance criteria for model verification and delivery, and (2) to provide inputs to the design team for selecting design options that reduce modeling uncertainties by building a system that is predictable and/or controllable, and which avoids over-designing the system by implementing e2e design optimization and margin management.

5.3 Modeling Methodology Validation

Each M&MV methodology on TPF-C falls into one of three broad and distinct categories, each of which represent the individual technologies required for successful delivery of a validated system model:

1. Development and validation of analysis tools
2. Characterization and validation of basic physics models
3. Validation of models and scalability on component testbeds.

Each of these M&MV technology areas is described in more detail below, as well as the approach by which it will be validated. Although there may appear to be overlap in the sub-

categories, in reality each of the sub-categories contribute to the three main M&MV technology areas in a distinct manner, as described in the table descriptions for Tables 5-1, 5-2, and 5-3.

Development and Validation of Analysis Tools

This technology area addresses the analysis tools that will be developed and validated in order to meet the TPF-C modeling needs, as summarized in Table 5-1.

The goal is to develop and verify analytical capabilities required for future analyses of the TPF-C flight system and testbeds. These include the ability to efficiently and accurately analyze multi-disciplinary systems in an integrated environment, to develop tools to introduce localized non-linearities and perform time-dependent and transient temperature-dependent simulations, to develop approaches to propagate uncertainties from component level to contrast, and to validate optical analysis tools for diffraction and polarization applications by benchmarking results from multiple codes.

Characterize and Validate Basic Physics Models

This technology area addresses the need to collect physical data to incorporate into TPF-C models at the required level of accuracy, as summarized in Table 5-2.

Table 5-1. Development and Validation of Analysis Tools

Technology	Description	Validation Approach
Integrated Modeling Tool	e2e simulation of thermal, structural and optical performance. Includes capability for multi-disciplinary control and optimization. Requires improved accuracy and effectiveness.	Compare closed form and textbook problems Benchmark with commercial codes Validate predictions on testbeds
Error Budget and Performance Modeling	Error budget allocation process, including sensitivity flow down and margin allocation strategy	Validate HCIT error budget, and exercise error sensitivities and modeling tolerances
Nonlinear Mechanical Analysis	Develop analysis tools to incorporate models of localized non-linearities (e.g., hinge/latch, geometric imperfections, and mirror seal plane micro-cracking), bound μdynamics, and update models from tests	Validate bounding analyses and system response predictions on benchmark problems and on testbeds (Precision Stability Testbed and SM Tower Testbed)
Optical Analysis	Evaluate existing capability to accurately model diffraction, polarization, WFSC, scattered light	Compare benchmark problems on existing codes: MACOS, Code V Validate models on HCIT
Uncertainty Analysis	Develop approach and tools to propagate analytical errors from model form, physical parameters, tool accuracy	Develop benchmark problems Apply and validate results on all testbed models Verify sensitivity to errors in testbeds.

Table 5-2. Characterization and Validation of Basic Physics Models

Technology	Description	Validation Approach
Material Properties	Collect high accuracy material properties for critical thermal, mechanical, and optical analyses. Include assessment of property variability, stability, temperature dependency, wavelength dependencies	Develop error budget for determining measurement accuracy of test facilities. Develop new facility where appropriate and verify results on benchmark materials. Collect all material property information in a Project-controlled document.
Nonlinear Mechanics	Investigate friction models as a function of pre-load, coeff of friction, stiffness, hysteresis, temperature Develop bounding analysis techniques to predict μdynamics disturbances	Validate model sensitivities to driving parameters on generic friction test article. Validate μdynamics bounds and system propagation on generic test article.

This area addresses two sets of particular concerns. The first assures that material properties relevant to TPF-C will be collected and controlled. Specifically, the data needs to be at levels of accuracy consistent with the goal of the end metric (e.g., tolerances in picometers of WFE), and all material property information will be delivered with verified error bars reflecting the test facilities' systematic and random errors.

The second area assures that we develop a physical understanding of what drives nonlinear behavior in mechanisms like hinges and latches or composite subassemblies. A goal is to develop constitutive mechanism models to include in system analyses and to generate component-level requirements on flight hardware that will meet the TPF-C specifications. Of particular importance is the physical understanding of micro-slip, spontaneous energy release, micro-yield, hysteretic behavior, delayed stress relaxation, and all other nonlinear mechanical physics affecting the prediction of structural stability to picometer levels. Another goal is the study of composite material variability and stability, especially at bonded interfaces. Overall, investigations will be performed to establish scaling laws for predicting sub-nanometer and 0-G behavior, and to define component level test protocols for model validation of flight hardware in later phases of the project.

Validate Models and Scalability on Component Testbeds

This area addresses the need to develop and validate component level models on testbeds, as summarized in Table 5-3.

Technologies described previously in the areas of Tool Development and Physics Characterization will be incorporated into component level models for validation in the testbeds addressed herein. Activities under this area include investigation of scaling law when testing conditions do not match flight environments, validation of the error budget architecture and sensitivity propagation, evaluation of modeling error sources and validation of uncertainty propagation methodology, and stitching of the various components and interfaces where appropriate. Since many of these testbeds are design dependent and will eventually be competed to industry, there is very little detail available at this time. However, in later sections of this document, the component testbed descriptions highlight what aspects of model validation will be verified on a case by case basis.

Table 5-3. Validation of Models and Scalability on Component Testbeds

Technology	Description	Validation Approach
Mirror Technology	Optical material and fabrication uniformity, stability, PSD, 1-g sag, coating uniformity ….	Develop models using tools, material properties and optics models validated previously. Use TDM data to validate models and assess performance in flight-like environment.
Coronagraph Technology	Diffraction, polarization, WFSC, coatings, contamination, masks and stops.	Develop models using tools, material properties and optics models validated previously. Use HCIT and Planet Simulator Testbed data to validate models and assess performance in flight-like environment.
Mechanisms and Structures	Validate subsystem model of a full-scale subsection of the SM tower hinge/latch and boom assemblies.	Develop models using tools, material properties and nonlinear latch models validated previously. Establish experiments to validate models and assess performance in flight-like environment.
Thermal control	Demonstrate predictability of thermal models for active/passive control of the isothermal cavity.	Develop models using tools, material properties and thermal models validated previously. Establish experiments to validate models and assess performance in flight-like environment.
Vibration Isolation	Develop models for RWA and active/passive isolators. Investigate possibility for active/ passive damping strategies.	Develop models using tools, material properties and dynamic models validated previously. Establish experiments to validate models and assess performance in flight-like environment.
SM Position Control	Metrology system and performance, actuator models, position control and stability.	Develop models using tools, material properties and dynamic models validated previously. Establish experiments to validate models and assess performance in flight-like environment.

In general, all technology development work for M&MV will take advantage of past and relevant technology developed for other Projects. In particular, we will review model validation work performed under the SIM and JWST projects, and fold into our activity where appropriate. We will also survey industry and academia for availability of test facilities and information consistent with the M&MV technology goals.

5.4 Error Budget Validation

As explained previously, the actual requirements and MUF allocations within the margin have not been defined. As the design and project matures, the V&V matrix will be developed through a systematic approach by identifying which terms in the error budget, starting from Level 2 requirements on down, will be validated by analysis and which will be directly validated by tests. Each of the terms validated by analysis will be linked to a metric, such as contrast, wavefront error, line-of-sight jitter, and so on. In turn, each of these metrics will be associated with a type of analysis (e.g., static errors, thermal distortion analysis, and dynamic jitter analysis), each of which requires a set of parameters and assumptions for the development of the models. In turn, each of the models, parameters, and assumptions used for validating the error budget terms will then need to be validated themselves through a series of tests or testbed results. During this process, MUFs will also be allocated and verified on the testbeds.

In the current configuration, the TPF Coronagraph will operate at 4 λ/D system with an 8m primary to achieve the top level goal of 10^{-11} contrast. Work has yet to be done to flow down these requirements to engineering performance specifications for mechanism and sub-component stability. But based on preliminary sensitivity analyses of the Contrast metric to WFE, we know that expected levels of stability over a 20-deg dither are as defined in Table 5-4.

Table 5-4. Required Stability Levels over a 20-Degree Dither

Description	Stability	Comment
Primary-Secondary Relative Motion	26 nm (z)	SM position controlled to compensate thermal
Primary Mirror Deformation	0.4 nm	3 σ
Structural Deformation (other than secondary)	100 nm / 10 nrad	3 σ
Rigid Body Pointing	4.0 mas	1 σ per axis
Spot Centration on Mask	0.3 mas	1 σ per axis

5.5 Model Validation

Table 5-5 is a matrix summarizing which testbeds will be used to validate the various M&MV technologies described previously. It is shown that there exists at least one testbed to validate each of the M&MV technologies. The model development roadmap is shown in Figure 5-2.

5.6 Progress to Date on Integrated Modeling

Technology infusion is the process of transition of the products, techniques, lessons learned, test environments and personnel from the technology development effort to the TPF-C Flight System. Model validation and lessons learned documentation are considered important aspects of technology infusion and are described in the following subsections.

5.6.1 Modeling Methodology Validation

Because TPF-C cannot be fully tested on the ground, successful implementation of the mission requires that models accurately predict sub-nanometer level performance prior to launch, currently beyond the state-of-the-art. TPF-C will address model development as "software fabrication" by including additional margin in the error budget to account for modeling uncertainties or tolerances much as is done for hardware fabrication. This implies that the accuracy of the prediction will be quantified by tracking contributions to the modeling errors during the project lifecycle. In effect, the TPF-C modeling validation is now treated as validation of analysis bounds, where the uncertainty is quantified and managed by the error budget. Through the use of the modeling error margins, we will derive rational and consistent acceptance criteria for the validation and delivery of models.

5.6.2 Error Budget Validation through Modeling

A systematic approach will be used to identify which error budget terms, starting from Level 2 requirement levels on down, will be validated by analysis and which will be directly validated by tests. Each of the models, parameters and assumptions used for validating the error budget terms, will then need to be validated themselves through a series of tests or testbed results, starting from the lowest level of assembly on up. Validation of TPF-C models will fall in one of two categories, validation of *absolute* predictive accuracy and validation of *relative* predictive accuracy. In either case, the approach implemented on TPF-C will require that validated accuracy be bound by the modeling uncertainties.

Table 5-5. M&MV Technology Validation vs. Testbed Matrix

Testbed Traceability Matrix to Modeling Technologies	Modeling Technologies													
	Basic Physics			Component Models						Tool Development & Validation				
	Material Property Characterization	Non-linear Mechanics	Light Propoagation	Mechanisms & Structures	Thermal modeling and control	Vibration Isolation	Mirror Technology	Coronagraph Technology	Uncertainty Propagation	Integrated Modeling	Error Modeling	Nonlinear analysis tools	Optical Analysis	Uncertaintuy Analysis Tools
Sub-Scale Sun Shield DeploymentTB		■		■								■		
Sub-Scale Isothermal Enclosure TB					■					■				
Sub-Scale PM Thermal Stability TB				■	■				■	■				
Sub-Scale PM Optical Performance TB			■				■		■	■	■		■	■
Closed Loop SM Position Control TB						■			■	■				■
Fabricate EM SM							■						■	
Pointing Control TB						■				■				
Vibration Isolation TB						■				■				■
Precision Hexapod TB				■					■					
SM Tower Partial Structure TB		■		■		■			■	■	■	■		■
Precision Sub-Structure Test Facility	■	■		■					■	■				
Microslip Tribometer		■		■								■		
Dilatometer TB	■													
High Contrast Imaging TB			■					■	■		■		■	■
Planet Detection Simulator			■					■		■	■		■	
Scatterometer	■		■										■	
Technology Demonstration Mirror							■		■				■	
Apodizing Mask & Stops			■				■	■					■	

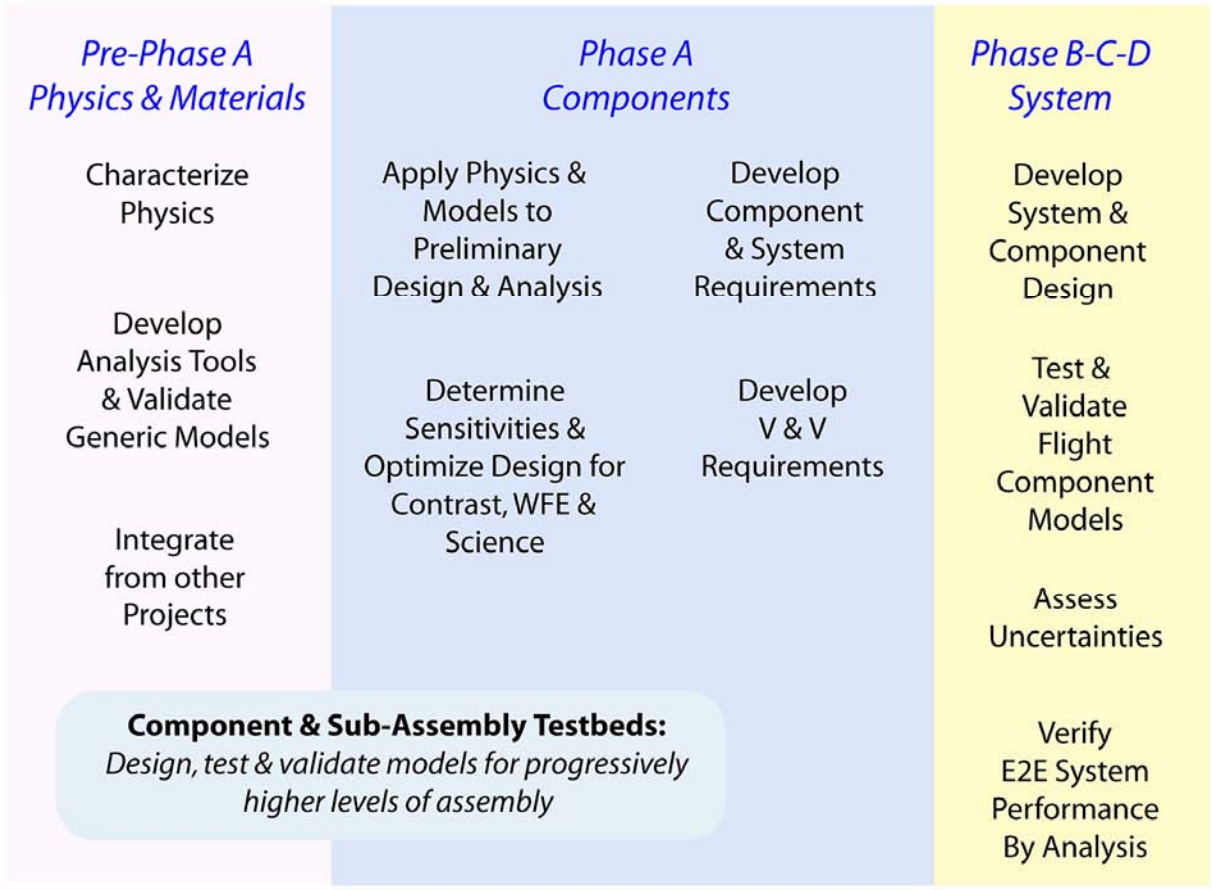

Figure 5-2. Model technology implementation timeline.

5.6.3 Model Validation

The following schematic depicts the overall M&MV technology development timeline as defined by the various phases of the Project. For now the actual schedule of the Phase gates has not been agreed upon, but this information will be included in the next release of the Technology Plan. In terms of the individual M&MV technology validation dates, those are identical to the schedules of the testbeds used for validation. The testbed plans and schedules are described in detail in the previous sections.

5.7 Integrated Modeling Tools

Two concerns that are central to the demonstration of a TPF Coronagraph are the characterization of the telescope system's point-spread function and its stability at a contrast ratio of 10^{-11} over long periods of time in the presence of numerous system perturbations.

From an analytical perspective, a TPF Coronagraph is of particular significance in that it is one of the first in a series of planned future precision optical missions which, given the impracticality of system-level, ground-based environmental testing, will necessarily be launched partly on the

strength of computer simulation and analysis. For such scenarios, system-level mission confidence can only hope to be achieved via:

- Analyses that are based on computational components whose theoretical formulations, assumptions, and implementations are well understood at all levels and which are capable of excellent correlation with available test facility data, to unprecedented levels of numerical precision.
- Knowledge of the range of applicability of the analyses as a result of necessary approximations made in the models and computational algorithms themselves.
- A consistent, computationally-based approach to analysis model parameterization and design space exploration in order to rationally address issues such as error budget limits and the assurance of optimally-tolerant designs.

The objective of this technology development effort will be to produce a general-purpose, common-model capability for precise computation of time-dependent optical aberrations resulting from radiation heat transfer-induced structural deformations. While intended to complement processes built using commercial off-the-shelf-components, it nevertheless seeks to fundamentally address issues relating to multidisciplinary analysis model integration in a manner that fully exploits recent advances in computer science and parallel computing platforms, and is expected to result in an open, extensible code base that can be used for continued methods research and development by other programs.

Progress to Date

In an area as rich in commercially available technologies as is finite element-based structural analysis, development efforts have focused on aspects unique to TPF classes of problems, in areas unlikely to be addressed in a timely fashion (if at all) by commercial vendors. Recent developments include:

- Creation of an open, extensible, large-problem-capable architecture:
  In order to adequately address issues relating to transient thermal stability and its effects on observatory performance, the use of thermal models with discretization levels approaching those of the structural models is anticipated. In addition to the architectural demands placed by such a common-model, integrated approach, the desire to readily extend the code as engineering experience with such systems is gained has led to development of strongly object-based data structures, core computational modules written in C, and Matlab-level hosting for robust extensibility on virtually all code levels.
- Integration with existing engineering processes:
  To facilitate interchange among engineers at JPL and other NASA centers and contractors, input to this new code can be specified using fully data-driven formats in NASTRAN (NAsa STRuctural Analysis) syntax for both model description and solution control. Though this de facto standard for finite element model description has been generalized for the new capabilities developed under TPF (and, indeed, other external code inputs are allowed as well), the approach nonetheless supports the use of existing CAD tools having NASTRAN-based pre- and post-processors, and should facilitate the complementary analyses seen as necessary in helping to achieve system-level confidence.
- Thermal and structural finite elements:

Fundamentally integrated analyses are supported via a set of scalar, 1-D, and 2-D finite elements having both thermal and structural properties. Though one might argue that such development reproduces that which is already available commercially, having an element library that includes, for example, a hierarchical set of 2-D shell elements (linear, quadratic, cubic) with point, edge, and surface structural and thermal loading capabilities readily lends itself to complementary activities. Opportunities for benchmarking, test/analysis correlation, and error investigation that would be impossible were the underlying code available only in a proprietary, closed-source form. Recent examples include investigation of through-thickness temperature gradients and the use of higher-order elements to describe optical surfaces for higher-quality optical aberration calculation.

- Nonlinear transient heat transfer:
  Making extensive use of the preceding components, an extremely high-precision solution procedure has been written at the hosting level with externalized controls for adaptive time-stepping and nonlinear convergence detection and control. Supporting computational modules include routines for automated vehicle orbit positioning, gray-body diffuse view factor calculations (specular exchange coefficients are currently under development), automatic computation of Earth albedo and/or solar flux loads (including re-reflection effects) and radiation exchange matrix generation including multiple radiation exchange cavities. The solution approach and underlying code architecture will allow for other embedded solution types (for example, linear structural thermal deformation calculations for all converged heat transfer solutions), and is expected to provide a basis for automated design sensitivity and optimization analyses for controlled thermal systems.

6 Instrument Technology and Advanced Concepts

6.1 Instrument Technology

An announcement of opportunity for Instrument Concept Studies was released early in 2005 for the purpose of soliciting the best ideas from academia and industry. The instruments defined in these studies along with the technical requirements that their accommodation would place on the observatory system will be considered by the Science and Technology Definition Team for inclusion in their final report. These studies are expected to expose technology needs for classes of instruments, and those identified for the most promising candidates will be addressed when the TPF-C Technology Development Plan is updated next. This section serves as a placeholder for those activities.

6.1.1 Detectors

The PIs of the selected Instrument Concept Studies will be asked to determine detector requirements and assess the needs against the state-of-the-art for fabrication and characterization. If a technology need is identified, a development plan will be added in the next version of this document.

6.2 Advanced Concepts

Currently there are two advanced concepts under development. The visible nulling architecture and the phase-induced amplitude apodization represent alternatives to the baseline coronagraphic approach to achieving the necessary starlight suppression. These efforts are carried as options to reduce risk to the Project through a development ending with proof-of-concept demonstrations.

6.2.1 Visible Nulling “Coronagraph” Testbed

Objective

The object of this technology development is to demonstrate the principle of nulling interferometry as applied to exo-planet imaging at visible wavelengths. The visible nulling testbed integrates all component and subsystem technologies developed for starlight suppression

and is intended ultimately to demonstrate 10^{-10} light suppression to $3\lambda/D$ or better. The testbed demonstrates proof-of-concept control of the amplitude, phase, spectral band pass, and polarization of the light to achieve target performance levels.

Approach

The visible nulling testbed achieves high contrast imaging via interferometry. [35,36,37] Using the telescope pupil, we synthesize a "nulling interferometer-based coronagraph" by dividing the light into two or more copies, applying π phase changes to selected copies, and recombining them with a lateral shear proportional to the required baseline. The pupil overlap region is then projected into the far-field, i.e., sent to an image plane, so that the resulting image is the superposition of the star and planet system with an interference fringe pattern. The star is in the dark portion of the fringe and is deeply attenuated, whereas the planet falls within the light or unattenuated location of the fringe.

Previous nulling experiments used a rotational shearing interferometer and a single mode optical fiber.[38,39] For TPF applications, rotational shearing is not acceptable because of the multiple baselines induced. Consequently, a linear shear is introduced via a modified Mach-Zehnder interferometer.[40]

A coherent array of single mode fibers filters starlight over a wide field of view.[41] Its principal function is loosely analogous to the filtering of scattered starlight in the Lyot plane of a 'conventional' coronagraph. Starlight that leaks past the diffraction suppression of the nulling interferometer is spatially filtered by each optical fiber in the array while the planet light is allowed to propagate without attenuation. The residual leaked starlight is also incoherent with planet light, thus the filtered planet light will focus into an image (a single pixel in the field) while the leaked starlight will be evenly distributed over the field of view. Thus to achieve the 10^{-10} contrast between star and planet, it is sufficient for the nuller to operate at 10^{-7} with the residual light spread over 1000 sub-apertures in the single mode fiber array (SMFA).[42] This fiber array may also be a valuable component in a conventional coronagraphic imaging system.

---

[35] Angel, R. (1990), "Use of a 16-m Telescope to Detect Earthlike Planets," *Proceedings of the Workshop on The Next Generation Space Telescope*, P. Bely and C. Burrows, eds., Space Telescope Science Institute, pp. 81–94.

[36] Angel, J.R.P, and Woolf, N.J. (1997),"An Imaging Nulling Interferometer to Study Extrasolar Planets,"*Astrophysical Journal*, v475, pp. 373-379.

[37] Shao, M., (1991), "Hubble Extra Solar Planet Interferometer," SPIE v1494.

[38] Serabyn, E., Wallace, J.K., Hardy, G.J., Schwindthin, E.G.H., and Nguyen (1999), "Deep Nulling of Visible LASER Light," *Appl. Opt.*, v38, p7128.

[39] Wallace, K., Hardy, G, and Serabyn, E. (2000), "Deep and stable interferometric nulling of broadband light with implications for observing planets around nearby stars," *Nature*, v406.

[40] Serabyn, E. and Colavita, M.M. (2001), "Fully Symmetric Nulling Beam Combiners," *Applied Optics*, v40, pp. 1668–1671.

[41] Shao, M., Serabyn, E., Levine, B.M., Mennesson, B.P., and Velusamy, T. (2002), "Visible nulling coronagraph for detecting planets around nearby stars," SPIE v4860.

[42] Levine, B.M., Shao, M., Liu, D.T., Wallace, J.K., and Lane, B.F. (2003), "Planet Detection in Visible Light with a Single Aperture Telescope and Nulling Coronagraph," SPIE v5170.

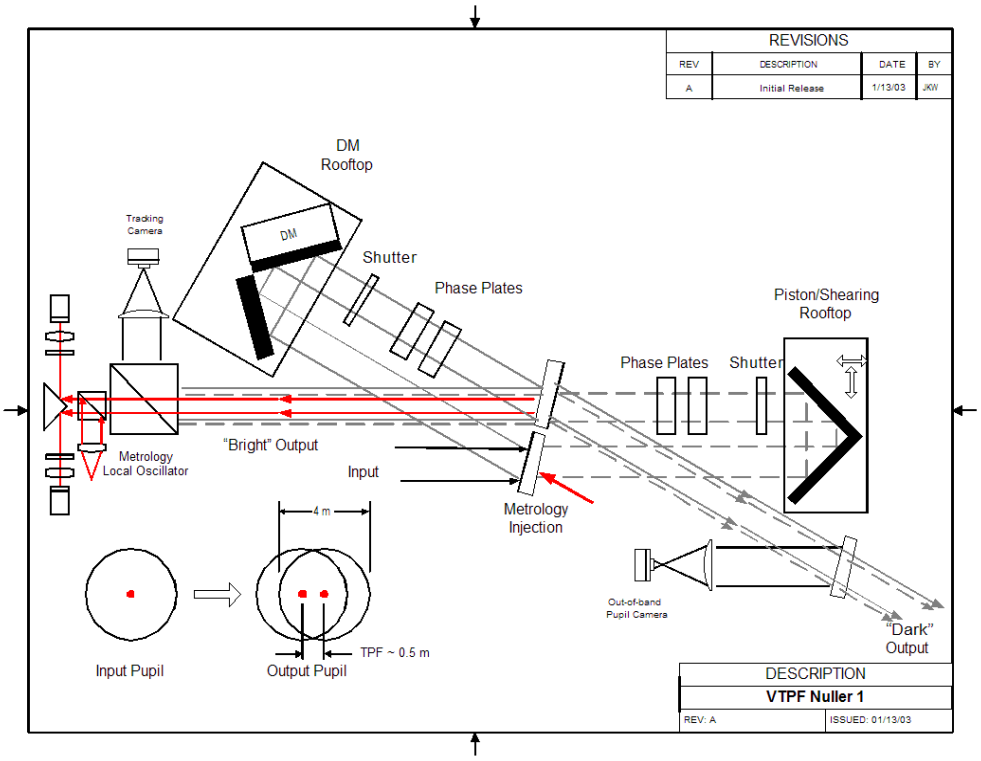

Figure 6-1. Detailed concept for the Visible Nulling Testbed.

Progress to Date

The components of the nulling coronagraph currently under development are the nulling interferometer including the phase plates and the laser metrology system, the single mode fiber array, and the deformable mirror, shown in Figure 6-1. These will all be integrated in the Visible Nulling Testbed in order to demonstrate the full 10^{-10} contrast required for TPF-C.

6.2.1.1 Visible Nulling Interferometer

The nulling interferometer has achieved nulls of 5×10^{-6} in polarized laser light (equivalent to 5×10^{-9} assuming a 1000 sub-aperture SMFA) and 10^{-4} in unpolarized broadband light with a 10% band pass as seen in Figure 6-2.[43] Improved broadband light results are expected with recently upgraded optics and inside a vacuum chamber.

[43] Wallace, .K. (2004), "Experimental Results from a Visible Nulling Interferometer," *Proc IEEE* Big Sky Conference.

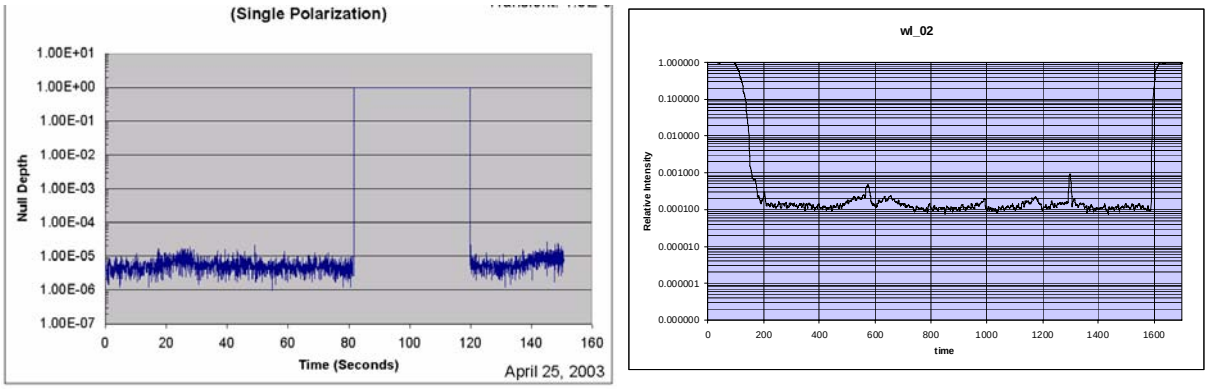

Figure 6-2. Left: Deep nulls from a laser source under control of a metrology system. Right: Deep nulls from an unpolarized white light source at 10% bandpass around 635 nm.

6.2.1.2 MEMS Deformable Mirror

A segmented MEMS deformable mirror (DM) is currently in development led by Boston University.[44] A design has been completed for a DM with 61 segments, each with tip, tilt, and piston, shown in Figure 6-3.

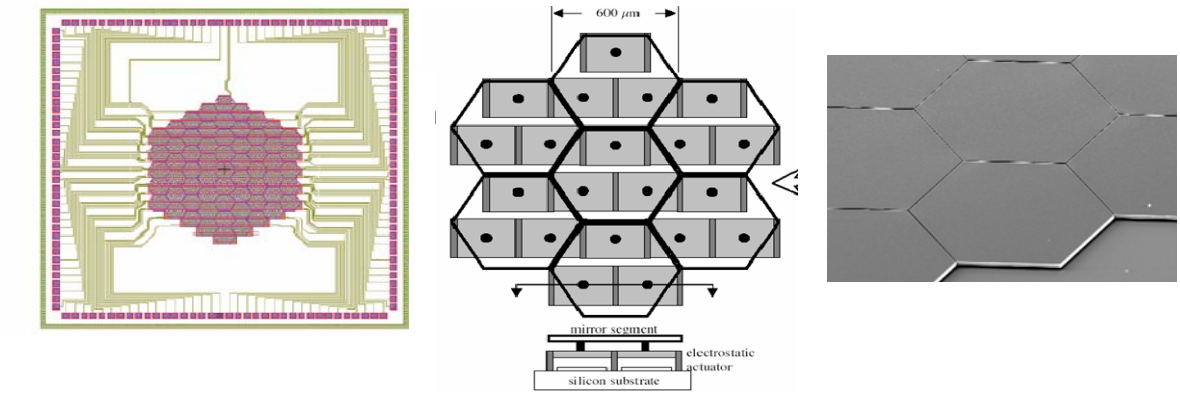

Figure 6-3. Left: Design of a 61-segment pathfinder DM. Center: Schematic placement of actuators under each segment. Right: Photomicrograph of segments from this device.

6.2.1.3 Single Mode Fiber Array

The alignment of the lens array to fiber array must be performed to a precision level of 0.5 μm because the mode field diameter of common visible single mode optical fibers are small and their numerical apertures are relatively large. Currently, two independent technologies are being pursued for the fiber array.[45]

---

[44] Krulevitch, P. A. Bierden, P, A., Bifano, T. G. Carr, E. Dimas, C. E. Dyson, H., Helmbrecht, M. A. Kurczynski, P. L Muller, .R. S. Olivier, S. S. Peter, Y. Sadoulet, B., Solgaard, O. Yang, E. H., 2003, "MOEMS spatial light modulator development at the Center for Adaptive Optics," *Proc SPIE*, 4985, 26.
[45] Liu, D.T., Levine, B.M., Shao, M., Aguyao, F. (2005), "Single Mode Fiber Array for Planet Detection using a Visible Nulling Interferometer", *Proc. IEEE* Big Sky Conference.

The first method is self-assembly with fibers stacked like soda straws within the constraints of a triangular space. In the center third of the triangle, the fibers form a hexagonal array as shown in Fig. 6-4. The challenge is to overcome electrostatic forces to stack successive rows without any placement error. To date, 51 rows have been successfully placed in this fixture to form a 496 fiber array. This method is expected to achieve its goal of 1000 fibers within the central aperture (101 rows on the triangle).

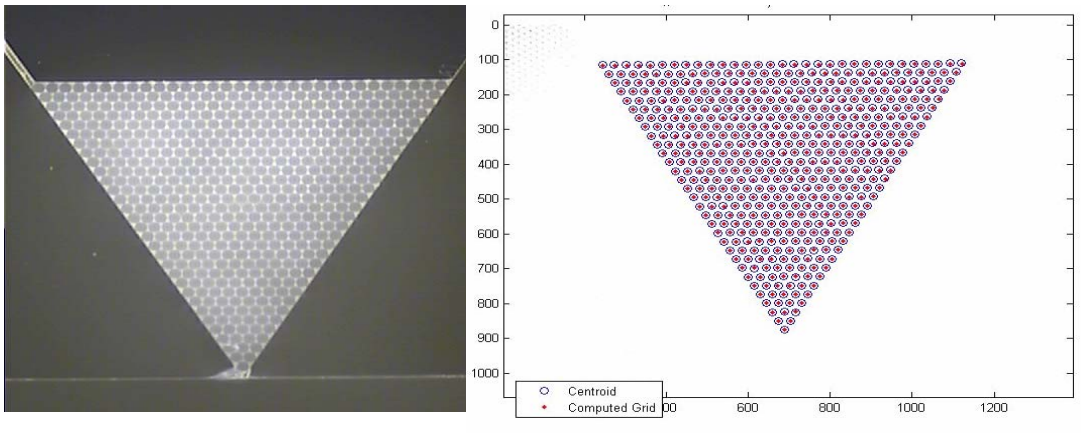

Figure 6-4. The polished end of the 496-fiber array shows effectively 331 fibers within its central hexagon. The fiber-placement error is 2.78 μm rms.

The second method is under development at the University of Florida and uses silicon fabrication technology to etch precision v-grooves on wafers. Fibers are bonded within the grooves to placement accuracies much less than a micron. This method is extended to two dimensions by etching grooves on both sides of a wafer and then stacking the wafers. Progress to date includes establishing the process for precision etching of two-sided wafers. A preliminary 10 × 10 fiber array, shown in Figure 6-5, has been fabricated and is being evaluated.

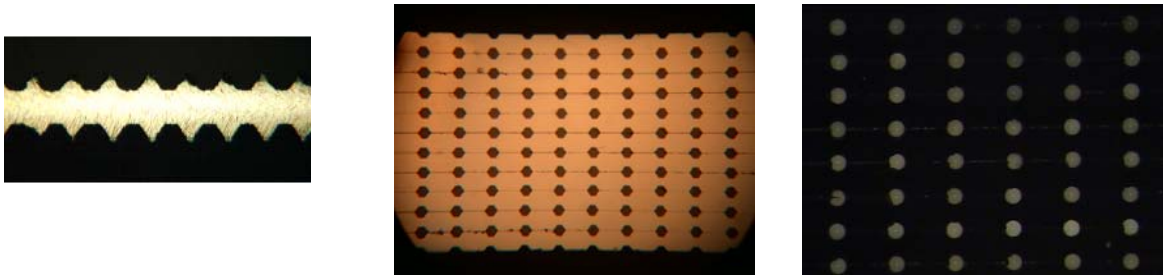

Figure 6-5. Preliminary results of a 10x10 fiber-array fabrication using silicon etching precision v-groove technology. Left: Enlarged image of a two-sided etching of grooves on a silicon wafer. Center: A preliminary array made by stacking multiple wafers. Right: Transmitted light through fibers in this array.

6.2.2 Phased Induced Amplitude Apodization

Objective

The Phase Induced Amplitude Apodization testbed is located at the University of Hawaii. It is being developed jointly by the University of Hawaii (UH) and the National Optical Astronomy Observatory (NOAO) with an independent study taking place at Smithsonian Astronomical Observatory (SAO). The phase induced amplitude apodization (PIAA) concept is an alternative to mask-and-stop coronography that uses aspheric optics to transform the pupil by geometric redistribution of the star light rather than absorbing it. This concept has advantages over traditional coronagraphs and visible nulling because it does not lose any light and preserves both sensitivity and angular resolution, making it possible to use a smaller telescope for efficient exoplanets detection or to effectively observe more distant stars with a same size telescope. This technique also has the advantage that it could be implemented along with a classic Lyot coronagraph or a pupil plane coronagraph by rotating the PIAA optics into the starlight suppression beam path to replace masks and stops. Figure 6-6 shows the three non-interferometric, starlight suppression schemes. The objective of this study is to establish the feasibility of this technique through simulations and laboratory demonstration.

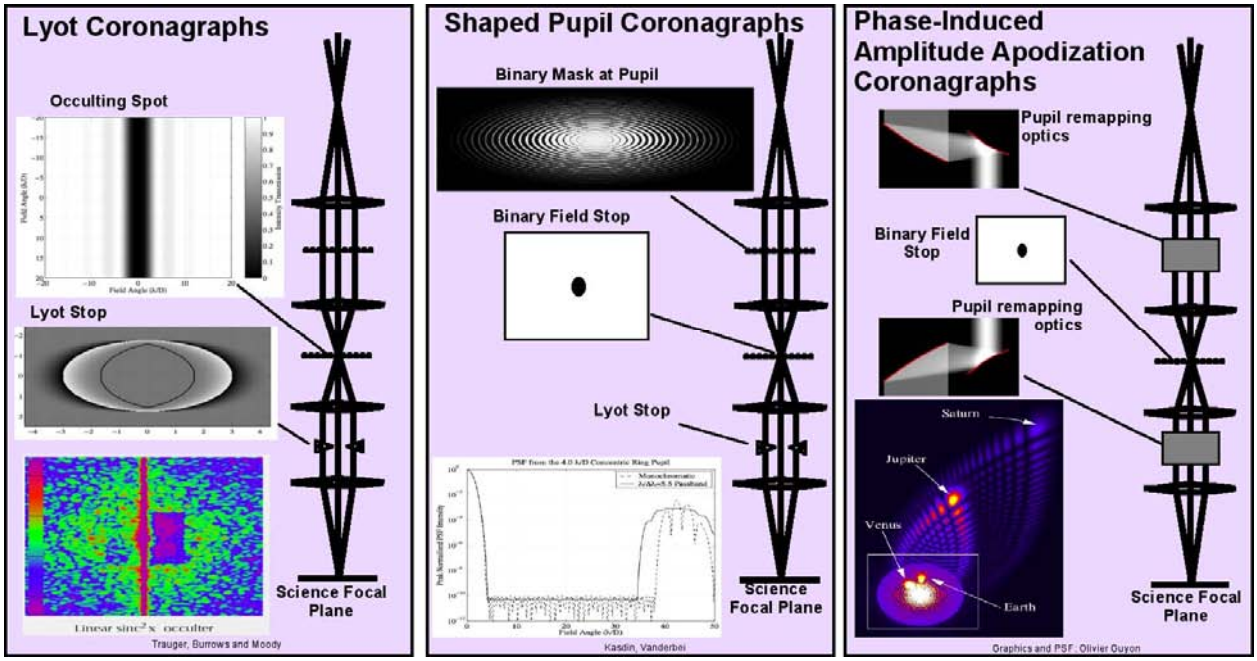

Figure 6-6. Layouts of several starlight suppression architectures.

Approach

NOAO and UH are working together to simulate and demonstrate a fully reflective implementation of the PIAA concept. At SAO, a refractive system is being simulated only, with no hardware implementation. Two phases will be pursued in a testbed at UH. The first phase was a proof-of-concept using low-quality plastic optics. The second phase will be a performance demonstration using fine-quality metallic optics. Fourier optics simulation is being performed on

super computers and is used to develop the shapes for the optics. Software development will be in parallel with the experimental effort. High priority will be given to matching experimental results with the numerical model of the concept.

SAO, working with Princeton, is studying a unique architecture for this concept. The study will include devising a method to minimize the off-axis aberrations and optimize the stellar image concentration. This study will work through mathematical simulations without producing hardware.

Progress to Date

UH and NOAO have built the first phase testbed successfully using low-quality plastic optics. Results from this testbed qualitatively verified the concept and were comparable to the simulated predictions. Figure 6-7 shows a picture of the detector output from this testbed as well as a photo of the optics. The second phase testbed is now underway. The first phase testbed is disassembled while updated component fixtures are being designed and fabricated. Optics have been ordered and are due Summer 2005. A MEMS deformable mirror has been ordered and the electronics and control software are underway. Simulations are continuing.

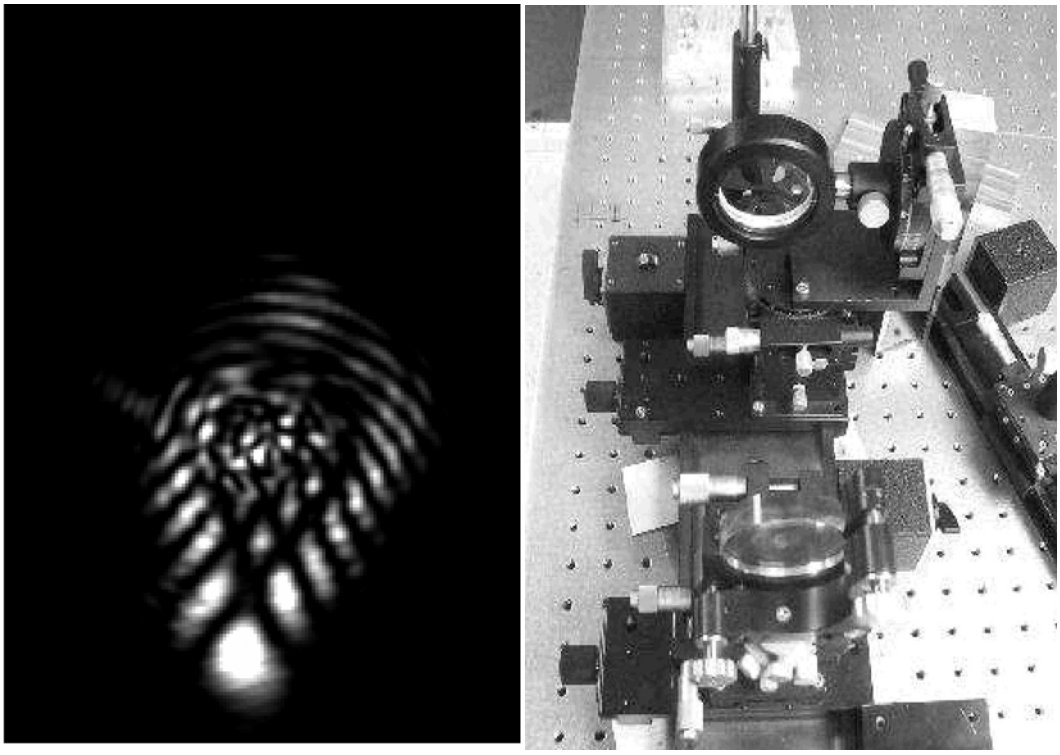

Figure 6-7. Detector output and optical components.

SAO, partnering with Princeton, started on contract in May 2004. To date, they have developed a refractive design with simulated performance that meets requirements within a narrow waveband. Figure 6-8 shows the design. Modeling is continuing with efforts focusing on optimizing the shape of the optics versus performance and fabrication.

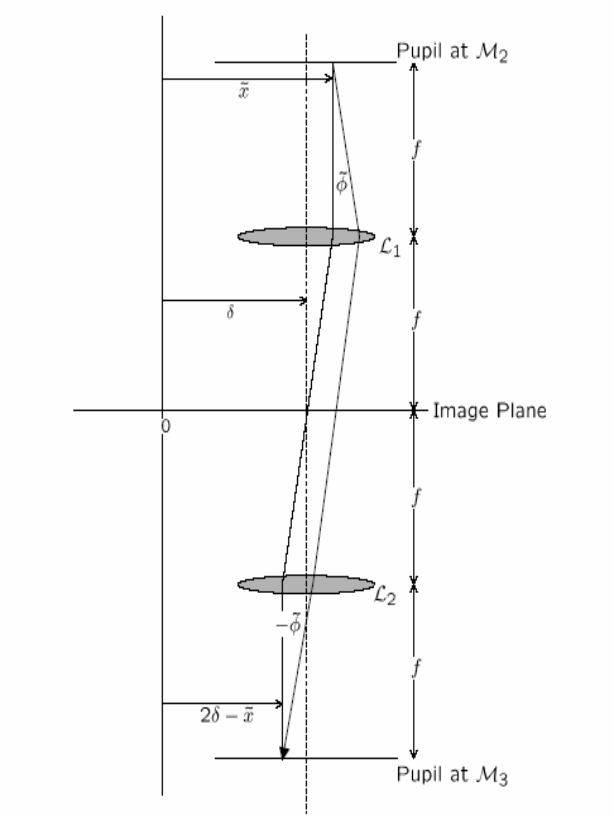

Figure 6-8. SAO refractive design.

Beyond the optimization of the conception design and laboratory demonstrations, there is much research that must be done in order to understand the issues related to system integration, operation and requirements flow down. For example, while conventional pupil-apodized or shaped-pupil coronagraphs enjoy a relatively low level of aberration sensitivity, it is not known whether a phase-induced apodization would offer the same benefits. Areas of needed study are issues related to PIAA optical alignment sensitivity and the PIAA interaction with the wavefront control system architecture that affect continuous, searchable, discovery spaces.

7 Plan for Technology Development

7.1 TPF-C Technology Roadmap

A very preliminary TPF-C technology roadmap based on our early assessment of the technical risks for TPF-C is shown in Figure 7-1. It shows that all the identified technical risks will be retired by the end of Phase B. A number of the testbed facilities used to retire technical risk will be utilized in Phases C/D and potentially even E to test flight units and support observatory level I&T.

As expected, the plans for the pre-Phase A activities are developed to higher fidelity than those for Phase A and B. Below are the pre-Phase A top level development activities, which continue the focus on the detection and characterization objectives described earlier in this document. Adequate progress against the top level technology milestones related to the detection and characterization objectives described in this document is a requirement for entering Phase A. Following is a brief description of the top level technology activities in pre-Phase A, Phase A and Phase B.

Top-Level Pre-Phase A Technology Development Activities:

It will be necessary to demonstrate starlight suppression on the High Contrast Imaging Testbed within an order of magnitude of the flight performance requirement that, in combination with an analytical model that is validated against the testbed, shows flight performance is feasible by end of pre-Phase A. The pre-Phase A testbeds include the currently functional breadboard instrumentation in the HCIT, Apodizing Masks and Stops, Dilatometer, and Scatterometer, all of which will continue to be used into Phase A. The Technology Demonstration Mirror (TDM) is currently in fabrication and testing and will be initiated before the end of pre-Phase A. Definition for a number of Phase A testbeds, including the Instrument Technology and Planet Detection Simulator, will begin as well.

By the end of pre-Phase A, a number of activities will be completed in addition to the technology risk identification and mitigation plan as described in this document. It will also be necessary to have a sufficiently complete and mature design by end of pre-Phase A to show that an exo-planet detection and characterization mission is feasible. Primary mirror procurement strategy must be sufficiently mature and complete by end of pre-Phase A to support the early procurement required to reach launch readiness in 2016.

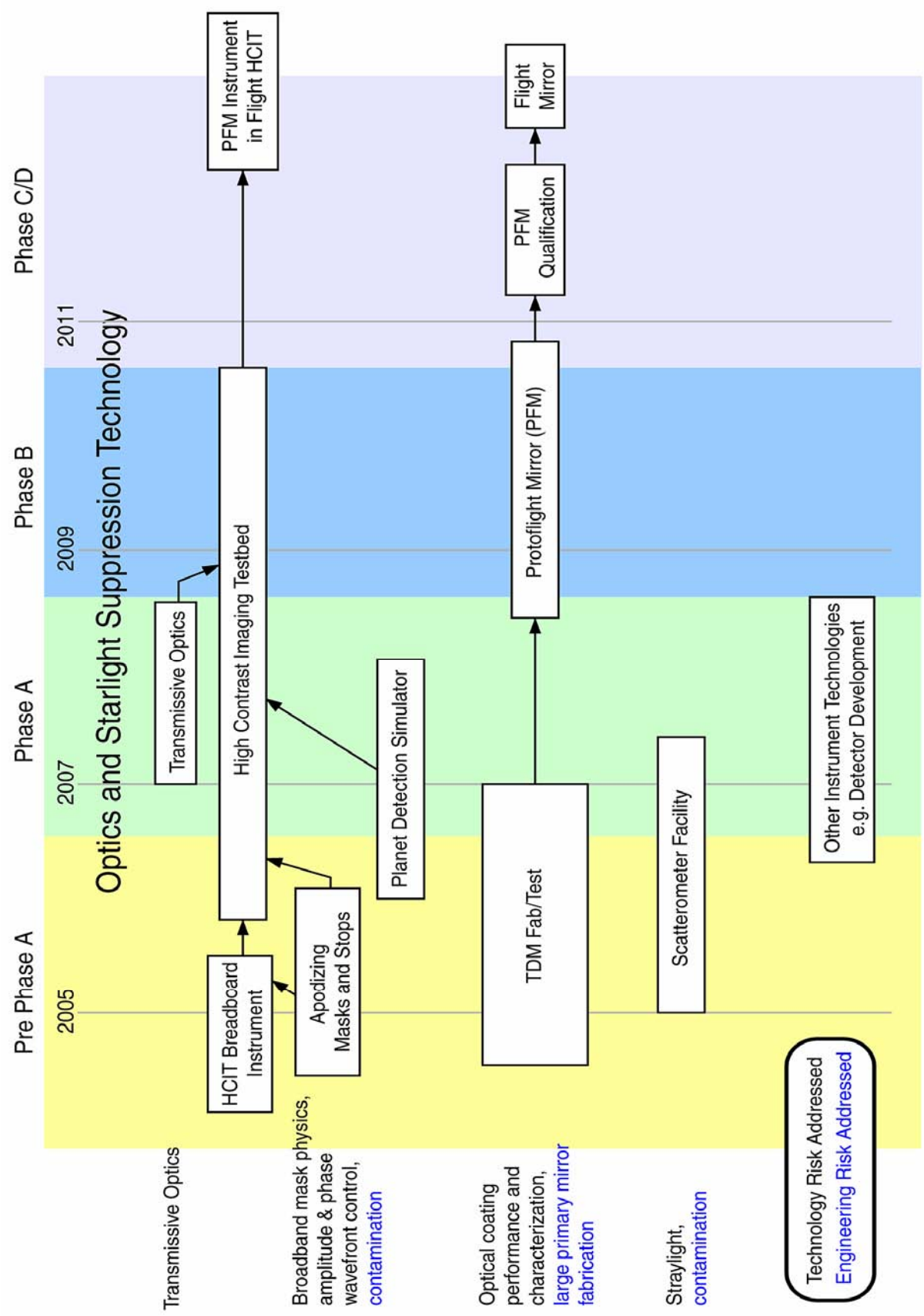

Figure 7-1. TPF-C Technology Development Roadmap (continued on next page)

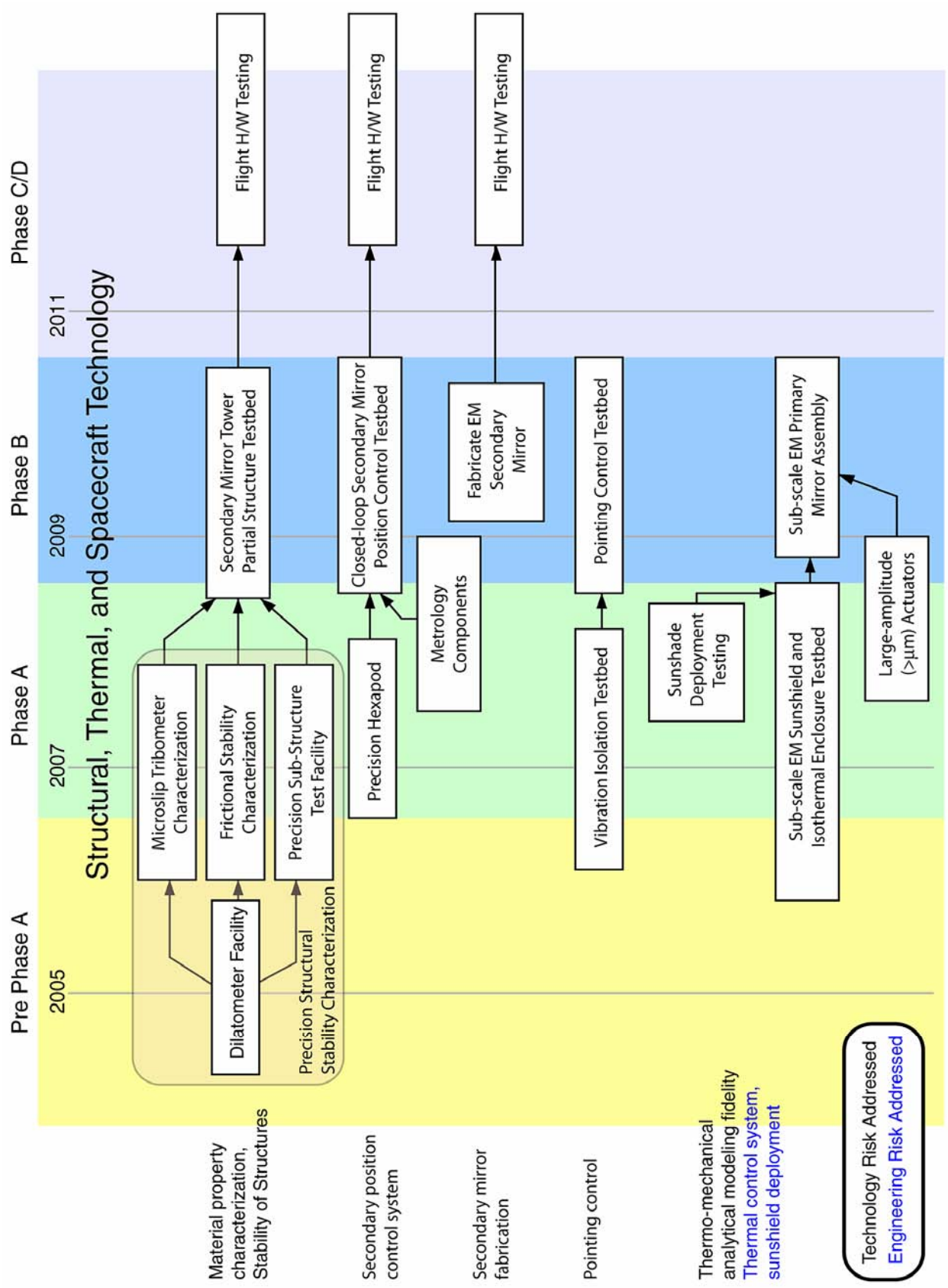

Figure 7-1. TPF-C Technology Development Roadmap (continued)

Top-Level Phase A Technology Development Activities:

For Phase A, the pre-Phase A testbeds (HCIT, Mask Characterization, Dilatometer, micro-slip, and scatterometer) continue to be utilized. In addition, the TDM is fabricated and tested. A laser frequency stability testbed and a precision hexapod testbed are developed. A protoflight primary mirror and mount *may* be initiated during this period. The protoflight mirror (PFM) will be specified to enable flight qualification. The microslip characterization facility is extended to accommodate testing of hinge and latch component microdynamics. Pointing control and subscale thermal shroud testbeds are initiated. Deployment of the sunshade is demonstrated. An effort focused on large-amplitude wavefront actuators is initiated if an actuated PM has been selected. Instrument technology developments are defined and initiated.

Top-Level Phase B Technology Development Activities for the Terrestrial Planet Finder Coronagraph:

As Phase B begins, the work on the dilatometer, the TDM, transmissive optics, micro-slip, mask characterization, and instrument technology has been completed. The HCIT continues to demonstrate masks and deformable mirrors. The laser frequency stability testbed flows into the closed-loop position control testbed. The work on a hinge and latch testbed and the pointing control testbed continues. A thermal shroud will be tested for isolation at a sub-scale level in an overdriven condition and at close-to-flight levels. A sub-scale EM isothermal cavity control system testbed will be developed and extended later through the installation of a sub-scale primary for a full-assembly thermal-stability test. If the project has initiated the development of a protoflight mirror in Phase A, it is expected to be under development though probably not complete by the end of Phase B. The PFM is expected to be qualified for flight in Phase C, thus becoming the TPF-C flight mirror. An EM secondary mirror will be fabricated.

7.2 Pre-Phase A Milestones

7.2.1 Milestone 1: Starlight Suppression on the HCIT

Planned Completion Date: Q3 FY05
Milestone #1 will demonstrate technology for Earth-like planet detection by coronagraphic starlight suppression to a level within an order of magnitude of the required TPF-C contrast at the required angle necessary to distinguish a planet signal from its star.

The HCIT has achieved 0.9×10^{-9} average contrast over an area ranging from 4 to 10λ/D, using a laser source (λ=785 nm). Contrast stability is on the order of 0.5×10^{-10} per hour. In near-term experiments, emphasis will be placed on speckles near 4λ/D, to demonstrate that performance is not near a fundamental limit at those angles. This will complete the milestone.

Monochromatic performance will benefit from the following planned improvements:

- Installation of a 64 × 64 DM, which should improve the contrast by up to a factor of two.
- Improved thermal stability of the testbed components, which will reduce the impact of thermal drift over the timescale of an experiment. The dominant contributor may be the DM, whose temperature variation is a factor of 10 larger than what was seen when testing DMs in a different vacuum chamber. (Actuator gain is a strong function of temperature.)

Improvements to the DM oven are underway. The chamber's thermal control system is currently inadequate to prevent the chamber from tracking changes in room temperature; elimination of this behavior will reduce the temperature variation of all testbed components. If sensitivity analysis and stability experiments dictate, thermal control can also be added to individual optical mounts and the optical bench.

- Improved calibration and algorithm efficiency, which will reduce the time required for an experiment and lessen the impact of testbed instability.
- Recoating the optics will reduce the stray-light level due to obvious contamination on the mirrors.
- Polarization of the input beam, which will improve performance when polarization becomes a limiting error source. A polarization analysis will be conducted for the testbed optical design.

7.2.2 Milestone 2: Broadband Starlight Suppression on the HCIT

Planned Completion Date: Q3 FY06
Milestone #2 will extend the technology demonstration of Milestone #1 to white light, using an optical bandwidth of 60 nm of the required bandwidth and to a level within an order of magnitude of the required TPF-C contrast at the required angle necessary to distinguish a planet signal from its star.

The current performance for white light (40 nm bandpass centered at 800 nm) is 5×10^{-9} contrast, within a factor of 5 of the milestone. The current limiting error source may be red-light leak in the filters or thermal stability of the components.

In addition to the plans discussed in the previous section, broadband performance will be improved by the following testbed modifications:

- Improved filters with reduced red leak (already installed in the HCIT).
- A brighter white light source. A supercontinuum source, which uses a nonlinear fiber to convert Nd:Yag laser pulses to pulsed broadband light (covering 500-1500 nm), is nearing completion. Preliminary testing suggests that this pseudo white-light source will provide greater than 100 times as much power as our current xenon lamp, cutting exposure times from 10s of minutes to 10 seconds.
- Enhanced white-light efficiency via design of an improved illumination system inside the testbed. The simple optical system used to image the fiber onto a pinhole will be replaced with a more advanced design, incorporating achromatic lenses, selectable (fixed) polarization, and finer, remote adjustment of fiber to pinhole alignment in vacuum.
- Improved optics. This will reduce phase-induced amplitude variation, which will reduce the chromatic effects of amplitude compensation. Improved coatings would also reduce these effects. Preliminary modeling suggests that the current HCIT optics are adequate to achieve 10^{-9} broadband contrast, so improved optics will probably not be procured until Phase A.

Other error sources uncovered during error budget development or experimentation will be addressed when needed. Diagnostic hardware will be designed and implemented when necessary to support contrast experiments and model validation.

7.2.3 Milestone 3A & 3B: Integrated Modeling of HCIT and TPF-C

Milestones 3A and 3B will demonstrate TPF-C's technology readiness to achieve system-level instrument performance at the 10^{-10} level. This milestone will be met using a combination of testbed results and models of the HCIT and TPF-C instrument.

Planned Completion Date: Q4 FY06
Milestone 3A will be achieved by demonstrating that HCIT models are consistent with experimental data. An error budget, currently under development, will be used to guide this activity. Each error source will be modeled, and experiments will be devised to validate the model. Data and model predictions ultimately need to match to better than 1×10^{-9} for a bandwidth of 60nm. Initial activity will focus on matching monochromatic performance.

There are two end-to-end optical models of the testbed. A science-oriented model, which uses plane-to-plane diffraction, is well developed and has been used to guide contrast experiments and algorithm improvement. An engineering-oriented model, which provides full raytracing capability in addition to diffraction, is also under development. In addition to verifying the results of the science-based model, the engineering tool enables sensitivity calculations (which can be compared to experimental measurements) and will be linked to structural and thermal models of the testbed in Phase A. Both models will be enhanced with better calibration of testbed components and incorporation of new features. The surface figures of the optics were quickly measured prior to their installation in the testbed; more careful characterization of the optics and their as-built alignments will be conducted. Mask characterization activities and better DM calibration will also feed into the testbed models. The science-oriented model already incorporates the algorithms that are used to control the testbed; these will soon also be added to the engineering-oriented model. A polarization model will be created using different tools in the near term, but eventually that capability should be added to the diffraction models. The results of a stray-light analysis, conducted by a specialist, will be incorporated into the error budget and experimentally validated where feasible.

Planned Completion Date: Q1 FY07
Milestone 3B will demonstrate, using the modeling approach validated against HCIT performance combined with appropriate telescope models and the current mission error budget, that TPF-C could achieve a baseline contrast of 1×10^{-10} at discrete wavelengths and over the required optical bandwidth necessary for detecting Earth-like planets, characterizing their properties and assessing habitability.

7.3 Error Budgets

7.3.1 Dynamic and Static Error Budgets

Scope

Current work is focused on adding new modeling capabilities and validating those capabilities in testbeds. Required models not presently in hand include: models of coating non-uniformities across large optics, stray-light and scattered light models validated at 1×10^{-11} fractional scattered energy, and wave-front sensing and control models that demonstrate the ability to identify speckles at the 1×10^{-11} level.

Presently, there are no models of coating non-uniformities related to large-scale anisotropies in the deposition process. These effects might limit the useful optical bandwidth. Stray light models treat forward-scattered light as being uniformly shifted in phase relative to the non-scattered beam. This approximation must be validated or superseded by new models. Stray-light (multiply-reflected from baffles, edges, etc.) is calculated using standard stray-light software, but the accuracy of the calculations at the 1×10^{-11} level has never been validated.

Model validation for these new models and for existing ones (see below) is of the utmost importance. The HCIT is used to verify/validate the models that are used to predict requirements. These include diffraction, stray-light, scattered-light, polarization, mask performance, and pointing. In contradistinction, the planned subsystem testbeds, namely the sunshield, primary-mirror stability, secondary tower, and pointing-control testbeds, are used to verify that dynamic requirements can be met. Unlike HCIT they do not verify models that are used to predict the fundamental engineering requirements.

The schedule for the dynamic and static error budgets is given in Table 7-1.

State of the Art **TRL N/A**

Static error budget terms are based on near-field propagation models, mask non-uniformity models, polarization ray-trace, and bidirectional reflectance distribution function based particulate-scattering models. The near-field propagation is calculated over the full bandwidth (500-800 nm) and includes the power spectral density (PSD) profiles for surface phase and amplitude. Mask design models evaluate complex transmission errors arising from design limitation and manufacturing errors, leading to derived requirements on substrate transmission PSD, lithographic/e-beam accuracy, and material dispersion. Ideal coronagraph mask performance is based on Fourier-plane (image/pupil conjugate) computations that have a noise floor better than contrast = 1×10^{-13}. Polarization ray-traces are used to determine cross-polarization level, the effectiveness of coating designs, and tolerances on those designs. Scatter models assume that forward-scattered radiation dominates back-scattered radiation and is coherent with the specular beam. At present there is no wavefront sensing and control model per se. Instead, a WFSC performance limit is assumed, consistent with results obtained in the HCIT testbed extrapolated to a more stable environment.

Dynamic error budget terms (jitter and thermal terms) are calculated using linear ray-trace aberration and beam-walk sensitivity matrices combined with the Fourier-plane coronagraph performance model. This model is used to evaluate the contrast leakage related to Zernike aberrations. These models lead to optical surface and structural stability requirements, from which thermal stability, structural damping and isolation are derived by the integrated modeling team.

Table 7-1. Dynamic and Static Error Budget Schedule

Planned Completion Date	Planned Activities	Performance Targets
Pre-Phase A	Sensitivity matrix validation using HCIT	Verification to 10-20% of contrast sensitivity
	Near-field diffraction modeling and mask imperfection modeling	Inclusions of wavelength dependent design parameters, random mask errors, and systematic errors
	Develop full static error budget that describes the contrast in an initial state and the contrast after WFSC using a pair of DMs in a Michelson configuration	Ability to model individual static WFE contributions at the 10^{-12} contrast level
Phase A	Validation of static WFE budget using HCIT	
	Iterative refinement of error budget in conjunction with end-to-end modeling activities	
Phase B	Validation of dynamic error budget using other testbeds	

7.4 Optics and Starlight Suppression Testbeds

7.4.1 Phase A and B Plans for HCIT and PDS

Scope

All the pre-Phase A milestones will probably be met using the half-dark hole configuration. Full-dark hole performance requires two deformable mirrors to control both phase and amplitude. Trade studies to determine the optimum architecture (Michelson configuration or two DMs in series) and necessary control algorithms are underway as part of the Wavefront Sensing and Control task. Design and fabrication of opto-mechanical hardware is planned for FY06, with installation in the HCIT and experimentation commencing at the beginning of Phase A. Completion of this activity had been planned for pre-Phase A, but it resulted in an unreasonable schedule that put required milestone performance at risk. If modeling shows that two DMs are needed to get the broadband performance required in Milestone 2, the HCIT schedule and resources will be adjusted. Also in Phase A, a custom bench and mounts will be designed and fabricated for the HCIT, with completion at the end of Phase A. This will provide the thermal stability needed to achieve and maintain 1×10^{-10} contrast, as well as enabling full structural and thermal modeling of the testbed. Initial study work for the Planet Detection Simulator will commence near the end of pre-Phase A, with detailed design and fabrication of the hardware during Phase A and installation in the HCIT occurring at the beginning of Phase B, after the custom testbed bench has been integrated. During Phases A and B, the spectral bandwidth will be increased and the center wavelength shifted to lower wavelengths, with the performance target for Phase B matching the required TPF-C planet detection bandpass (currently 500-600 nm). The HCIT and PDS milestone schedule is given in Table 7-2.

State of the Art TRL 4

Laboratory results from the HCIT have shown an average contrast of 0.9×10^{-9} for laser light as measured in the half-dark hole over angles from 4 to 10 λ/D.

Table 7-2. HCIT and PDS Milestone Schedule

Planned Completion Date	Planned Activities	Performance Targets	TRL
Pre-Phase A (Q3 FY05)	Monochromatic starlight suppression	Milestone 1: 10^{-9} contrast, 4 λ/D, laser light (λ=785 nm)	4
Pre-Phase A (Q3 FY06)	Broadband starlight suppression	Milestone 2: 10^{-9} contrast, 4 λ/D, 60 nm bandwidth centered at 800 nm	4
Pre-Phase A (Q4 FY06)	Modeling of testbed	Milestone 3A: Correlation of experimental testbed data and optical models of the testbed at 10^{-9} level	4
Pre-Phase A (Q1 FY07)	Integrated modeling of mission	Milestone 3B: Demonstrate viability of 10^{-10} contrast in flight mission using modeling approach validated against testbed and current mission error budget	4
Phase A	Demonstrate full-dark hole using 2 DMs; design/build custom bench and mounts.	1×10^{-9} contrast, full dark hole, 4 λ/D, 100 nm bandwidth centered at 675 nm; correlation of experimental testbed data with optical models of the testbed at 1×10^{-9} level	5
Phase B	Experiments with custom bench; install and operate Planet Detection Simulator	1×10^{-10} contrast, full-dark hole, 4 λ/D, 100 nm bandwidth centered at 550 nm (or current requirement for planet detection); correlation of experimental testbed data with integrated models of the testbed at 1×10^{-10}	6

7.4.2 Apodizing Masks and Stops

Scope

HEBS and binary masks for both focal plane and pupil plane configuration will be fabricated and tested, including the new 8th-order masks, which have been predicted to yield lower sensitivity to aberrations as well as better error budgets due to improved tolerances. Basic characteristics of mask materials and devices and their spectral dependence will be measured precisely with a dedicated component-level test setup being developed at JPL. The schedule for the apodizing masks and stops is given in Table 7-3.

State of the Art TRL 3

Candidate masks have been fabricated and tested on the HCIT. More promising designs are now being prepared.

Table 7-3. Apodizing Masks and Stops Schedule

Planned Completion Date	Planned Activities	Performance Targets	TRL
Pre-Phase A **Q1 FY05**	Fabrication of initial set of candidate masks; fabrication and evaluation of HEBS and binary masks	Compare performance impact of each type of mask on HCIT.	3
Q4 FY05 **Q4 FY06** **Q4 FY06**	Iterate fabrication of candidate masks, based on performance results. Fabricate and test 8th order masks in both binary and HEBS implementations. Fabricate and test silicon type masks. Test and compare pupil plane masks and focal plane masks. Incorporate analysis results to improve design and fabrication.	Measurement of candidate masks at component level to quantify and control fundamental properties such as optical density, amplitude variations and phase retardation/advance including wavelength dependence with better than ±1% measurement precision. A dedicated test setup and methodologies for such precision measurements will be fully developed.	3-4
Phase A	Optimization of apodization functions and fabrication methods. Mask set delivery.	Receive masks consistent with 10^{-9} contrast requirement.	4-5
Phase B	Summary report on mask design and fabrication. Mask set delivery.	Receive masks consistent with 10^{-10} contrast requirement.	6

7.4.3 Technology Demonstration Mirror

Scope

Although the mirror will be completed in March 2007, a critical milestone will be the delivery of the PSD for the coated TDM in September 2006. Earlier near term milestones are the delivery of the fused planar blank to ITT, from Corning, in April 2005 and the completion of slumped mirror in August 2005. From August 2005 to August 2006 the mirror will be fine ground and polished using small tool lap, full tool active lap, and ion beam figuring. The schedule for the TDM is given in Table 7-4.

State of the Art TRL 3

The required mid-spatial frequency performance for the TDM has not been demonstrated on the scale needed for TPF. Smaller mirrors (with a higher areal density) have demonstrated the required MSF, but in the class of the TDM, the requirement has only been met over part of the MSF range.

Table 7-4. Technology Demonstration Mirror Schedule

Planned Completion Date	Planned Activities	Performance Targets	TRL
Pre-Phase A			
April 2005	Delivery of fused planar blank from Corning to ITT	CTE uniformity meets or exceeds requirement	3
August 2005	Completion of slumped mirror	Mirror is within 0.5mm of net shape and cell structures are not deformed due to slumping process	4
August 2006	Delivery of PSD for coated TDM from ITT to JPL	Mirror meets or exceeds spatial surface performance requirements as described in Table 7	5
Phase A			
March 2007	Mirror completed		5

7.4.4 Wavefront Sensing and Control

Scope

This effort includes the development and establishment of the flight baseline wavefront sensing and control architecture. Development and implementation of wavefront sensing and control methodologies on HCIT will continue in support of the pre-Phase A Milestone requirements, as well as Phase A and B plans for the HCIT. A flight baseline wavefront sensing and control architecture will be developed and established in Phase A. The selection will be based on trades between interferometric and multi-conjugate configurations for dual deformable mirror correction. Once a baseline is established, it will be implemented on HCIT. Control methodologies traceable to flight design will be developed, implemented and demonstrated. The simulated performance of the WFSC system will be flowed up to the TPF system requirements to determine the operational capacity of the observatory. The schedule for wavefront sensing and control work is given in Table 7-5.

State of the Art TRL 3

The HCIT has demonstrated repeatable control to $\lambda/10^4$ in a laboratory environment.

Table 7-5. Wavefront Sensing and Control Schedule

Planned Completion Date	Planned Activities	Performance Targets	TRL
Pre-Phase A	Implement wavefront sensing and control methods on HCIT	Wavefront sensing and control performance consistent with HCIT pre-Phase A milestone requirements	3
Phase A	Complete trade study between interferometric and multi-conjugate systems for 2-DM	Baseline WFSC architecture selected	3
	Implement flight baseline design on the HCIT and demonstrate multi-DM control algorithms traceable to flight	WFSC performance consistent with HCIT Phase A performance targets	5
Phase B	Simulate the performance of the TPF-C system	Verify that the observatory operational capacity meets requirements for the baselined WFSC design	5
	Demonstrate WFSC baseline on combined HCIT/PDS testbed	WFSC performance consistent with HCIT Phase B performance targets	6

7.4.5 Deformable Mirrors

Scope

The objective is to develop DMs that are reliable and robust to support the TPF-C/High Contrast Imaging Testbed with the goal of demonstrating contrast performance of 1×10^{-10} or better at angular separations of 4 λ/D or greater from the central point source by May 2006. The scope of work for Xinetics is to demonstrate robust performance in all fundamental elements of the modular deformable mirror process for TPF/Coronagraph Science.

The products to be developed are 32 × 32, 48 × 48, 64 × 64, and 96 × 96 deformable mirrors leading toward technical hardware that are reliable, large enough and robust to support flight performance levels required by September 2008. Module development and combinations will enable best understanding of last path for flight hardware development.

The schedule for the deformable mirror work is given in Table 7-6.

State of the Art TRL 4

Xinetics has delivered five 32 × 32 actuator DMs and two of four 64 × 64 actuator DM. The 32 × 32 DMs have been used in HCIT to achieve suppression approaching 10^{-9} with speckle nulling. See Figure 3-11 in Section 3.2.1 for recent HCIT experimental results.

Work is currently progressing on the 48 × 48 DM 2,304-channel single module manufacturing pathfinders; this work includes module development, actuator machining and delineation pathfinder, interconnect evolution pathfinders, and facesheet development.

Table 7-6. Deformable Mirror Schedule

Planned Completion Date	Planned Activities	Performance Targets	TRL
Pre-Phase A	Manufacture of 64 × 64 and 48 × 48 DMs	Contrast performance of 1×10^{-10} or better at angular separations of 4 λ/D in the HCIT	4
Phase A	Manufacture of 96 × 96 DMs: 3 × 3 format of 32 × 32 and 2 × 2 format of 48 × 48	Contrast performance of 1×10^{-10} or better at angular separations of 4 λ/D in the HCIT	5

7.4.6 Transmissive Optics

Scope

If it is decided that a configuration similar to that of the minimum design mission is needed, the following technology development steps can be outlined further in Phase A and pursued. The schedule for transmissive optics work is given in Table 7-7.

First the system requirements would be defined through detailed modeling of the system using values for the state of the art and allowing for error correction via DMs.

A detailed design including material identification would be performed and investigated with vendors for manufacturability. Demonstration optics would be procured and tested at the manufacturers, for example from Corning for fused silica and from Schott for the beamsplitter glass. Measurements if selected, specially prepared blanks would include dispersion of optical constants, birefringence, striations, bubbles and inclusions, through-thickness homogeneity of index, surface and internal scatter over wavelength; this is estimated to be a ~1-year-long process. The properties of the optical cement and the cemented assembly must also be addressed at the same time, through modeling and measurement, specifically with respect to induced stress.

The alternative approach of large-scale wire grid polarizers fabricated through electron beam lithography might also be addressed.

State of the Art TRL 2

With samples of fused silica, homogeneity values in the range of 0.5 ppm have been published, birefringence levels as low as 0.07 nm/cm have been obtained, and scatter (transmission loss) at a level just over 10^{-5}/cm has been reported

Table 7-7. Transmissive Optics Schedule

Planned Completion Date	Planned Activities	Performance Targets	TRL
Phase A	Large blanks of transmissive optics glass completed	Blanks of a size consistent with 10-cm clear aperture optics	3
	Characterization data from large blanks delivered	Blanks meet or exceed performance requirements as outlined in the contracts as consistent with the error budget	4-5

7.4.7 Coatings

Scope

In order to achieve TRL 6 at the end of Phase B, we will progress through a series of steps from identification of suitable designs and confirmation of their performance on small parts ("witness samples"), to developing the processes for coating on large scales (for the primary and secondary mirrors) and confirmation of performance using the TDM as a large test system. In addition, test coatings for all optics throughout TPF-C and confirmation of their properties on witness samples will be demonstrated to ensure their performance conforms to the established requirements. The coatings have achieved TRL 3.The schedule for coatings work is given in Table 7-8.

Table 7-8. Coatings Schedule

Planned Completion Date	Planned Activities	Performance Targets	TRL
Pre-Phase A	Design of critical coatings Sensitivity analysis of coating performance Measurement of small samples confirm design performance Initiate lifetime measurements Input to definition of TDM coating requirements & process	Nominal designs for all optics completed Small samples of critical coatings meet required performance	1-3
Phase A	Define tests to be used on large optics to confirm performance Test coatings for TDM Test sample coatings for all components to confirm performance	TDM coating performance meets or exceeds requirements Samples of all critical coatings meet or exceed performance requirements	4-6

7.4.8 Scatterometer

Scope

The scatterometer provides checks on how the physics of scatter and contamination effects are handled in various engineering codes, judges impacts on the project and informs the selection of a code for use during baffle design. Scatterometer capabilities allow surface testing to levels comparable to the TDM tests across the relevant range of spatial frequencies. Initially precision optics will be tested followed by baffle materials. The results will validate the models, inform baffle design, and refine the error budget. The schedule for the scatterometer work is given in Table 7-9.

State of the Art TRL 3

The scatterometer testbed at GSFC has measured near-angle scatter to ~<5% accuracy on ~15-cm optics.

Table 7-9. Scatterometer Schedule

Planned Completion Date	Planned Activities	Performance Targets	TRL
September 2005	BRDF models & measurements on 30-50 cm precision optics	Confirmation of model to 2%	4
September 2006	Near-wide-angle BRDF on baffle materials	Confirmation of models to 1%	4
	Verification of near-angle differential scatter from particulate contamination	Confirmation of models to 1%	

7.4.9 Small Precision Optics

Scope

The key issues for masks are surface roughness, transmitted wavefront, and material homogeneity. We will fabricate and test substrates that meet the mask PSD requirements with emphasis on 15-100 micron spatial scales.

For the cube beamsplitters, stress birefringence is identified as the primary limiting factor. Two approaches will be explored: redesign to eliminate cube beamsplitters and work with manufacturers to develop techniques and materials for ultralow-stress birefringence.

For the remaining small optics, we will work with manufacturers to obtain 1 nm surface flatness on mounted optics. The small precision optics have achieved TRL 3.Their schedule is given in Table 7-10.

Table 7-10. Small Precision Optics Schedule

Planned Completion Date	Planned Activities	Performance Targets	TRL
Pre-Phase A	Work with manufacturers to define specifications	Set of specifications manufacturers are willing to attempt	3
Phase A	Build components	Substrate meets mask PSD requirements, 1 nm surface flatness for 10-20 cm reflective optics	4

7.5 Structural, Thermal, and Spacecraft Testbeds

7.5.1 Metrology Components

Scope

The baseline approach is to follow SIM progress on the external metrology truss development while periodically revisiting the project requirements. If for any reason SIM technology is deemed insufficient for TPF-C needs, this task will be expanded to address TPF-C requirements. In addition, as the verification plan matures, metrology requirements will emerge. Any necessary technology development activities will be captured in the next update to this plan. The schedule for metrology components is given in Table 7-11. The metrology components have achieved TRL 3.

Table 7-11. Metrology Components Schedule

Planned Completion Date	Planned Activities	Performance Targets	TRL
Pre-Phase A	Study and monitor metrology sensing scheme based on SIM components		3
Phase A	Implement metrology scheme on Closed-loop Secondary Mirror Position Control Testbed.	6 DOF control to ~50 nm over 24-hour timescale	4

7.5.2 Precision Hexapod

Scope

The testbed development begins in pre-Phase A with design work and requirements definition. By the end of pre-Phase A the metrology sub-system will demonstrate 15-nm measurement. In Phase A, components and full hexapod systems will be acquired where possible, and designed and built where necessary to develop a baseline concept. In Phase B, the EM of the hexapod system will be designed, fabricated and demonstrated to meet performance requirements. This characterization facility will be used during the I&T program to verify the performance of the flight hexapod. The schedule for the precision hexapod is given in Table 7-12.

State of the Art TRL 3

A hexapod built by JPL for SIM in 1997 was designed for a 20 kg payload. It used precision ball screw actuators to achieve a piston accuracy of 1 micron, a pointing accuracy of 3 arcsec, a pointing range of 15 degrees from nominal, and a maximum travel range of 8 cm. The hexapod was designed with low CTE materials and the struts were conductively decoupled from its surroundings to aid with thermal stability.

Table 7-12. Precision Hexapod Schedule

Planned Completion Date	Planned Activities	Performance Targets	TRL
Pre-Phase A Q4 FY05	Planning of the testbed	Clearly define the goals and uses of the testbed	3
Pre-Phase A Q2 FY06	Proposed initial development of the test-bed facility (pending availability of resources)	Demonstrate the ability to measure 6 degrees of freedom to a level of 15 nm over a 5 mm range	4
Phase A	Characterization of actuators and hexapod systems	Procure/fabricate actuator and hexapod systems and characterize using the facility	5
Phase B	Characterization of EM hexapod system	Facility used to verify performance of an EM hexapod system	5
Phase C/D	Utilize the facility to perform initial verification of the flight Hexapod system	Facility is used to verify the performance of the flight hexapod system	6

7.5.3 Precision Structural Stability Characterization

Scope

The goals of the Precision Structural Stability Characterization activity will be achieved through staggered delivery of test facilities and testing of materials and components representing progressively higher levels of assembly and higher levels of flight hardware fidelity. In pre-Phase A, we will focus on collecting material data and validating models for the basic physics of microdynamic stability. Data will be obtained for a regime consistent with the end requirement of 10^{-9} contrast, and scaling laws will be validated where appropriate. Material properties will be maintained within a controlled TPF-C Material Database for approved use on all Project modeling activities. Information on material variability and modeling errors will be assessed to develop a modeling uncertainty propagation approach for TPF-C. This implies that all test facilities will be required to perform an error calibration prior to performing tests to incorporate experimental accuracy within the formulation of the modeling uncertainty factors. In Phases A through B, the focus will progressively shift towards using the validated physics models of pre-Phase A to building and validating models representing higher levels of assembly. Ultimately, the technology developed herein will be delivered to the Flight Design team for use in the flight analyses, and to the Secondary Mirror Tower Partial Structure Testbed for validation of the testbed models. The schedule for precision structural stability characterization is given in Table 7-13.

Table 7-13. Precision Structural Stability Characterization Schedule

Planned Completion Date	Planned Activities	Performance Targets	TRL
Pre-Phase A September FY05	Measure CTE and dimensional stability of relevant optics class materials Calibrate MTC, deliver to JPL and measure microslip for relevant hinge/latch materials Design and build PSS and FSC testbeds	Establish Project controlled Material Database document Measure CTE and stability to 10 ppb Calibrated performance of MTC better than nm-level measurements	N/A
Pre-Phase A September FY06	Calibrate measurement accuracy of PSS and FSC Collect composite material dimensional stability data Characterize friction parameter sensitivity to system dynamic performance	Validate material dimensional stability and dynamic hinge/latch stability models to an accuracy consistent with 10-9 contrast requirement.	N/A
Phase A	Collect dimensional stability and dynamic stability for representative composite structure sub-assembly	Deliver material dimensional stability and dynamic hinge/latch stability requirements consistent with 10-9 contrast requirement	N/A
Phase B	Incorporate model and material property results into flight design analyses Test actual flight sub-component hardware and validate models	Validate that flight design meets 10-9 contrast requirement	N/A

7.5.4 Vibration Isolation Testbed

Scope

During pre-Phase A stage, significant effort will be invested in developing high-fidelity models of the candidate isolation designs. The analytical models will be correlated with existing test data to ensure that the actual behaviors of the isolators are properly captured. These isolation models will also be incorporated in the integrated model, combining structure, optics, and control models, to support end-to-end disturbance-to-performance analyses. The objective during pre-Phase A is to demonstrate the vibration suppression capabilities of the isolators via analysis and show that the stability requirements described in the error budget can be met.

Since the vibration isolation architecture has significant implications to different subsystems within the TPF-C system, system engineering trades that account for these interdependencies must be completed before down-selecting the isolation architecture. The system-level trades will take into account cost, risk, and how performance margins may affect other subsystems requirements. By the end of pre-Phase A, the relative merits of different isolation point designs will be assessed, and an isolation design will be selected based on its vibration-suppression performance and the results of the system engineering trades. At this point, it is also necessary to develop detailed test plans to improve the maturity level of the isolation component technology and determine testbed requirements.

The Phase A isolation sub-system test is envisioned to use the flight payload isolator design attached to mass simulators that mimic the mass and inertia of the payload and the spacecraft (i.e., a 1:1 scaled test). The mass simulators will need to be gravity offloaded so that their fundamental suspension frequencies are significantly below the isolator mode (on the order of 0.01-Hz suspension frequencies). The spacecraft mass simulator will be excited using 6 force shakers arranged to give 6 DOF forcing (e.g., in a Stewart platform). Two types of tests will be performed. The first type measures the 6×6 transfer function matrix from disturbance inputs to payload response. The next type will measure the isolator performance when the motion at each side of the isolator is actively driven to mimic the behavior of analytical models of the spacecraft and the payload. The spacecraft mass simulator response will be actively driven to mimic the behavior of the analytical flexible spacecraft model, driven by the reaction wheel disturbances. The response at the payload interface will be actively driven to mimic the analytical model of the payload. The performance metrics will be the optical stability of the payload analytical model. The metrics for isolation acceptance will include the isolator resonant frequencies (below a specified frequency), damping (greater than a given percent damping), and attenuation above the isolator resonance (greater than a specified, frequency-dependent requirement). The test will need to be conducted in a thermal-vacuum chamber since the damper performance is a function of temperature, and joint pumping and acoustics can introduce additional damping. The input forcing levels should be consistent with expected disturbance force magnitudes to ensure that nonlinear effects show up properly in the test results. Test data must be comprehensive enough to tune the isolator models, and to characterize variability and uncertainty in the isolator behavior. The correlated isolator models (with uncertainty model) will be used to generate an improved system performance prediction, with uncertainty bounds produced by isolator variability.

During Phase B, the isolation sub-system testbed will be integrated with the pointing testbed to demonstrate the pointing and stability performance of TPF-C. This testbed should be a subscale

model of TPF-C and should include appropriate flexible dynamics of the spacecraft and instrument module.

The vibration isolation testbed has achieved TRL 3. The testbed schedule is given in Table 7-14.

Table 7-14. Vibration Isolation Testbed Schedule

Planned Completion Date	Planned Activities	Performance Targets	TRL
Pre-Phase A (Q4 & September FY05)	Design and analyze three types of isolation systems: passive, augmented passive, and active.	Develop models for each isolation design to support analysis. Demonstrate via analyses that each isolation design meets the following payload pointing and stability requirements: rigid body pointing, structure deformation, and optics deformation.	2, 3
Pre-Phase A (Q2 & March FY06)	Improve isolation designs, add higher-fidelity models to analyses, and conduct detailed sensitivity analyses. Complete system-level trade studies sufficient to assess the relative merits of isolation point designs. Identify testbed requirements needed to mature the technology.	Select isolation design that achieves dynamics stability requirements based on analytical results including uncertainty parameter factors and trade study results.	3
Phase A	Fabricate selected isolation devices and supporting testbeds for isolation subsystem test. Perform isolation subsystem tests. Update performance predictions based on isolation test results.	Pointing and stability requirements met with analyses anchored from isolation subsystem test.	4, 5
Phase B	Perform integrated pointing and isolation tests.	Experimentally demonstrate performance of pointing and isolation system	5, 6

7.5.5 Closed-loop Secondary Mirror Position Control

Scope

Our plan is to start the testbed operation using stabilized lasers of wavelength 1.06 μm, currently in operation on the testbed. The first step will be to demonstrate active positioning at the 0.1 nm level along the beam axis (1 DOF), by the middle of FY05. By the middle of FY06, the goal will be to show the required secondary mirror positioning along all 6 DOF, using the down-selected TPF stabilized laser system described above. In Phase A we envision operating an engineering prototype, of order ¼ scale, that will lead to the design of the full mission system. Finally, in Phase B a realistic mission design will be tested, including the use of a 3 m tower to support the hexapod. The closed-loop secondary mirror position control has achieved TRL 3. The schedule is given in Table 7-15.

Table 7-15. Closed-loop Secondary Mirror Position Control Schedule

Planned Completion Date	Planned Activities	Performance Targets	TRL
Pre-Phase A Q3 FY05	Demonstrate required length control along optical axis (1 DOF)	$\Delta x \sim 10^{-10}$ m over 8 hour timescale	3
Q2 FY06	Demonstrate required length control along transverse axes, and in tip and tilt (6 DOF)	$\Delta y, \Delta z \sim 10^{-10}$ over 8 hour timescale	4
	Incorporate TPF down-selected stabilized laser system in testbed	$\Delta\theta, \Delta\phi \sim 10^{-10}$ over 8 hour timescale	4
Phase A	Implement Closed-loop Secondary Mirror Position Control on ¼ scale engineering prototype.	TPF secondary mirror positioning requirements in 6 DOF	5
Phase B	Test of realistic system including 3 m tower support of hexapod	TPF secondary mirror positioning requirements in 6 DOF	6

7.5.6 Secondary Mirror Tower Partial Structure Testbed

Scope

The current plan is to have this testbed competed, designed and built through Phase A, with model validation and other technology objectives completed in the early-to-mid-Phase B time frame. The secondary mirror tower partial structure testbed has achieved TRL 3. The testbed schedule is given in Table 7-16.

Table 7-16. Secondary Mirror Tower Partial Structure Testbed Schedule

Planned Completion Date	Planned Activities	Performance Targets	TRL
Phase A	Design and build testbed Test materials and sub-components individually prior to testbed integration Validate sub-component models	Design testbed, hinge/latch and metrology system consistent with 25 nm SM stability requirement above 1 Hz	3, 4
Phase B	Perform tests and validate testbed models	Validate microdynamic bounding analyses on flight-like hardware for 25 nm SM stability requirement above 1 Hz	5, 6

7.5.7 Pointing Control Testbed

Scope

The goals of the Pointing Control Testbed are to demonstrate both the capability to deliver very high precision pointing and to reject disturbances at the coronagraph using fine guidance sensor (FGS) measurements coupled with a fine steering mirror (FSM) pointing control. Additional capabilities required are rigid body pointing of the entire payload using reaction wheels, low-bandwidth steering of the secondary mirror, and perhaps pointing offset of the payload using active isolation actuators.

In pre-Phase A, we will focus on analysis and data collection of the various sensor components. In Phase A, we will develop key pieces of the testbed, and perform open-loop tests of the FSM and FGS. In Phase B, the method for verifying the measured performance versus the modeled performance (a "scoring system") will be developed; the requirements for isolation levels will be defined; and closed-loop performance of the FGS/FSM/optical path, acquisition sensor, and disturbance rejection will be tested. The pointing control testbed has achieved TRL 3. The testbed schedule is given in Table 7-17.

Table 7-17. Pointing Control Testbed Schedule

Planned Completion Date	Planned Activities	Performance Targets	TRL
Phase A	Implement FGS camera	Demonstrate open-loop pointing control accuracy, resolution and 50 Hz bandwidth on FSM	5
	Implement FSM control loop	Demonstrate measurement accuracy of 1 mas on FGS sensor at 500 Hz; meet tighter requirements in Phase B	
	Develop disturbance generators	Develop capability to induce modeled vibration into testbed, required in Phase B	
Phase B	Develop validation "scoreboard"	Demonstrate capability for validating high-precision pointing	5,6
	Design and build isolated testbed	Demonstrate isolation required for integrated testing	
	Test FSM/FGS/optical path subsystem element.	Demonstrate pointing accuracy to 0.3 mas jitter, 0.3 offset at subassembly level with controlled disturbances, in vacuum chamber	
	Test acquisition camera accuracy	Show 10 mas accuracy/axis for stars brighter than roughly 10,000 electrons signal	
	Test integrated system with disturbance input.	Demonstrate ability to reject disturbances to testbed using FSM/FGS/optical path simulation to full performance (currently ~0.3mas 1 sigma jitter)	

7.5.8 Sub-scale EM Sunshield and Isothermal Enclosure

Scope

The testbed development begins during pre-Phase A, roughly at the beginning of FY06, and concludes at the end of Phase A. Testbed design will be strongly affected by the need to minimize thermal noise arising from the simulated space environment. Measurements will evaluate the design of the sunshield, the thermal enclosures and the temperature control systems. It is understood that there is a significant risk that the design verified by the testbed during Phase A will change significantly by the time that the final flight design is set at the critical design review. Early demonstration of thermal design feasibility in Phase A is judged a worthwhile investment. Significant flight design changes may be incorporated and verified in a updated testbed, if necessary, later in the program. The sub-scale EM sunshield and isothermal enclosure have achieved TRL 3. Their schedule is given in Table 7-18.

Table 7-18. Sub-scale EM Sunshield and Isothermal Enclosure Schedule

Planned Completion Date	Planned Activities	Performance Targets	TRL
Pre-Phase A **Q4 FY05**	Select baseline sunshield configuration	Characterize specularity of sunshield layers based on scattering measurements of previously folded material	
	Select candidate isothermal cavity components	Survey available 10-100 micro-K thermometry components (sensors and PID controllers) for room temperature control. Consider the need for component space qualification	4-5 (comp)
Q2 FY06	Design the sunshield	Complete thermal model of sunshield assembly including IR BRDF, micrometeoroid effects, rip-stop features, deployment system effects, etc.	2-3 (sys)
	Design the isothermal cavity	Requirements summary for the Isothermal Cavity testbed completed and approved	2-3 (sys)
		Preliminary design including the dummy mirror and the supporting AMS/PSS structure completed	
		Plan for preliminary qualification testing is established on EMs sensors/controllers by early in Phase A if need is identified	
Phase A	Complete design, construction and checkout of the Sun/Iso testbed with an installed dummy mirror system.	By mid-Phase A, select a site for the testbed, update the testbed requirements, complete a final design, and have it reviewed and approved. Procure the components and assemble the testbed late in Phase A. Perform any critical component qualification testing per plan from pre-Phase A	5-6 (comp)
	Complete thermal performance testing of above testbed.	In the presence of external thermal disturbances simulating the effects of dithers and slews, demonstrate mirror temperature control at the required flight levels.	5-6 (sys)
		Correlate analytical models to the test data to validate models that can later be scaled to predict the PM thermal response of the full-scale TPF-C to dithers and slews.	

7.5.9 Sub-scale EM Primary Mirror Assembly

Scope

This testbed is essentially the same testbed as described in the preceding section but with added features. In the initial build-up of the testbed, vibration isolation will be included for convenience and efficiency, but is not required for the thermal control system evaluation. The interferometer and its attendant controls can be added after the tests on the sunshield/thermal enclosure systems have been completed. Optical testing of the thermal control system will occur during Phase B. The sub-scale EM primary mirror assembly has achieved TRL 3. The assembly schedule is given in Table 7-19.

Table 7-19. Sub-scale EM Primary Mirror Assembly Schedule

Planned Completion Date	Planned Activities	Performance Targets	TRL
Phase B	Convert the Sunshield/Isothermal Cavity testbed into the Sub-scale PM Assembly testbed, and test the sub-scale PM in the new testbed.	Design and procure the high-quality sub-scale mirror needed for the optical testing of the Sunshield/Isothermal Cavity testbed. This will likely need to be started sometime late in Phase A. In the presence of external thermal disturbances simulating the effects of dithers and slews, demonstrate optical shape control at the required flight levels. Correlate analytical models to the test data to validate models that can later be scaled to predict the optical response of the full-scale TPF-C to dithers and slews.	5-6 (sys)

7.6 Integrated Modeling and Model Validation

7.6.1 Integrated Modeling Tools

Scope

Code architecture, optical aberration calculations, large problem numerics (parallel processing) and design sensitivity and optimization components are currently supported by JPL R&TD development funding for use in future missions such as TPF-C; TPF specific components include element development and nonlinear heat transfer methods development. Within these TPF-funded areas, technology completion will include:

- Completion and validation of nonlinear transient solution procedures:
  Gray-body diffuse exchange by the end of pre-Phase A, specular exchange with thermal control by Phase A. Validation will consist of performance benchmarking against commercial tools currently used by design teams, and test validation using JPL in-house test programs.

- Thermal and structural finite elements:
  Completion of initial library by end of pre-Phase A, validation using theoretical, commercial, and test fixture results.

- Optical aberration calculation:
  Automated optical aberration calculations for the purpose of interfacing with codes such as SPICA, MACOS, Code-V, etc. are seen as fundamental to the success of the analytic methods development task, and should be available by the end of pre-Phase A. Validation will consist of demonstrated higher levels of precision that with existing tools, in support of contrast ratios on order of 10^{-9}.

The integrated modeling tools have achieved TRL 3. Their schedule is given in Table 7-20.

Table 7-20. Integrated Modeling Tools Schedule

Planned Completion Date	Planned Activities	Performance Targets	TRL
Pre-Phase A	Completion of nonlinear transient heat transfer solutions, completion of initial thermal/structural finite element library.	Demonstrate ability to compute thermal, structural responses to degree of accuracy required by TPF, correlate performance with commercially-available tools, validate performance against HCIT.	
Phase A	Nonlinear transient specular exchange, thermal control module.	Utilization of code by TPF design team members for integrated thermal, structural and optical aberration calculations, testbed validation, system error budget investigation.	
Phase B	Nonlinear structural analysis capabilities for local mechanical, material nonlinearity investigation.	Continued use by design teams to increasing level of sophistication including incorporation of nonlinear optical element, hinge, latch behaviour.	

7.7 Instrument Technology and Advanced Concepts

7.7.1 Instrument Technology

The classes of instruments defined in the Instrument Concept Studies and included in the Science and Technology Definition Team final report are likely to require technology development. Once identified, the high-priority developments will be addressed in the next update to the TPF-C Technology Development Plan. This section serves as a placeholder for those activities.

7.7.2 Advanced Concepts: Visible Nuller Testbed

Scope

The visible nuller testbed must integrate existing component technologies and demonstrate the concept of starlight suppression on a system basis in white light, and at the 10^{-10} contrast required for detection and spectroscopy of extra-solar planets. The 2-mirror rooftop design will be replaced by 3 mirrors to facilitate reimaging the deformable mirror onto the single-mode fiber array. When the deformable mirror and fiber array are in place, this testbed will demonstrate the ability of a coherent single-mode fiber array to spatial-filter over a full aperture, showing enhanced nulling over a full field of view. The visible nuller testbed schedule is given in Table 7-21.

State of the Art TRL 3

The visible nuller has achieved nulls of 5×10^{-6} in polarized laser light and 10^{-4} in unpolarized white light with a 10% bandpass in a single optical channel. A single-mode fiber array having 51 rows has been successfully implemented to form a 496-fiber array.

Table 7-21. Visible Nuller Testbed Schedule

Planned Completion Date	Planned Activities	Performance Targets	TRL
Pre-Phase A **Q4 FY05**	Establish Visible Nuller Testbed configuration. Convert to 3 mirror arm nuller. Demonstration of nulling interferometer component for instrument.	Single pixel contrast $\leq 10^{-6}$ in white light (λ=650 nm, 5-10 % bandpass)	3
Q2 FY06	Demonstrate deep nulling required for Earth-like planet detection and spectroscopy	Single pixel contrast $\leq 10^{-7}$ in white light (λ=650 nm, 5-10 % bandpass)	3
Q3 FY06	First demonstration of multiple channel nulling. Integration of component technologies, nuller, DM, SMFA for system demonstration capability in a vacuum environment. Predict contrast performance.	Multiple pixel contrast less than single pixel contrast over 100 pixels or more. Contrast performance prediction at the 10^{-10} level.	3

7.7.3 Advanced Concepts: Phase-Induced Amplitude Apodization

Scope

This work is focused on developing the mathematical formalism for this concept. This work will contribute to the design of optical surfaces and minimization of system aberrations. A number of implementations, including hybrid concepts, will be explored. A laboratory demonstration of hybrid PIAA/conventional apodization approach in the visible is planned. The demonstration includes wave-front control employing a deformable mirror, and results will be compared to simulations. Optical fabrication issues will be addressed through this experimental effort. The phase-induce amplitude apodization schedule is given in Table 7-22.

State of the Art TRL 2

The PIAA principal has been demonstrated in a laboratory experiment. Detailed analyses have been published. The technique has been applied in radio dishes for decades. Optics suitable for 1e-6 diffraction control are currently being fabricated. These optics meet unique requirements for radius-of-curvature and accuracy at the edge of the optic.

Table 7-22. Phase-Induce Amplitude Apodization Schedule

Planned Completion Date	Planned Activities	Performance Targets	TRL
Pre-Phase A	Contracts with NOAO and U of Hawaii for analysis and proof of concept.	10^{-7} contrast at 4 λ/D	3

8 TPF-C Pre-Phase A Project Schedule

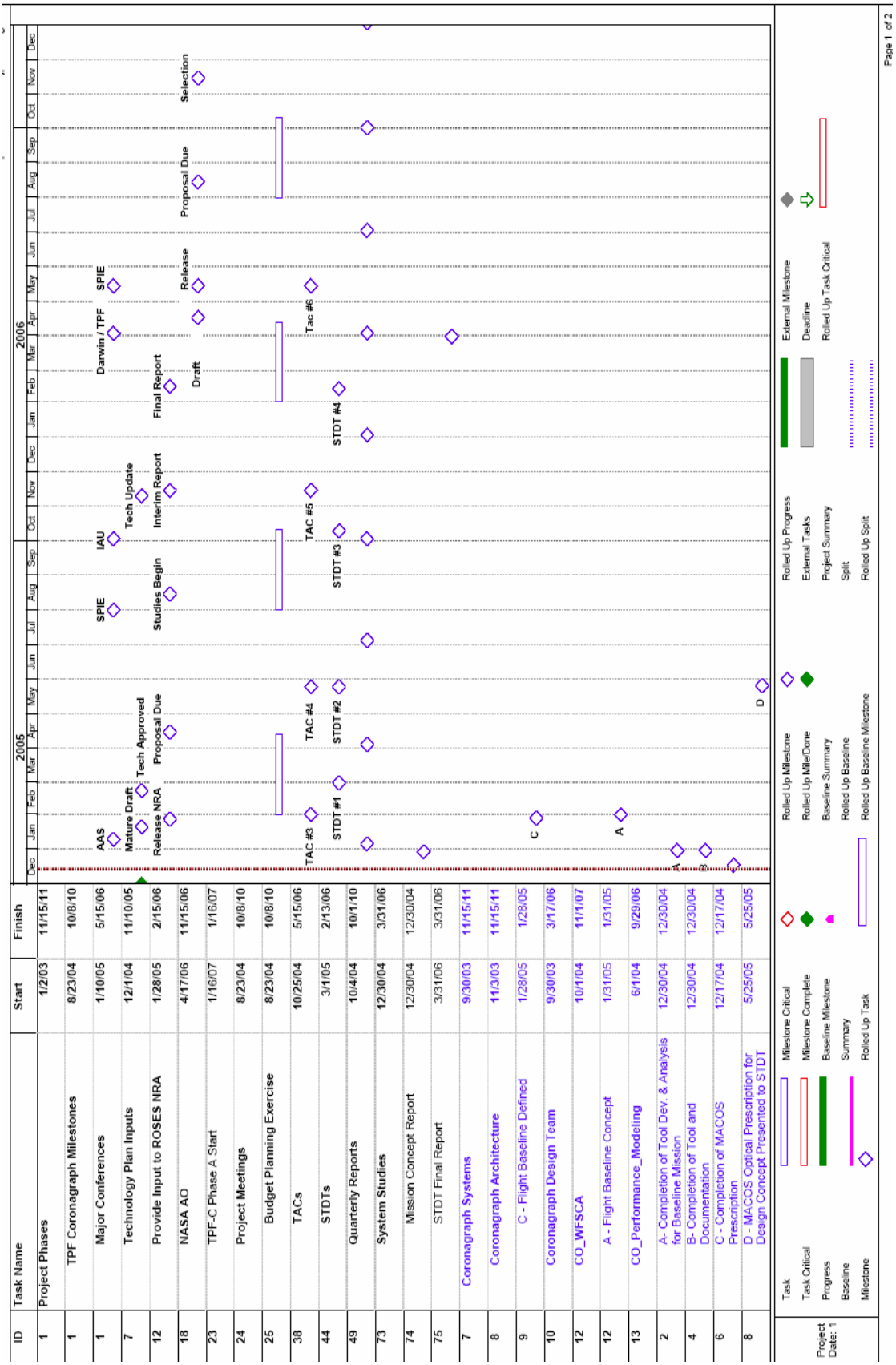

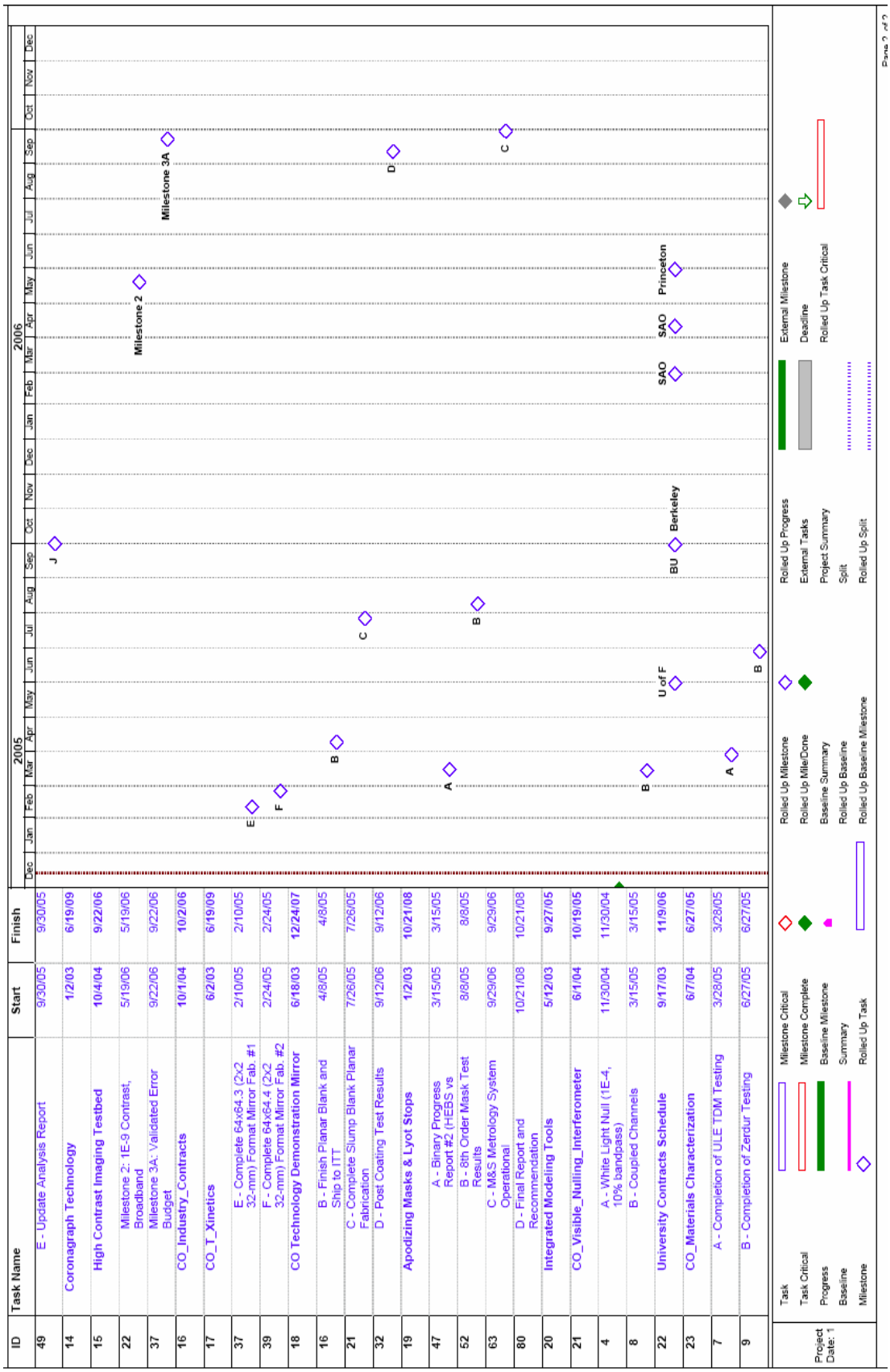
ID
Task Name
Start
Finish
2005
2006
Milestone 2
Milestone 3A
SAO
Princeton
Berkeley
U of F
Project Date: 1
Task
Task Critical
Progress
Baseline
Milestone
Milestone Critical
Milestone Complete
Baseline Milestone
Summary
Rolled Up Task
Rolled Up Milestone
Rolled Up Mile/Done
Baseline Summary
Rolled Up Baseline
Rolled Up Baseline Milestone
Rolled Up Progress
External Tasks
Project Summary
Split
Rolled Up Split
External Milestone
Deadline
Rolled Up Task Critical

Appendix A: TPF-C Project Organization

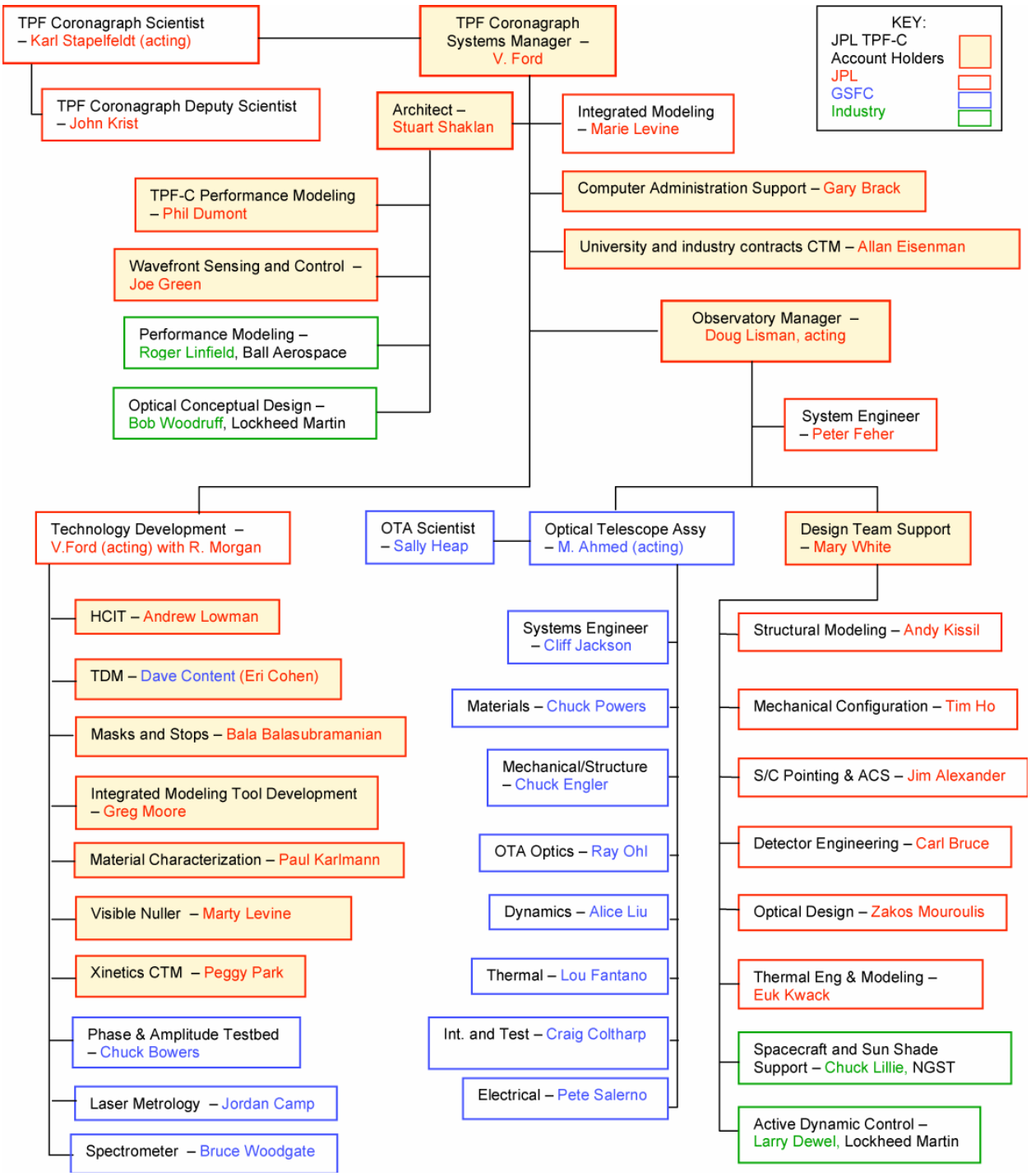

Appendix B: TPF-C Detailed Milestone Schedule

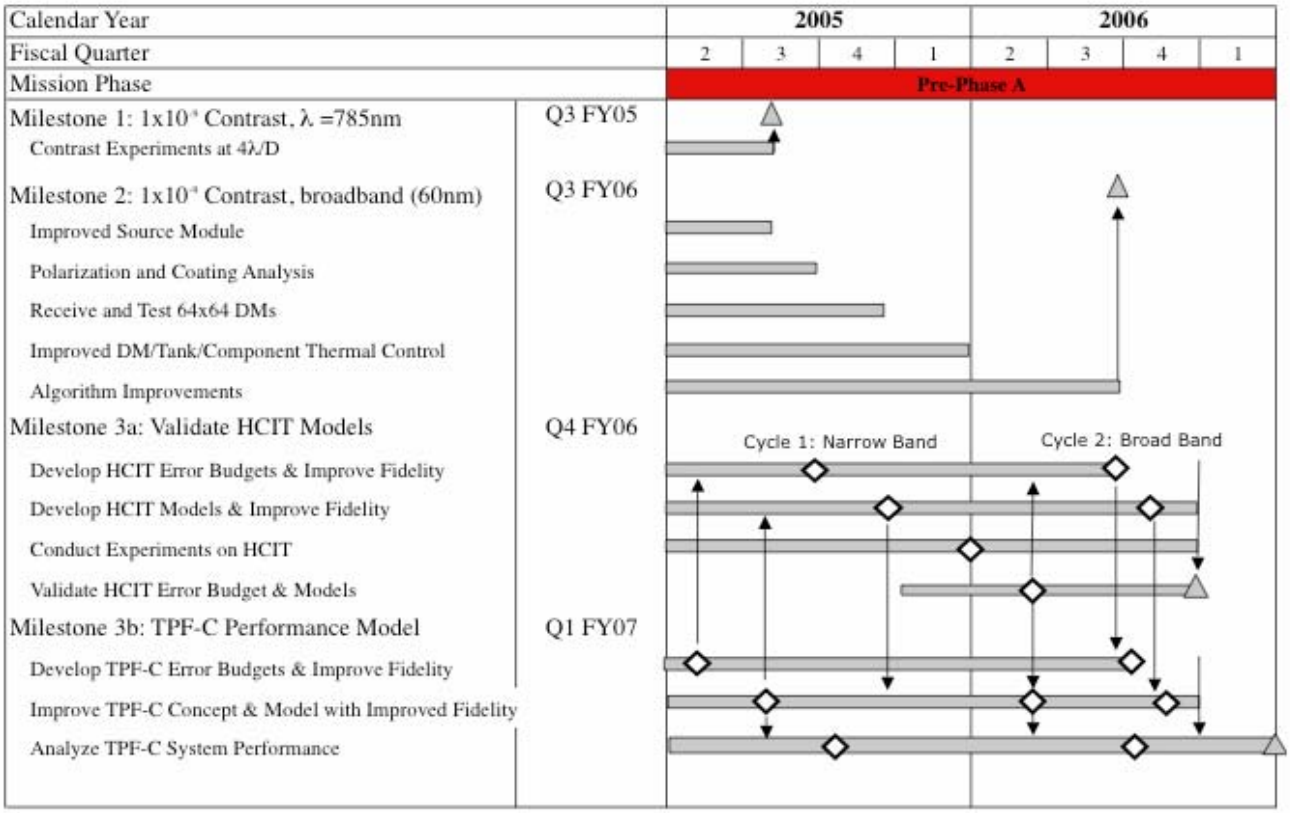

Appendix C: TPF-C Science and Technology Definition Team

Table C-1. Science and Technology Definition Team Members

Name	Institution
James Kasting (Chair)	Penn State University
Roger Angel	University of Arizona
Mike Brown	California Institute of Technology
Robert Brown	Space Telescope Science Institute
Chris Burrows	Metajiva Scientific
Mark Clampin	NASA Goddard Space Flight Center
Alan Dressler	Carnegie Institute of Washington
Harry Ferguson	Space Telescope Science Institute
Heidi Hammel	Space Telescope Science Institute
Scott Horner	Lockheed Martin
Garth Illingworth	University of California Observatories Lick
Jeremy Kasdin	Princeton University
Marc Kuchner	Princeton University
Doug Lin	UC Santa Cruz
Mark Marley	NASA Ames
Vikki Meadows	IPAC, NAI
Charley Noecker	Ball Aerospace
Ben Oppenheimer	American Museum of Natural History
Sara Seager	Carnegie Institute of Washington
Wesley Traub	Smithsonian Astrophysical Observatory
John Trauger	Jet Propulsion Laboratory
Sally Heap (ex officio)	NASA Goddard Space Flight Center
Karl Stapelfeldt (ex officio)	Jet Propulsion Laboratory

Appendix D: TPF-C Technology Advisory Committee

Table D-1. TPF Technology Advisory Committee

Name	Institution
Jennifer Dooley (Chair)	Jet Propulsion Laboratory
Ron Allen	Space Telescope Science Institute
Chris Burrows	Metajiva Scientific
Rich Capps	Jet Propulsion Laboratory
Dick Dyer	Schafer Corporation
Mike Krim	Perkin-Elmer, retired
Bruce Macintosh	Lawrence Livermore National Laboratory
Pete Mason	California Institute of Technology
Dave Mozurkewich	Seabrook Engineering
Jason Speyer	UCLA

Appendix E: Technology Readiness

TPF-C technology progress is tracked against several metrics. One set of metrics is the technology gates discussed above in Section 1.6. In terms of coverage of technology risk areas, these gates are not all-inclusive, but they do offer a concrete measure of TPF-C's progress toward full technology validation. Another metric is the Technology Readiness Level (TRL) scale. The entire TRL scale is given below for reference.

- **TRL 1:** Basic principles observed and reported
- **TRL 2:** Technology concept and/or application formulated
- **TRL 3:** Analytical and experimental critical function and/or characteristic proof of concept
- **TRL 4:** Component and/or breadboard validation in laboratory environment
- **TRL 5:** Component and/or breadboard validation in relevant environment
- **TRL 6:** System/subsystem model or prototype demonstration in a relevant environment (ground or space)
- **TRL 7:** System prototype demonstration in a space environment
- **TRL 8:** Actual system completed and "flight qualified" through test and demonstration (ground or space)
- **TRL 9:** Actual system "flight proven" through successful mission operations

Appendix F: Acronym List

Table F-1. Acronym definitions used in this technology plan.

Acronym	Definition
ACS	Advanced Camera for Surveys
AMS	Aft Metering Structure
AMSD	Advanced Mirror System Demonstrator
AOM	Acousto-optic Modulator
ASAP	Advanced Systems Analysis Program
ASIC	Application-Specific Integrated Circuit
BRDF	Bidirectional Reflectance Distribution Function
CEB	Contrast Error Budget
CGH	Computer Generated Holography
COPHI	Common Path Heterodyne Interferometers
CTE	Coefficient of Thermal Expansion
DFP	Disturbance Free Payload
DGEF	Diffraction Grating Evaluation Facility
DM	Deformable Mirror
DOF	Degree of Freedom
EELV	Evolved Expendable Launch Vehicle
EM	Engineering Model
ESA	European Space Agency
FGS	Fine Guidance Sensor
FSC	Frictional Stability Characterization
FSM	Fine Steering Mirror
FY	Fiscal Year
GSFC	Goddard Space Flight Center
HEBS	High Energy Beam
HCIT	High Contrast Imaging Testbed
HST	Hubble Space Telescope

HSF	High Spatial Frequency
HRC	High Resolution Channel
I&T	Integration and Test
IPEX	Interferometry Program Experiment
IR	Infrared
IWA	Inner Working Angle
JPL	Jet Propulsion Laboratory
JWST	James Webb Space Telescope
LISA	Laser Interferometer Space Antenna
LIGO	Laser Interferometer Gravity Wave Observatory
LOS	Line of Sight
LSF	Low Spatial Frequency
M&MV	Modeling and Model Validation
MACOS	Modeling and Analysis for Controlled Optical
MAP	Microwave Anisotropy Probe
MATLAB	Matrix Laboratory
MDL	Micro Devices Laboratory
MSF	Mid Spatial Frequency
MTC	Microslip Tribometer Characterization
MUF	Modeling Uncertainty Factor
NASA	National Aeronautics and Space Administration
NASTRAN	NASA Structural Analysis
NGST	Next Generation Space Telescope (see also JWST)
NIST	National Institute of Standards and Technology
NOAO	National Optical Astronomy Observatory
OAP	Off-axis Parabola
OSAC	Optical Surface Analysis Code
OSCAR	Optical Systems Characterization and Analysis Reseach
OTA	Optical Telescope Assembly
PCT	Pointing Control Testbed
PDF	Precision Dilatometer Facility
PDS	Planet Detection Simulator
PIAA	Phased Induced Amplitude Apodization
PFM	Protoflight Mirror
PM	Primary Mirror
PSD	Power Spectral Density
PSS	Payload Support System
RMS	Root Mean-Square

RWA	Reaction Wheels Assembly
SAO	Smithsonian Astrophysical Observatory
SBIR	Small Business Innovative Research
SIM	Space Interferometry Mission
SM	Secondary Mirror
SMFA	Single-Mode Fiber Array
SPIE	International Society for Optical Engineering
STDT	Science and Technology Definition Team
SWG	Science Working Group
TAC	Technology Advisory Committee
TDM	Technology Demonstration Mirror
TPF-C	Terrestrial Planet Finder Coronograph
TPF-I	Terrestrial Planet Finder Interferometer
TRL	Technology Readiness Level
U of A	University of Arizona
UH	University of Hawaii
ULE	Ultra-low Expansion
V&V	Verification and Validation
VN	Visible Nuller
WA	Work Agreement
WBS	Work Breakdown Structure
WFE	Wavefront Error
WFSC	Wavefront Sensing and Control